

DIGITAL ACCESS TO SCHOLARSHIP AT HARVARD
DASH.HARVARD.EDU

HARVARD LIBRARY

Identification of a privileged scaffold to accelerate DUB drug discovery

Citation

Ayala, Anthony. 2024. Identification of a privileged scaffold to accelerate DUB drug discovery. Doctoral dissertation, Harvard University Graduate School of Arts and Sciences.

Link

https://nrs.harvard.edu/URN-3:HUL.INSTREPOS:37377844

Terms of use

This article was downloaded from Harvard University's DASH repository, and is made available under the terms and conditions applicable to Other Posted Material (LAA), as set forth at

https://harvardwiki.atlassian.net/wiki/external/NGY5NDE4ZjgzNTc5NDQzMGIzZWZhMGFlOWI2M2EwYTg

Accessibility

https://accessibility.huit.harvard.edu/digital-accessibility-policy

Share Your Story

The Harvard community has made this article openly available.
Please share how this access benefits you. Submit a story

HARVARD UNIVERSITY
Graduate School of Arts and Sciences



DISSERTATION ACCEPTANCE CERTIFICATE

The undersigned, appointed by the

Department of Chemistry & Chemical Biology

have examined a dissertation entitled:

Identification of a privileged scaffold to accelerate DUB drug discovery

presented by: Anthony Ayala

candidate for the degree of Doctor of Philosophy and hereby certify that it is worthy of acceptance.

Signature _____
Typed name: Professor Sara Buhrlage

Signature _____
Typed name: Professor Theodore Betley

Signature _____
Typed name: Professor Matthew Shair

Date: 6 September 2023

Identification of a privileged scaffold to accelerate DUB drug discovery

A dissertation presented by

Anthony Ayala

to

The Chemistry and Chemical Biology Program

In partial fulfillment of the requirements

for the degree of

Doctor of Philosophy

in the subject of

Chemistry and Chemical Biology

Harvard University

Cambridge, Massachusetts

September 6, 2023

Copyright

© 2023 Anthony Ayala

All rights reserved

Dissertation Advisor: Dr. Sara Buhrlage Anthony Ayala

Identification of a privileged scaffold to accelerate DUB drug discovery

Abstract

The ubiquitin/proteasome (UPS) is a highly regulated protein modification pathway, where the covalent attachment of one or more ubiquitin proteins promotes proteolysis, or other non-proteolytic fates, of substrate proteins.[1] Three distinct enzymes, E1, E2, and E3 ligases, are required to conjugate the C-terminus of ubiquitin to the target protein. Substrates that are destined for degradation are proteolyzed in a ubiquitin-dependent manner. Deubiquinating enzymes (DUBs) oppose the activity of ligases and remove ubiquitin from target proteins. Improper function of the UPS has been linked to several human pathologies, including neurodegeneration, inflammation, and cancer.[2] Due to their central role in UPS regulation, DUBs are increasingly recognized as attractive targets for therapeutic intervention in these diseases. The clinical success of the proteosome inhibitor, Bortezomib, has validated the ubiquitin system as a target for cancer therapy.[3] However, despite extensive research into the basic function and disease relevance of the ubiquitin system, high quality chemical probes and clinical agents have been developed for only a small fraction of proteins that write (E1-E2-E3), read, and erase (DUB) ubiquitin PTMs.[4]

In this work, we embarked on a campaign to identify reversible small molecules that target recently described DUB pockets. To generate chemical starting points for inhibitors that target these new pockets, we screened a chemically diverse small molecule library across a set of eight DUBs. We subsequently used our established suite of DUB assays and computational analysis to credential new chemotypes as “leads” for a noncovalent library targeting non-catalytic pockets conserved across most DUBs. Importantly, we identified analogs from these chemotypes that inhibit DUBs relevant to cancer therapy. We leveraged the additional sequence and structural diversity represented in these pockets to

develop selective inhibitors across the gene family. Our new chemical tools will accelerate the development of selective probes for promising DUB targets and enable detailed mechanism studies to decipher the function of DUBs in oncology.

Table of Contents

Title Page ..... *i*

Copyright ..... *ii*

Abstract ..... *iii*

Table of Contents ..... *v*

Abbreviations ..... *viii*

Acknowledgements ..... *xiii*

Chapter 1: Deubiquitinase background *1*

1.1 Ubiquination and deubiquinating enzymes **1**

1.2 Challenges with identifying DUB inhibitors **5**

Chapter 2: Identification and validation of leads for USP8 inhibitors *7*

2.1 Introduction **8**

2.2 Results **12**

2.2.1 USP8 confirmatory biochemistry with XL-9872-040 12
2.2.2 Orthogonal validation of XL-9872-040 by target engagement 14
2.2.4 XL-9872-040 structure activity relationship (SAR) data 14
2.2.5 Ubiquigent Selectivity Profiling for select XL-9872-040 analogs 20
2.2.6 USP8 confirmatory biochemistry with SB1-B-68 27
2.2.7 Orthogonal validation of SB1-B-68 by Microscale Thermophoresis (MST) 29
2.2.8 Computational docking studies with SB1-B-68 series 30
2.2.9 SB1-B-68 structure activity relationship (SAR) data 32
2.2.10 Ubiquigent profiling for SB1-B-68 series 38
2.2.11 SB1-B-68 readily oxidizes, confounding the "hit" result 39
2.2.12 USP8 confirmatory biochemistry with M058-0519 40
2.2.13 M058-0519 structure activity relationship (SAR) data 40
2.2.14 Redox activity of select M058-0519 analogs 42

Table 2.5 (Continued) **51**

2.3 Discussion **51**

2.4 Materials and methods **54**

2.5 Author contributions **75**

Chapter 3: A pyrrolo-pyridine motif is a foundational chemotype for DUB inhibition. *76*

3.1. Introduction **77**

3.2. Results **81**

3.2.1 Ubiquigent profiling revealed selective M058-0519 series hits of USP28 and USP25 81
3.2.2 Computational docking studies of YL-12826 and USP28 81
3.2.3 YL-12826-4 structure activity relationship (SAR) data 86
3.2.4 Additional Ubiquigent profiling of select USP28-active analogs 86
3.2.5 Orthogonal validation of USP28 inhibitors by Activity-Based Protein Profiling (ABPP) .. 87

3.2.4 M058-0519 analogs selectively inhibit USP4 and USP15 95
3.2.7 YL-12826-7 structure activity relationship (SAR) data 97
3.2.7 An alignment of the USP28 and USP4 distal pockets reveals further insights into selectivity. 104
3.3 Discussion 104
3.4 Materials and methods 107
3.5 Author contributions 114

List of Figures		Page
Figure 1.1	Role of deubiquitinating enzymes in the ubiquitin proteosome system	3
Figure 1.2	DUB family tree	4
Figure 2.1	IC_{50} values and selectivity profiles of USP8 inhibitors	9
Figure 2.2	Studies of USP8 biology with early-generation USP8 inhibitors	11
Figure 2.3	USP8 screening hits from the Novartis library	13
Figure 2.4	USP8 target engagement	14
Figure 2.5	Ubiquigent profiling of select XL-9872-040 analogs	21
Figure 2.6	Validation of SB1-B-58 with biochemistry and Ubiquigent profiling.	28
Figure 2.7	MST confirmed binding of SB1-B-68 to USP14	29
Figure 2.8	Computational model of SB1-B-68 bound to USP8	31
Figure 2.9	Ubquigent profiling of SB1-B-68 analogs	39
Figure 2.10	Validation of USP8 inhibition by M058-0519 with biochemistry and Ubiquigent profiling	42
Figure 2.11	Resazurin redox assay results	44
Figure 3.1	Ubiquigent profiling revealed selective M058-0519 analogs of USP25/28	82
Figure 3.2	USP28 crystallography	83
Figure 3.3	Computational insights from the USP28 co-crystal structure	84
Figure 3.4	Select analogs are highly selective for USP25/28	86
Figure 3.5	ABPP studies with AXA-05-177, 191, and 193	92
Figure 3.6	Ubiquigent profiling revealed selective analogs of USP4/15	95

List of Tables		Page
Table 2.1	SAR studies of XL-9872-040 series analogs focused on the pyrrole region	18
Table 2.2	SAR studies of XL-9872-040 series analogs focused on the amide region	23
Table 2.3	SAR studies of SB1-B-68 series analogs focused on the amide position	33
Table 2.4	SAR studies of SB1-B-68 series analogs, focused on the phenyl region	36
Table 2.5	SAR studies of M058-0519 analogs against USP8	46
Table 3.1	SAR studies of M058-0519 analogs against USP28	89
Table 3.2	SAR studies of M058-0519 analogs against USP4	100

Abbreviations

µL	microliter
µM	micromolar
ABPP	activity-based protein profiling
AMSH	Associated Molecule With The SH3 Domain Of STAM
CRO	contract research organization
DBU	1,8-Diazabicyclo[5.4.0]undec-7-ene
DCM	dichloromethane
ddH_2O	double-distilled water
DMF	Dimethylformamide
DMSO	dimethylsulfoxide
DUB	deubiquitinating enzyme
EDTA	Ethylenediaminetetraacetic acid
ESI	electrospray ionization
Et_2O	ethyl ether
Et_3N	triethylamine

EtOAc	ethyl acetate
EtOH	ethanol
HATU	1-[Bis(dimethylamino)methylene]-1H-1,2,3-triazolo[4,5-b]pyridinium 3-oxide hexafluorophosphate
HCl	hydrochloric acid
HEPES	4-(2-hydroxyethyl)-1-piperazineethanesulfonic acid
HTS	high-throughput screening
IMiD	immunomodulatory drug
IPTG	isopropyl-1-thio-D-galactopyranoside
ISG15	interferon stimulated gene 15
ITC	isothermal titration calorimetry
JAMM	Jab1/Mov34/Mpr1 Pad1 N-terminal+ domain proteases
K_D	Dissociation constant
kDa	kilodalton
LCMS	liquid chromatography mass spectrometry
LSCC	lung squamous cell carcinoma
MALDI-TOF	matrix-assisted laser desorption/ionization time-of-flight
MeCN	acetonitrile
MHz	megahertz
MINDY	motif interacting with ubiquitin-containing novel DUB family proteases
MJD	Machado-Josephin domain proteases
mL	milliliter

Na_2SO_4	sodium sulfate
NaCl	sodium chloride
$NaHCO_3$	sodium bicarbonate
NEDD8	neuronal precursor cell-expressed developmentally downregulated protein 8
NIBR	Novartis Institutes for BioMedical Research
Ni-NTA	nickel(II) nitriloacetate
nL	nanoliter
nM	nanomolar
NMR	nuclear magnetic resonance
NSCLC	Non-small cell lung cancer
OTU	ovarian tumor proteases
OTUD3	Ovarian Tumor Deubiquitinase 3
PAINS	Pan-assay interference compounds
PLpro	papain-like protease
PMSF	phenylmethanesulfonylfluoride
$POCl_3$	Phosphoryl chloride

PTM	post-translational modification
ROS	reactive oxygen species
SAR	structure activity relationship
SARS-CoV-2	severe acute respiratory syndrome coronavirus 2
SDS PAGE	sodium dodecyl sulfate–polyacrylamide gel electrophoresis
SUMO	Small ubiquitin-like modifier
TCEP	tris(2-carboxyethyl)phosphine
TEAB	Triethylamonium bicarbonate
TFA	trifluoroacetic acid
THF	tetrahydrofuran
TMS	tetramethylsilane
TMT	tandem mass tag
Tris	tris(hydroxymethyl)aminomethane
Ub	Ubiquitin
Ub-AMC	ubiquitin-aminomethylcoumarin
Ubl	ubiquitin-like protein
Ub-PA	ubiquitin propargylamine
Ub-Rho	ubiquitin-rhodamine110
Ub-VME	ubiquitin vinyl methyl ester
UCH	ubiquitin C-terminal hydroxylase
UCHL1	Ubiquitin C-Terminal Hydrolase L1

UPS	ubiquitin proteasome system
USP	ubiquitin specific protease
USP10	Ubiquitin Specific Protease 10
USP17	Ubiquitin Specific Protease 17
USP25	Ubiquitin Specific Protease 25
USP28	Ubiquitin Specific Protease 28
USP30	Ubiquitin Specific Protease 30
USP7	Ubiquitin Specific Protease 7
USP8	Ubiquitin Specific Protease 8
ZUP1	zinc finger-containing ubiquitin peptidase 1

Acknowledgements

I would like to thank my advisor, Dr. Sara Buhrlage, for her mentorship and support over the past several years. When I joined her lab, we hit the ground running with experiments and grant writing, and she was there to guide me every step of the way. Her mentorship during those early days boosted my confidence and set me up for success. I learned so much about drug discovery and about the importance of working as a team. I can confidently say that I have grown as a scientist during my time in her lab and I feel extremely well-prepared for my next steps in industry and beyond.

I would also like to thank all members of the Buhrlage lab, past and present, who have provided moral support and academic and scientific advice. I am biased, but I believe the folks in the Buhrlage lab are some of the friendliest people at Harvard. While every Buhrlage lab member had a positive impact on me, there are a handful of people that I would like to name and appreciate. I would like to thank Dr. Xiaoxi Liu, a talented chemist and scientist who was my go-to person when I needed help with troubleshooting reactions and planning experiments. I would like to thank Dr. Robert Magin for very patiently listening to me practice my qualifying exam talk and for always offering to proofread my writing. Dr. Mona Sharafi provided so much scientific guidance over the course of my PhD, and I am very grateful for her friendship and support. Dr. Wei Pin Teh is a talented chemist that I constantly relied on for help and advice. Dr. Yanran Liu worked tirelessly on the USP28 and USP4 projects with me and synthesized many compounds. Dr. Anthony Varca was always willing to help me with anything I needed in the lab, and he helped me improve the quality of my thesis presentation. I would also like to thank my fellow graduate students Alejandra Felix, Binita Shah, Isabella Jaen-Maisonet, and Nick Girardi for making life in the lab filled with laughter.

I would also like to thank the mentors that have guided me along my path from undergrad to today. During my first semester at the University of Maryland, Dr. Josh Singer gave me the chance to work in his lab and to learn more about scientific research. Josh supported my growth both in and

outside of the lab throughout my time UMD, and I am very grateful today that I get to call him a friend. Dr. Efrain Rodriguez heavily influenced my interest in chemistry, and he encouraged me to pursue graduate school. Efrain convinced me that yes, I was smart enough to cut it at a top PhD program. His encouragement meant the world to me. I would also like to thank Dr. Luke Lavis and Jon Grimm, MA at the Janelia Research Campus for hiring me on as a technician and for teaching me everything I know about organic chemistry. I had a blast learning from them, and it was a tough decision to leave them for graduate school.

I am grateful for the love and support of my family. To my mom and dad, thank you for encouraging my curiosity from a young age. To my little brother and sister, thanks for being great listeners and for always making life fun. I don't have the words to adequately express my gratitude. I am so glad that I get to share this journey with you all, and the fact that I have made it this far is a testament to how awesome you all are.

I am fortunate enough to have several close friends support me along the way. To Elfadil and Jonah, thanks for always being there to provide a space for me to unwind, relax, and laugh. To Vayu and Alan, my time in Boston would not be the same without your friendship. Harvard can be an intimidating, and your warmth showed me the importance of finding and building a community. To my dear friend, confidant, and roommate Fred, thank you for providing me a safe haven as I got the hang of living in Boston. Rarely a day goes by that I don't think of you, and I miss you dearly. I appreciate all of the wonderful times we spent together. To Nada, I am amazed by how quickly our friendship took off, and I am grateful that you were there with me during my last year at the DFCI.

To Isabella, I feel incredibly lucky to have shared the last five plus years with you. Graduate school has provided some of the most exciting, but also the most frustrating moments of my life so far, and you were there with me for all of it. Your love, support, and friendship mean everything to me, and I am so excited for this next step in our journey.

Chapter 1: Deubiquitinase background

1.1 Ubiquination and deubiquinating enzymes

The ubiquitin-proteasome system (UPS) is a highly regulated protein modification pathway where the covalent attachment of one or more ubiquitin proteins promotes proteolysis, or other non-proteolytic fates, of substrate proteins.[1] Three distinct enzymes, E1, E2, and E3 ligases are required to conjugate the C-terminus of ubiquitin to the target protein Lys or Thr residues or the amino terminus.[2] Ubiquitin is a small 76-amino acid protein encoded by four genes (UBC, UBB, UBA52, and UBA80).[3] Ubiquitin can be appended to a target protein in multiple configurations, resulting in a complex code through which cells interpret different functional outcomes.[4] For example, polyubiquitin chains can be linked via one of the seven ubiquitin-lys residues or via the ubiquitin-amino terminus.[4,5] Polyubiquitin chains comprised of linear of Lys-63 linkages promote protein complex formation, whereas Lys11-and Lys48-linked chains promote protein degradation.[4] To add further complexity, target proteins can also be marked with ubiquitin-like proteins (Ubls) such as a small ubiquitin-like modifier (SUMO), neuronal precursor cell-expressed developmentally downregulated protein 8 (NEDD8), and interferon stimulated gene 15 (ISG15) either as stand-alone PTMs or as hybrid chains that contain ubiquitin.[4,6]

While ubiquitination is most often studied in the context of protein degradation, it plays a role in important cellular processes including protein trafficking,[7] cell cycle progression,[8–10] DNA repair,[11] and transcription.[12] Improper function of the UPS has been linked to a number of human pathologies including neurodegeneration,[13–15] inflammation/immune response,[16,17] and cancer.[18,19, 20] Targeting protein degradation has recently emerged as a promising therapeutic strategy for several indications. Due to their central role in UPS regulation, DUBs are increasingly recognized as attractive targets for therapeutic intervention in these diseases. The clinical success of the proteasome inhibitor, Bortezomib, has validated the ubiquitin system as a target for cancer therapy and heightened the

interest in the space.[21] Multiple DUB targeting agents have recently entered clinical development, including small-molecule inhibitors of the DNA damage repair regulator ubiquitin-specific protease 1 (USP1).[22–24]

Deubiquinating enzymes (DUBs) are isopeptidases that oppose the activity of ligases and remove ubiquitin from target proteins (**Figure 1.1**). The removal of ubiquitin rescues target proteins from degradation on and maintains a constant level of cellular ubiquitin.[25] In humans, DUBs are classified into seven gene families based on sequence and structural similarities: ubiquitin-specific proteases (USPs), ovarian tumor proteases (OTU), ubiquitin C-terminal hydrolases (UCHs), Machado-Joseph disease protein proteases (MJD), the motif interactive with ubiquitin (MIU)-containing novel DUB family (MINDY), Zinc Finger ubiquitin-specific protease (ZUP/ZUFSP), and JAMM/MPN motif proteases[26–29] (**Figure 1.2**). The USP, OTU, UCH, MJD, MINDY, and ZUP families are all cysteine proteases, while the JAMMs are zinc-dependent metalloproteases. Cysteine proteases use catalytic diads or triads to catalyze the hydrolysis of amide bonds between ubiquitin and the substrate.[25] DUBs vary highly by molecular weight, and many DUBs contain multiple domains, in addition to their catalytic domains that serve as interaction scaffolds with other proteins. Despite extensive research into the basic function and disease relevance of the ubiquitin system, high quality chemical probes and clinical agents have been developed for only a small fraction of proteins that write (E1-E2-E3), read, and erase (DUB) ubiquitin PTMs.[30]

Ubiquitination controls a myriad of human physiology. Deregulation of these processes contributes to many diseases. Notable examples include: USP6, translocated in aneurysmal bone bone cysts;[31] USP7, mutated in neurological disorders;[32] USP8 mutated in Cushing disease;[33,34] USP9X, whose mutations cause developmental disorders;[35] and USP15 is amplified in certain ovarian, breast, and glioblastoma cancers.[36] Moreover, DUBs play a known role in driving infectious diseases.

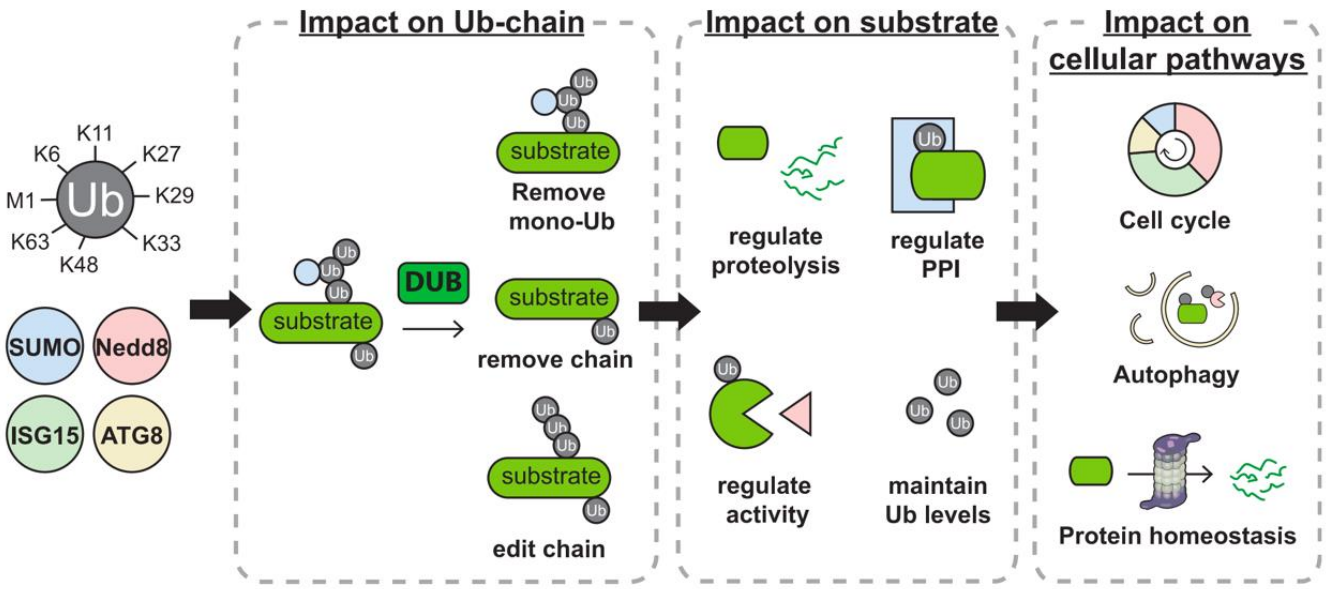


Figure 1.1 Role of deubiquitinating enzymes in the ubiquitin proteosome system.
Overview of DUB function.[37] Cells use ubiquitin as a multi-purpose signaling molecule. Ubiquitin proteasome system carefully controls protein degradation, a process that cells use to remove proteins that are no longer functional or whose function are no longer needed. A failure to degrade proteins results in the accumulation of toxic proteins, leading to many human diseases. The UPS uses ubiquitin as a signal for protein degradation: any protein labeled with the appropriate Ub mark are directed towards a degradation pathway. Deubiquinating enzymes play a critical role in regulating protein degradation pathways: they survey the ubiquinated proteome and remove ubiquitin marks stabilizing the protein and prolonging the protein's cellular life. Inactivation of DUBs causes specific proteins to undergo accelerated degradation and could offer a new avenue for the development of drugs leading to targeted degradation.

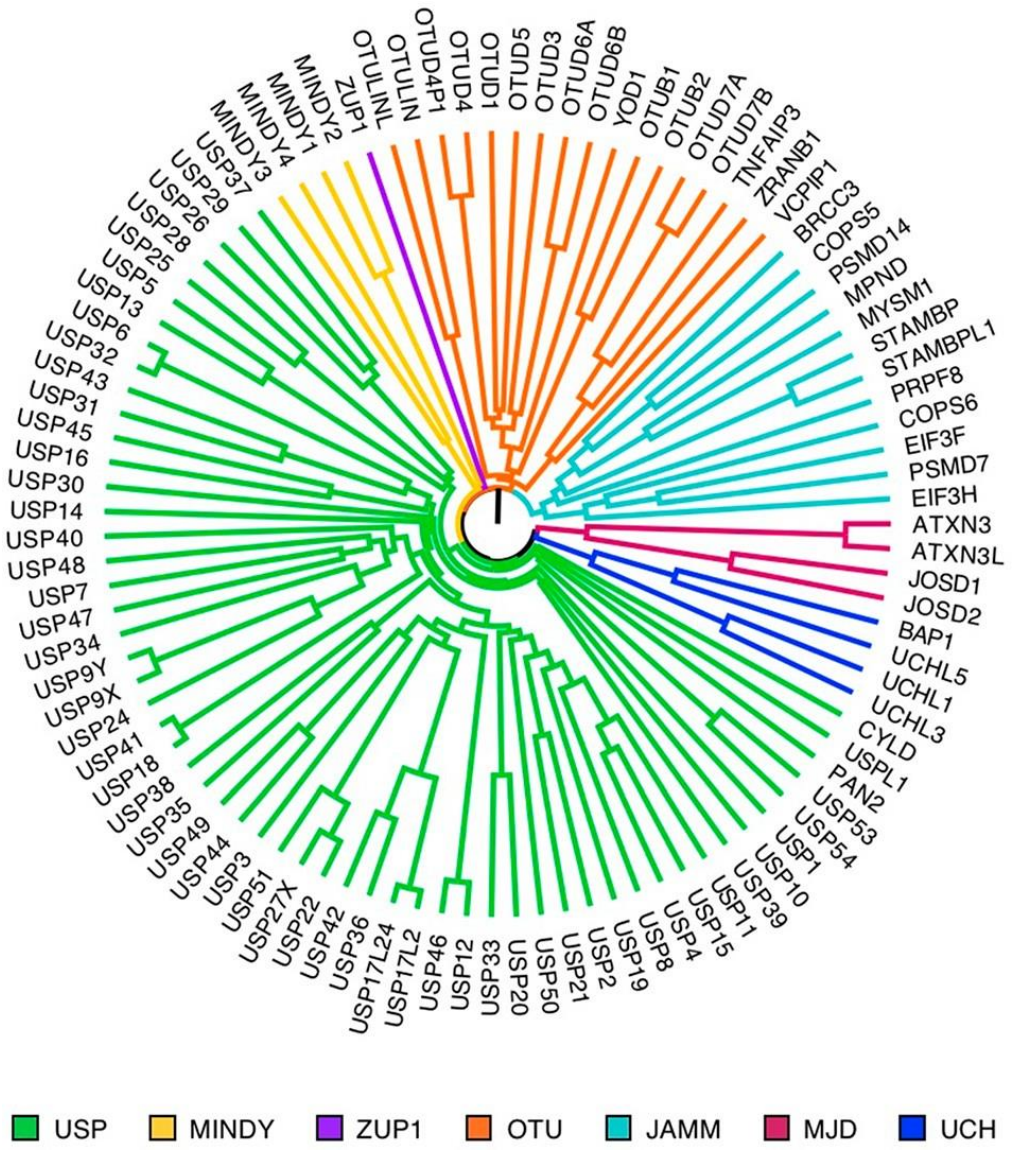


Figure 1.2. DUB family tree

DUB phylogenetic tree.[30] There are approximately 100 identified human DUBs, which cluster by the sequence similarity of their catalytic domains into seven families: ubiquitin-specific proteases (USP), ubiquitin C-terminal hydroxylases (UCH), Machado−Josephin domain proteases (MJD), Jab1/Mov34/Mpr1 Pad1 N-terminal+ proteases (JAMM), ovarian tumor proteases (OTU), and zinc finger containing ubiquitin peptidase 1 (ZUP1).

Pathogenic viruses use DUBs for replication and for diminishing the host immune response. For example, the severe acute respiratory syndrome coronavirus 2 (SARS-CoV-2) virus expresses the DUB papain-like protease (PLpro). PLpro has deubiqutinating activity, and can remove polyUb chains from host immune proteins, dysregulating the host immune defense mechanisms against the virus.[38] DUBs have also been shown to act on substrate proteins that are themselves drivers of disease. Thus, inhibiting DUBs offers the possibility of specifically degrading toxic proteins by ensuring ubiquitin mediated degradation by the proteasome. Some of these toxic proteins lack well-defined, druggable pockets. Notable examples include the transcription factors Myc and HIF1alpha.[39,40] USP8 has been shown to specifically deubiquitinate mutant EGFR, a well-known driver of drug resistant non-small cell lung cancer (NSCLC).[41] Despite the therapeutic potential of DUB inhibition, there is a lack of rigorously validated probe compounds for DUBs and no approved DUB targeting DUBs in the clinic.

1.2 Challenges with identifying DUB inhibitors

Despite the attractiveness of DUBs as drug targets, identifying bonafide DUB probes has been challenging, and researchers face several obstacles in the field. First, while DUB catalytic pockets are attractive starting points for the development of inhibitors, these pockets share a high degree of structural homology, making it challenging for chemists to optimize for selectivity within DUB families. Second, because most DUBs are cysteine proteases and rely on a reactive thiol group to catalyze the removal of ubiquitin molecules, most standard assays used to identify inhibitors are prone to non-selective redox false positives.[42] Third, DUBs alternate between active and non-active confirmations, making it challenging to design predictive biochemical assays. [43,44] Despite these challenges, the past few years has seen an increase in the rate of successful DUB inhibitor discovery campaigns. For example, multiple groups (including our own) converged on a series of compounds

which showed nanomolar potency and excellent selectivity for the DUB USP7.[45–50] Interest in USP7 was in part motivated by its role in deubiquinating and stabilizing the tumor supressor p53. While the work on USP7 shows that DUBs are amenable to inhibition, there are very few quality compounds beyond the reported USP7 inhibitors. Dr. Ritorto and coworkers used a matrix-assisted laser desorption/ionization time of flight (MALDI-TOFF) spectroscopy technique to screen a panel of 32 DUBs against 9 reported DUB inhibitors.[51] None of the compounds showed strong selectivity and many inhibited most of the DUBs on the panel. The result of this study highlights the need for the development of strategies for identifying high-quality probes with good potency and selectivity.

In this work, I embarked on a campaign to develop reversible small molecules that target recently described non-catalytic DUB pockets. Using our established suite of DUB assays and computational docking studies, I credentialed three chemotypes as leads for a noncovalent library targeting non-catalytic pockets conserved across many DUBs. I identified analogs from these chemotypes that inhibit DUBs that are relevant for cancer therapy. I leveraged the structural diversity represented in these pockets to optimize for selectivity. This work resulted in the generation of a chemical library that will accelerate the development of validated probes for therapeutically relevant DUB targets and enable mechanistic studies to understand the function of DUBs in cancer.

Chapter 2: Identification and validation of leads for USP8 inhibitors

2.1 Introduction

To identify high-quality lead compounds for DUB targeting agents, we executed a high throughput screen (HTS) placing a high priority on identifying selective hit scaffolds. We screened a diverse small molecule library against eight DUBs: USP7, 8, 10, 17, 28, 30, UCHL1, and OTUD3. This effort was part of a collaboration between our group and the Novartis Institutes for Biomedical Research's (NIBR) FAST Lab Program, which gives academic labs access to a nonproprietary compound collection assembled at NIBR. To read out inhibitory activity, the screening assay relied on a ubiquitin-rhodamine110 (Ub-Rho) substrate which consists of a rhodamine conjugated to the C-terminus of ubiquitin. This allows for the monitoring of the increase in fluorescence over time as active DUB cleaves the fluorogenic rhodamine off the ubiquitin. DUBs were included in the screen based on their association with interesting biology and/or the availability of well-validated chemical probes. The compound library was designed to contain compounds with good drug-like properties. Each compound was screened at a single high concentration of 25 or 50 μM. To confirm active hit compounds and provide early evidence of selectivity, we screened each hit against its target plus 1-3 additional DUBs in 8-point dose response in triplicate. Hits were further validated through a series of counter screens and orthogonal assays, which resulted in selective inhibitors of USP25, USP28, and USP30. A subset of these compounds was derived from the same core scaffold as other selective DUB inhibitors (see Chapters 2 and 3 . Full results for this were recently disclosed in a manuscript published by Dr. Anthony Varca and coworkers.[52] Following the HTS, I focused on the identification and validation of hit compounds for USP8. Efforts were placed on USP8 given its interesting biology and potential role in a stabilizing mutant EGFR.

USP8, also known as UBPY, is involved in the growth and regulation of various cancer cells.[53] Leeuween and coworkers reported that USP8 negatively regulates the ubiquination and lysosomal degradation of epidermal growth factor receptor (EGFR).[41] USP8 KO mice show embryonic lethality

due to significant growth retardation associated with the reduction of receptor tyrosine kinases such as ERBB2, ERBB3, EGFR, and c-MET. [54] Other studies have suggested that the

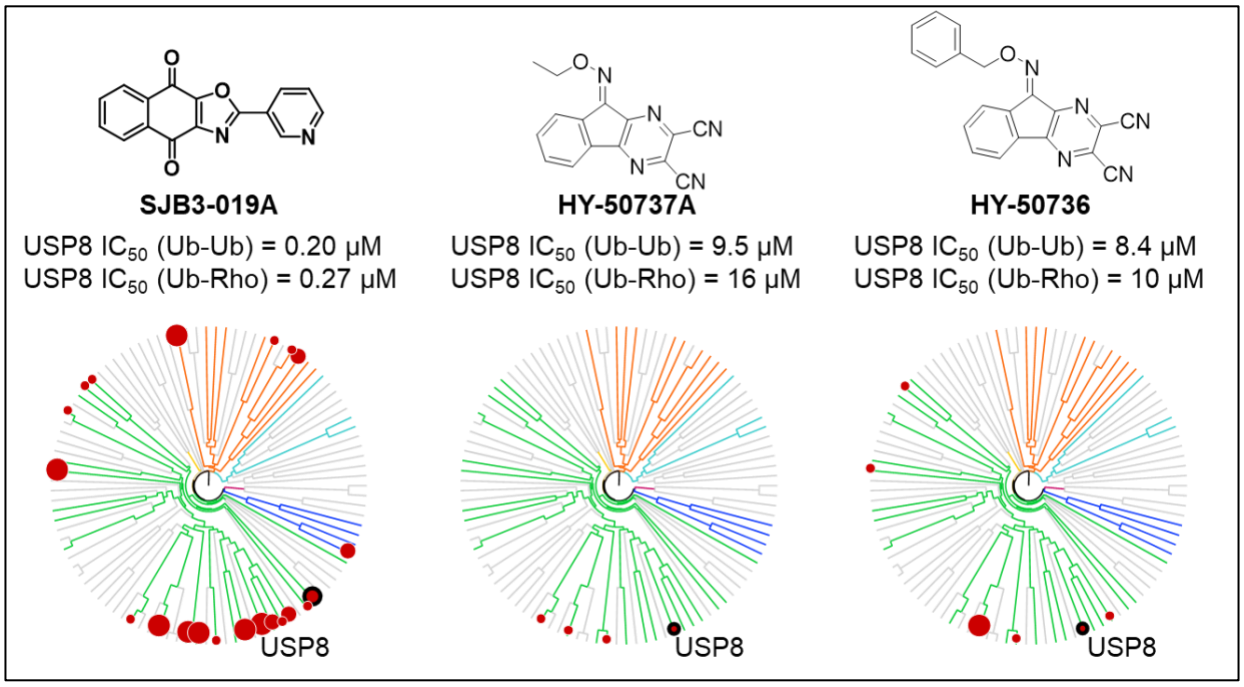


Figure 2.1. IC_{50} values and selectivity profiles of USP8 inhibitors. Each line in the selectivity tree represents an individual DUB and red dots indicated inhibitors activity against the dub. The larger the red circle, the more potent the inhibition.

depletion of USP8 leads to the suppression of STAM, HRS, RNF41, and Parkin, which lead to cell death.[55,18,19] Elevated expression of USP8 correlates with a poor prognosis in various cancers, suggesting that USP8 might be oncogenic and a potential target for cancer therapy.[54,58] The EGFR-TKIs gefitinib and erlotinib are frontline therapies for patients with NSCLCs.[53] However, despite initial positive responses to these inhibitors, treatment invariably leads to the emergence of drug resistance. Mechanisms of resistance include gatekeeper mutations in EGFR, and the activation of bypass survival signals via MET and ERBB3 receptors.[59–61] To overcome acquired resistance to EGFR-TKIs, conventional approaches have relied on developing second, third, and fourth- generation inhibitors to suppress the activity of mutant EGFR.

In 2013, Dr. Dong and coworkers reported that USP8 suppression, either by siRNA or inhibition by the small-molecule inhibitor HY50737A, lead to downregulation of EGFR and death of gefitinib-resistant NSCLC cells *in vitro* and *in vivo*.[54] These findings highlight the potential of USP8 inhibition as a means of overcoming drug resistance in EGFR-mutant driven NSCLC. Working with Dr. Pasi Janne, a physician scientist at Dana Farber and expert in NSCLC, we independently confirmed these results. Using HY50737A, analogs HY5037, HY50736, and a chemically distinct inhibitor SJB3-019A (**Figure 2.1**), we showed that USP8 inhibition suppressed growth of PC9 and HCC827 cells, which both harbor EGFR exon 19 deletion activating mutations. The compounds also showed similar levels of activity against the gefitinib-resistant cell lines PC9-GR (which harbors an EGFR T790M mutation), and HCC826 cells (which harbors a Met amplification) (**Figure 2.2a**). Follow-up Western blot analysis confirmed that treatment of EGFR mutant cells, those both sensitive and resistant to kinase inhibition, with either USP8 inhibitor led to downregulation of EGFR with specificity for the kinase over other key signaling molecules (**Figure 2.2b**).

Treatment with either scaffold led to increased ubiquitination of EGFR, which confirmed that EGFR reduction occurred via an ubiquitin-mediated degradation (**Figure 2.2c**). In agreement with cell-line data, we showed that primary cell tumors from a gefitinib resistant patient are sensitive to USP8 inhibitors HY50737A and SJB-019A (**Figure 2.2d**). The HY50737A and SJB3-019A compounds have been instrumental in preliminary studies of USP8 biology, but USP8 inhibitors with better potency, selectivity, and drug-likeness are required to rigorously investigate the detailed mechanisms by which USP8 contributes to disease. As shown in **Figure 2.1** SJB3-019A is a potent USP8 inhibitor but displays moderate selectivity, while HY50737A and HY50736 are weak inhibitors that display decent selectivity. To facilitate the development of highly potent and selective USP8 inhibitors, we executed a high throughput screening campaign to identify novel chemical leads for the enzyme.

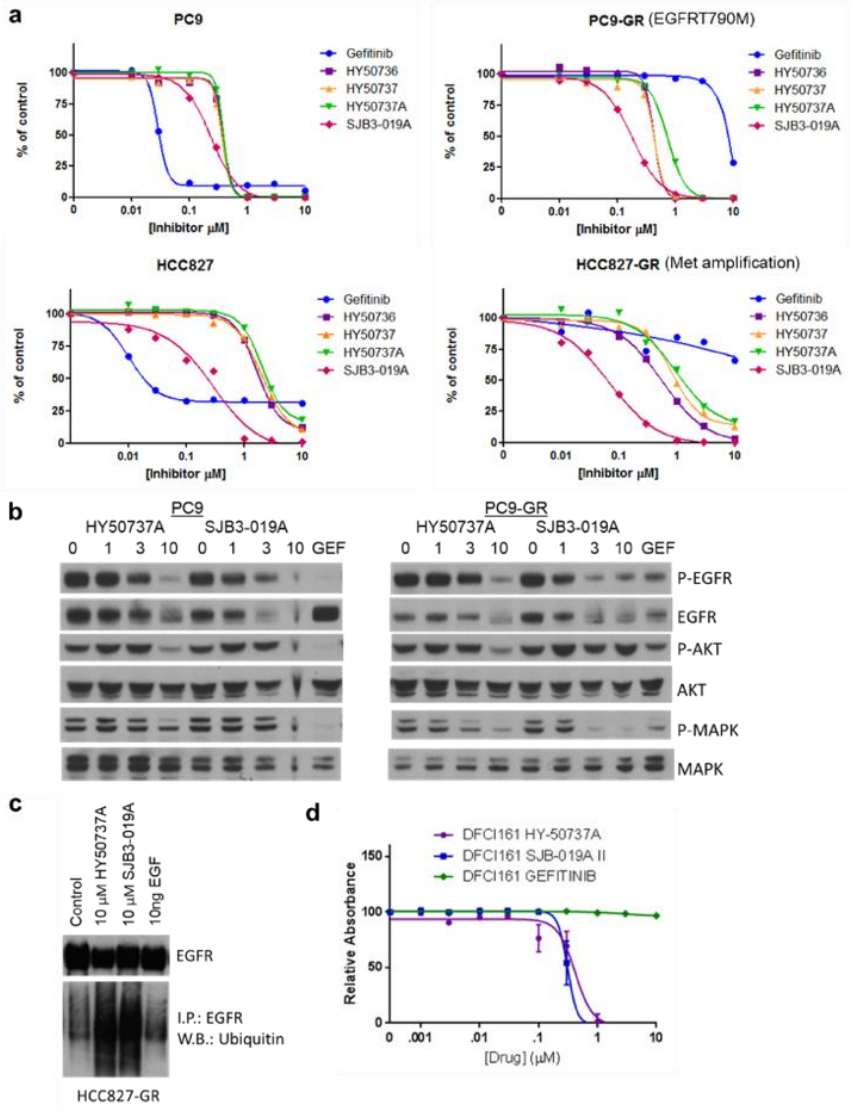


Figure 2.2. Studies on USP8 biology with early-generation USP8 inhibitors. a) Antiproliferative curves for USP8 inhibitors and gefitinib against gefitinib sensitive and resistant EGFR mutant cell lines. b) USP8 inhibitors reduce total levels of EGFR protein. c) USP8 inhibitors lead to increased ubiquitination of EGFR. d) USP8 inhibitors suppress growth of NSCLC cells that are resistant to kinase inhibition by gefitinib.

2.2 Results

2.2.1 USP8 confirmatory biochemistry with XL-9872-040

We identified 14 promising active USP8 compounds that inhibited USP8 with an IC_{50} of less than 20 μM and maximal inhibition greater than 30% while exhibiting little to no inhibition of the other DUBs tested (IC_{50} > 50 μM). All 14 compounds were resynthesized in-house and evaluated for their activity using the same assay as employed in the screen. Ten of the compounds inhibited USP8 with an IC_{50} less than 20 μM and maximal inhibition of > 90%. Given that the high-throughput screen utilized USP8 catalytic domain (residues 777-1109), we tested compounds for enzymatic inhibition of full-length USP8. Nine of the ten compounds exhibited equipotent inhibition of full-length enzyme. Based on a combination of potency, selectivity, and synthetic accessibility, I chose the quinoxalinone containing compound, XL-9872-040, and as a lead for follow up SAR studies (**Figure 2.3**). The quinoxalinone core structure is well represented in a number of molecules in clinical trials including the anxiolytic agent Panadiplon ($GABA_A$ partial agonist) [62,63] and the neuroprotective agent YM872 (AMPA antagonist).[64]

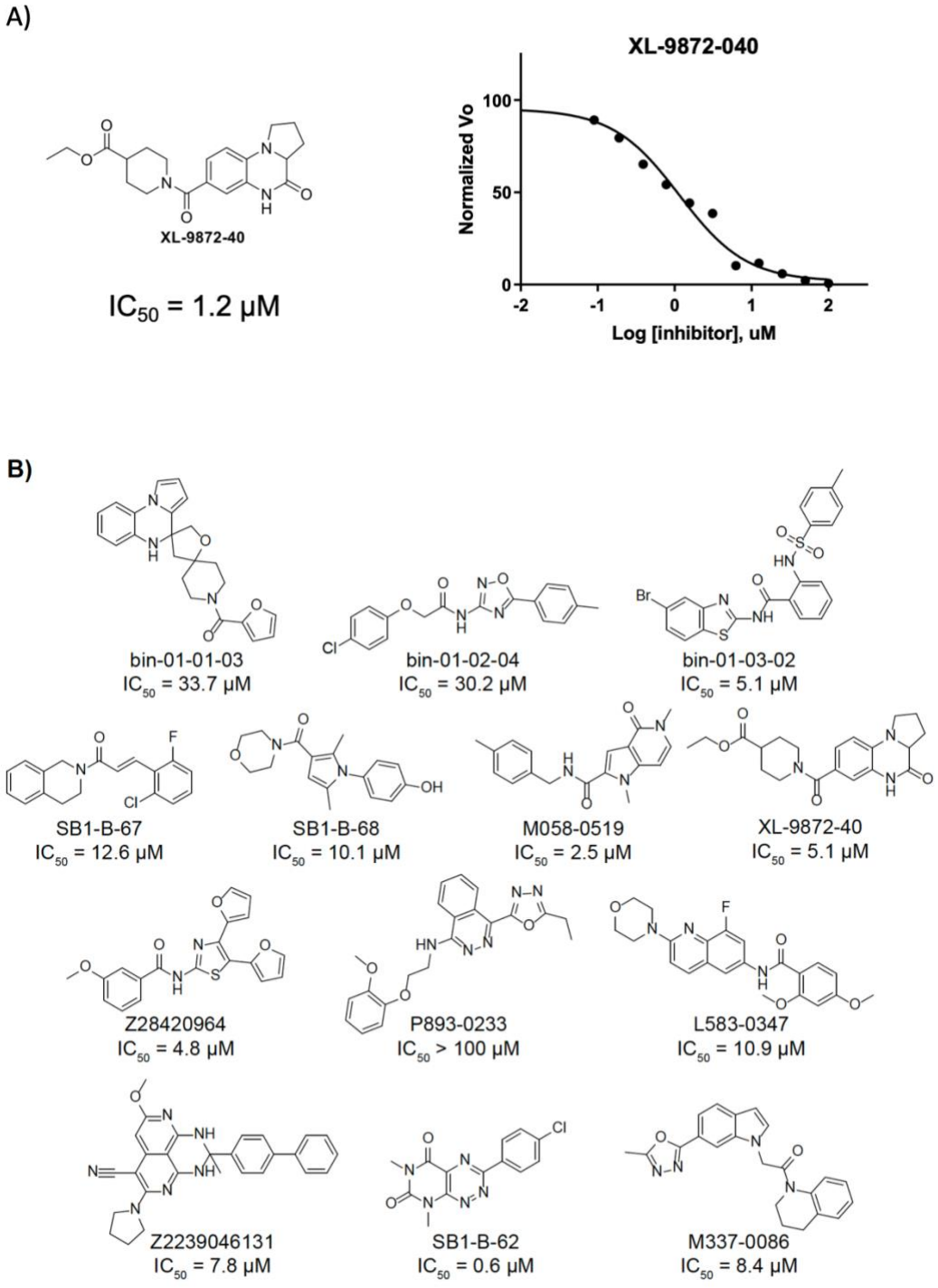


Figure 2.3. USP8 screening hits from the Novartis library

A) Structure and dose response curve of USP8 quinoxalinone hit, XL-9872-040, against USP8.

B) Structure of other USP8 inhibitors from the screening data. Compoundswere profiled in dose-response against USP8 and IC_{50}s are reported. Data shown represent $n \geq 1$.

2.2.2 Orthogonal validation of XL-9872-040 by target engagement

To instill confidence in XL-9872-040's activity, additional experimental validation was carried out to confirm the biochemistry results. XL-9872-040 was tested in a cell lysate-based target engagement experiment. For this experiment, XL-9872-040 was incubated in dose-response in HEK293T cellular lysate for 10 minutes followed by treatment with a 1:1 mixture of Ub-PA/Ub-VME. The samples are then read out by western blot for a specific DUB of interest using a DUBspecific antibody (in this case USP8).

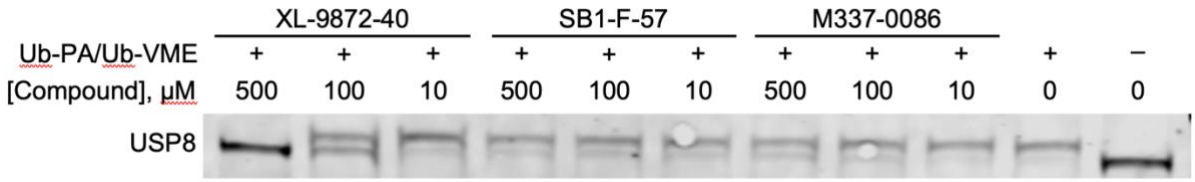


Figure 2.4. USP8 target engagement
Target engagement of select USP8 compounds in HEK293 cell lysate in dose response. XL-9872-040 is able to compete with the ubiquitin probe at 100 µM.
Compound binding prevents probe labeling resulting in the presence of a band on the blot corresponding to the native USP8. If the compound does not engage with the protein, the probe will bind to the DUB resulting in a higher molecular weight adduct, which can be observed as a band above the native protein band. **Figure 2.4** above shows the results of the USP8 target engagement with XL-040 along with other USP8 hits which showed weaker target engagement. A no probe control and DMSO control show the two distinct species of USP8 (native and DUB bound). Cell lysate samples were treated with three concentrations of compound (10 µM, 100 µM, and 500 µM). XL-9872-040 demonstrated dose-dependent effect in blocking probe labeling with full blockage at 500 µM, 50% blockage at 100 µM, and no blockage at 10 µM. These results confirm that XL-9872-040 binds to USP8 and prevents labeling by the covalent ubiquitin probe.

2.2.4 XL-9872-040 structure activity relationship (SAR) data

Based on the results from the Novartis screen, confirmatory follow-up Ub-rho experiments, and validation with the target engagement experiment, XL-9872-040 emerged as a clear choice for medicinal chemistry follow up. XL-9872-040's validated well upon resynthesis and the core scaffold is amenable to chemical derivatization toward the goal of further improving compound potency and understanding structure activity relationships. Additionally, XL-9872-040 exhibited no significant redox activity or other compound artifacts (such as autofluorescence or fluorescence quenching). The scaffold also showed good selectivity for USP8 in broader selectivity Ubiquigent profiling experiments. Toward the goal of improving compound potency to create better USP8 probes as well as better understanding the components of XL-9872-040 important for activity, derivatives for XL-9872-040 were synthesized following synthetic protocols established in house. Based on the synthetic routes, points of derivatization were identified and changes to these regions were made to assess the importance of each region of the molecule on measured activity. Following the synthesis of each derivative, compounds were tested in dose-response in a ubiquitin-rhodamine assay to determine IC_{50} values. Through multiple rounds of synthesis and biochemical assay screening, I assessed various positions on the scaffold to generate SAR and provide insight into compound activity. The full medicinal chemistry efforts and SAR trends for XL-9872-040 are reported below.

The XL-9872-040 scaffold contains a quinoxalinone core consisting of a phenyl ring fused to a piperazin-2-one with additional substituents installed at various positions. Further interrogation of the scaffold was performed, and multiple derivatives were synthesized to assess each region on the molecule. Based on the previously established synthetic route, the core intermediate for XL-9872-040 contains a fluoro leaving group positioned ortho to a nitro group on the phenyl ring that can be replaced with various amines. I leveraged this chemistry to replace the five-membered pyrrolidine ring present on XL-9872-040 with various saturated and aromatic cyclic moieties to establish if groups of differing size and electronic properties were preferred for binding (**Table 1.1**). Initially, I

focused on changing the size of the 5-membered pyrrolidine ring on the upper right-hand side of the hit compound. I introduced an azetidine (AXA-01-151), which resulted in a large reduction in potency. I tried to further reduce the size of the ring to a cyclopropane, however the final cyclization step did not afford the desired product. A close look at the H-NMR of this product indicated the formation of a hydroxyquinoxaline with an ethyl group at the 2-position, at a yield of 90%. In follow-up Ub-Rho experiments, this compound was inactve against USP8CD. This taught us that opening the ring at this position is not favored. Additionally, introducing saturated cyclic groups at that position also introduces unfavorable strain to the system, leading to challenges with chemical stability, purification, and storage. These observations were further confirmed with the synthesis of AXA-02-007, which features two methyl groups in place of the pyrrolidine ring. While this analog was chemically stable, opening the ring led to a complete loss in potency. The analogs AXA-01-203 (which features a hydroxy group at the 5-position of the pyrrolidine) and AXA-02-003 (which features a cyclopropane at the 5-position of the pyrrolidine) exhibited moderately improved stability, but weaker potency values. AXA-01-203 and AXA-02-003 were highly sensitive to acid and could only be purified in non-TFA conditions.

One of the major degradation products of XL-9872-040 features a double bond in the pyrrolidine ring. We hypothesized that the tricyclic ring system is highly strained, electronically unfavorable, and prefers to aromatize. To support this view, we made the analog AV-51, which has a fully aromatic pyrrole ring in place of the pyrrolidine. This compound was chemically stable compared to the parent, but it was inactive against USP8CD. Given this finding, it is likely that the binding pocket on USP8 prefers more flexible saturated groups over planar and aromatic groups. To follow up on this observation, I made the analogs AXA-01-117 and AXA-01-103. With AXA-01-117, I installed a S-methyl at the 3a-position of the core. AXA-01-103 was the enantiomer with a R-methyl at the same position. Interestingly, this quaternary substitution stabilized the compound. AXA-01-117 was

roughly equipotent to the parent compound, while AXA-01-103 was about 4-5x weaker, showing that the one enantiomer is preferred over the other. An ethyl group at this position (AXA-01-145) was also well tolerated (roughly equipotent to XL-9872-040) and chemically stable. Increasing the size of the group all the way up to a phenyl (AXA-02-197) penalized us on potency (IC_{50} = 50μM), but this substitution also had the effect of stabilizing the compound.

Table 2.1. SAR studies of XL-9872-040 series analogs focused on the pyrrole region. Table showing compound ID, structure, and IC_{50} determined in the Ub-Rho assay. This set focused on derivatizing at the pyrrole position.

Table 2.1 (Continued)

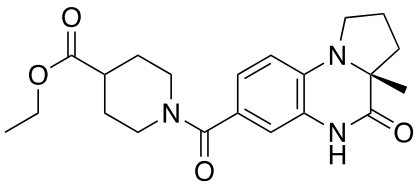
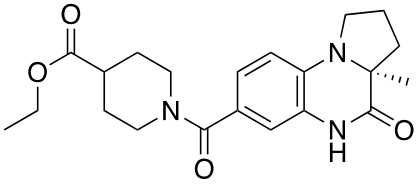
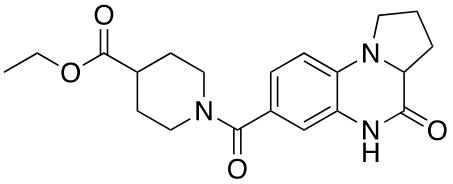
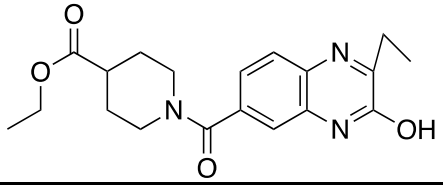
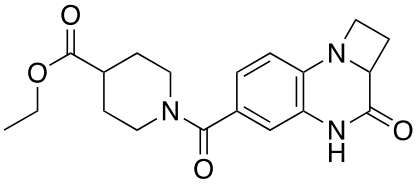
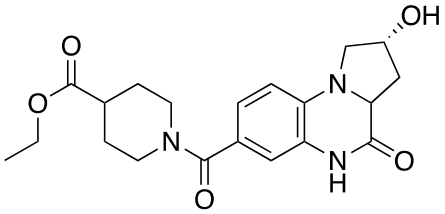
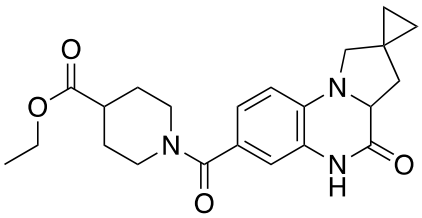
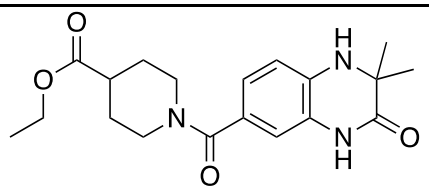
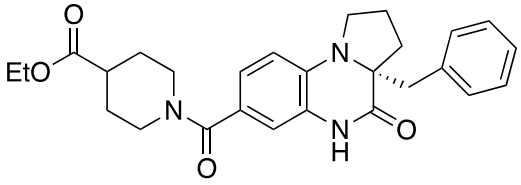
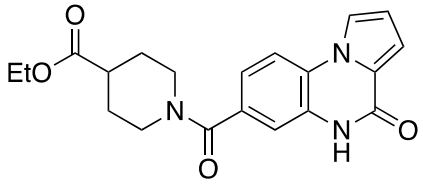
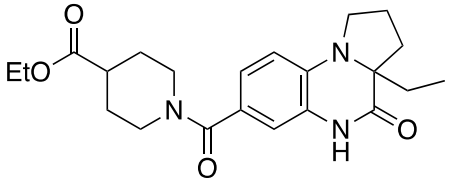
Compound	Structure	IC50 (μM)
AXA-01-103		88
AXA-01-117		4
XL-9872-040		5
AXA-01-157		> 100
AXA-01-189		56
AXA-01-203		> 100
AXA-02-003		23

Table 2.1 (continued)

AXA-02-007		> 100
AXA-02-197		50
AV-51		> 100
AXA-02-145		5

2.2.5 Ubiquigent Selectivity Profiling for select XL-9872-040 analogs

AXA-01-117 and AXA-02-197 showed improved stability over the parent compound, but lower overall potency against USP8, as measured by Ub-rho. However, we wanted to understand how these modifications to the core scaffold impacted selectivity. AXA-01-117 and AXA-02-197 were submitted to Ubiquigent to determine their selectivity against a larger DUB panel (**Figure 2.5)**. Ubiquigent's DUBprofiler platform is a commercially available service for assaying DUB inhibitors against a panel of 41 purified DUBs. Compounds are assayed at a single concentration against each DUB using a ubiquitin-rhodamine assay with conditions optimized for each DUB. The percent activity remaining following compound treatment is reported for each compound against each DUB

in the panel. The readout consists of a heatmap, where the intensity of color corresponds to the percent inhibition of that DUB. AXA-01-117 and AXA-02-197 both show on-target activity, and little inhibition of other DUBs. These compounds represent an excellent starting point for the further development of potent and specific USP8 inhibitors.

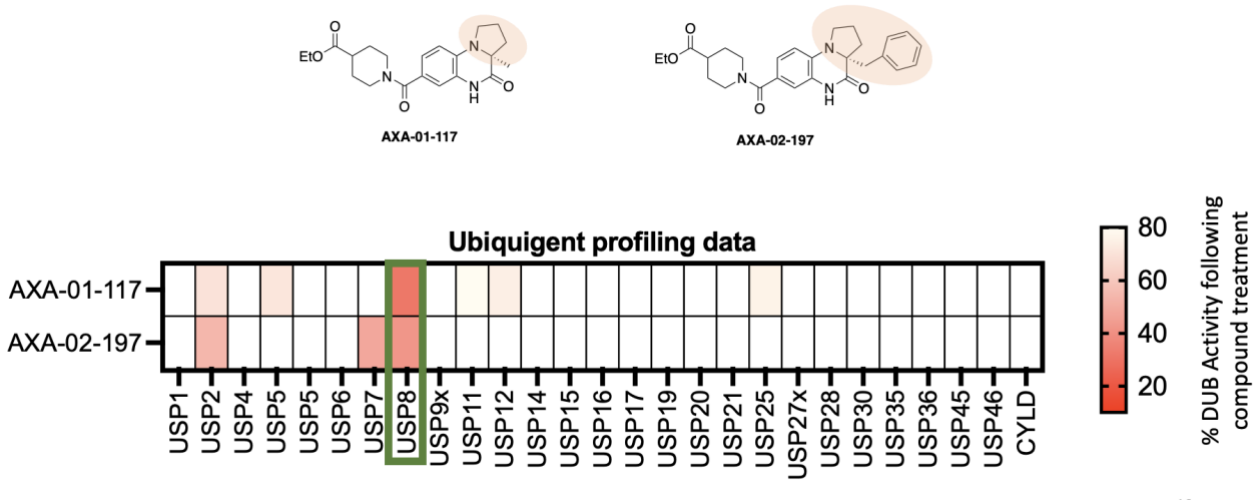


Figure 2.5. Ubiquigent profiling of select XL-9872-040 analogs. Introducing a quaternary methyl (as in AXA-01-117) or a quaternary phenyl (as in AXA-02-197) at the 4a position of the scaffold solved the chemical instability of this series and maintained good selectivity for USP8.

AXA-01-117 was the most stable and active analog that came out of our first round of chemistry. For the next round of SAR, I focused on making changes to the piperidine ring on the left-hand side XL-9872-040. I successfully completed a large-scale prep of the carboxylic acid intermediate AXA-02-149, which provided a convenient handle to introduce various amines. Our goal was to introduce a diversity of small alkyl groups, saturated rings, and solubilizing groups to determine the optimal hydrophobic and electrostatic interactions with USP8. In comparison to an ether, an amide moiety has more favorable drug like properties. The analog AXA-02-151, which has an ethyl amine in place of an ethyl ester, is equipotent to the parent compound showing that amides are well-tolerated at this position. We learned that the amide engages in important hydrogen bonding interactions, since introducing a dimethyl amine (AXA-02-203) lead to a significant decrease in potency. Changing the

ethyl group for an isopropyl (AXA-02-153) was not well-tolerated and resulted in an ~8-fold decrease in IC_{50}. Interestingly, installation of a terminal $-CF_3$ functionality moderately improved the IC_{50} suggesting that there might be an opportunity to introduce advantageous halide interactions. As we made more analogs, we observed a trend in size tolerance. Generally, as the bulk of the substituent increased, the potency was penalized. An isopropyl group (AXA-02-159) was weak (double digit micromolar) but still active. A slightly larger cyclohexyl group (AXA-02-157) was weaker still. Changing the cyclohexyl to a phenyl (AXA-02-167) did not similarly alter the IC_{50} value. Substituting the phenyl ring for a quinoline (AXA-02-175) ablated the compound's activity. Similarly, the analogs AXA-02-161 and AXA-0-163, which carry an ethyl morpholine and an ethyl piperazine respectively, were also inactive. Interestingly, we observed that a thiazole analog, AXA-02-171, inhibited USP8CD with an IC_{50} of 13 μM. A full summary of these efforts are summarized in SAR **Table 2.2**

Table 2.2. SAR studies of XL-9872-040 series analogs focused on the amide region. Table showing compound ID, structure, and IC_{50} determined in the USP8CD ub-rho assay. This set focused on derivatizing at the amide position.

Table 2.2 (Continued)

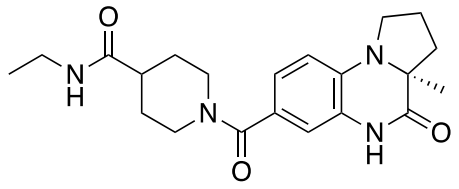
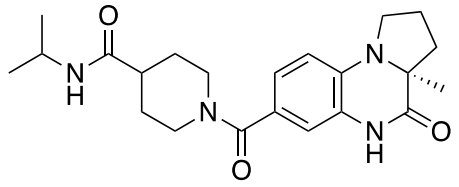
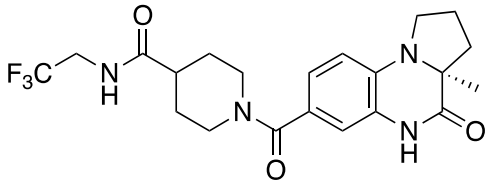
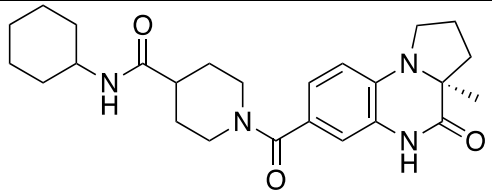
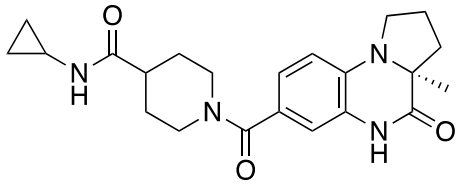
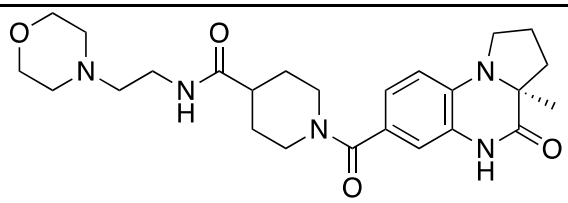
Compound	Structure	IC50 (μM)
AXA-02-151		5
AXA-02-153		48
AXA-02-155		2
AXA-02-157		30
AXA-02-159		20
AXA-02-161		> 100

Table 2.2 (Continued)

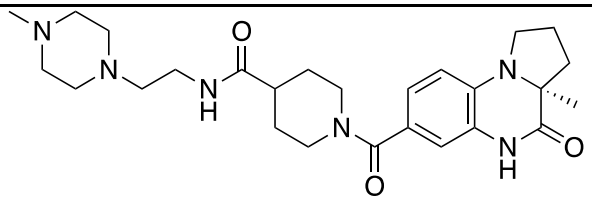
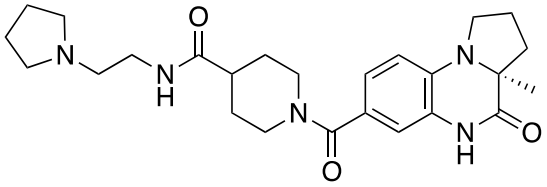
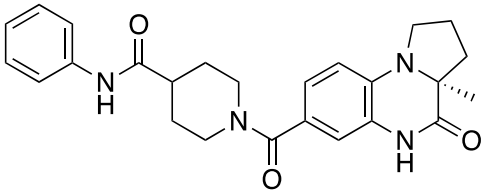
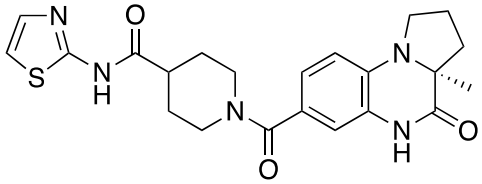
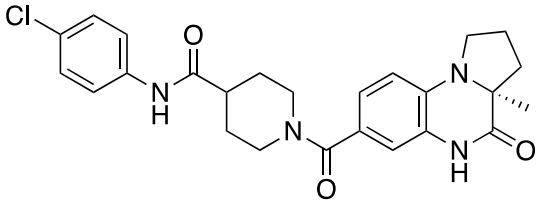
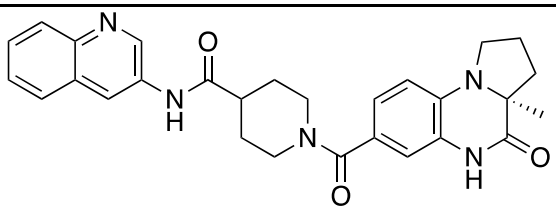
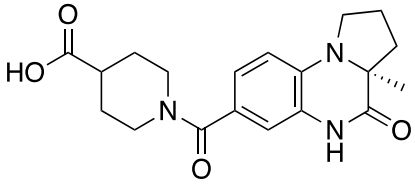
AXA-02-163		> 100
AXA-02-165		> 100
AXA-02-167		18
AXA-02-171		13
AXA-02-173		34
AXA-02-175		> 100
AXA-02-149		7

Table 2.2 (Continued)

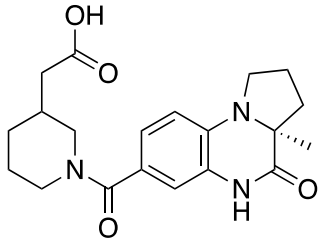
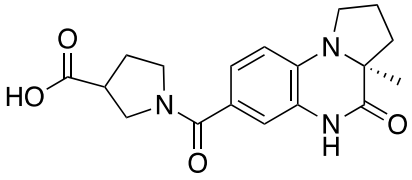
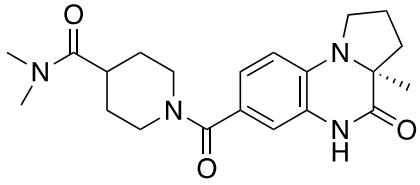
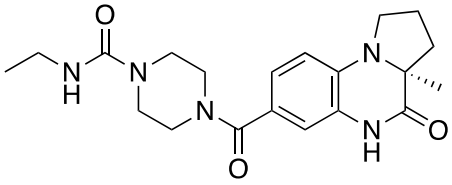
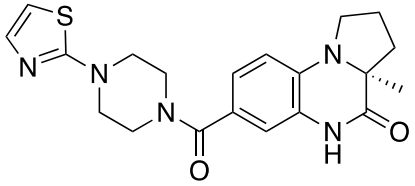
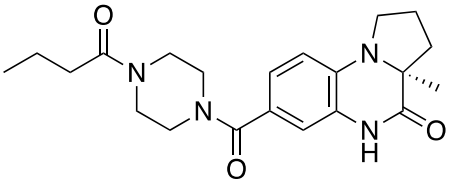
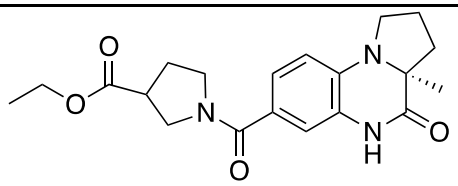
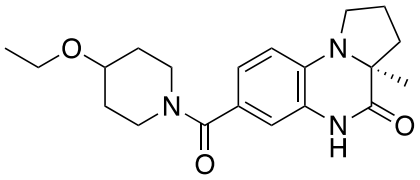
AXA-03-001		> 100
AXA-03-013		> 100
AXA-02-203		> 100
AXA-03-023		N/A
AXA-03-025		N/A
AXA-03-035		N/A

Table 2.2 (Continued)

AXA-03-031		N/A
AXA-03-029		N/A

2.2.6 USP8 confirmatory biochemistry with SB1-B-68

Parallel to my efforts on XL-9872-040, I revisited the results of the Novartis HTS to identify additional scaffolds as leads for optimization against USP8. The dimethyl pyrrole, SB1-B-68, was identified as a selective hit for USP8 with a single digit micro-molar potency of 4.2 μM (**Figure 2.6**). A close analog of SB1-B-68, IU1, was reported by Dr. Randall King's and Dr. Daniel Finley's groups at Harvard Medical School as 12.25 μM inhibitor of USP14.[65] I subsequently used the IU1:USP14 co-crystal structure to guide my own SAR efforts around SB1-B-68, the results of which are discussed later in this chapter.

I resynthesized SB1-B-68 and submitted the compound to Ubiquigent for selectivity profiling against a panel of 40 DUBs. While the compound is a weak hit, it shows good selectivity for USP8. To provide further confirmation of the SB1-B-68's activity, I tested the compound against full-length USP8 and USP8 catalytic domain, where it showed IC_{50} values of 4.2 µM and 2.1 µM, respectively.

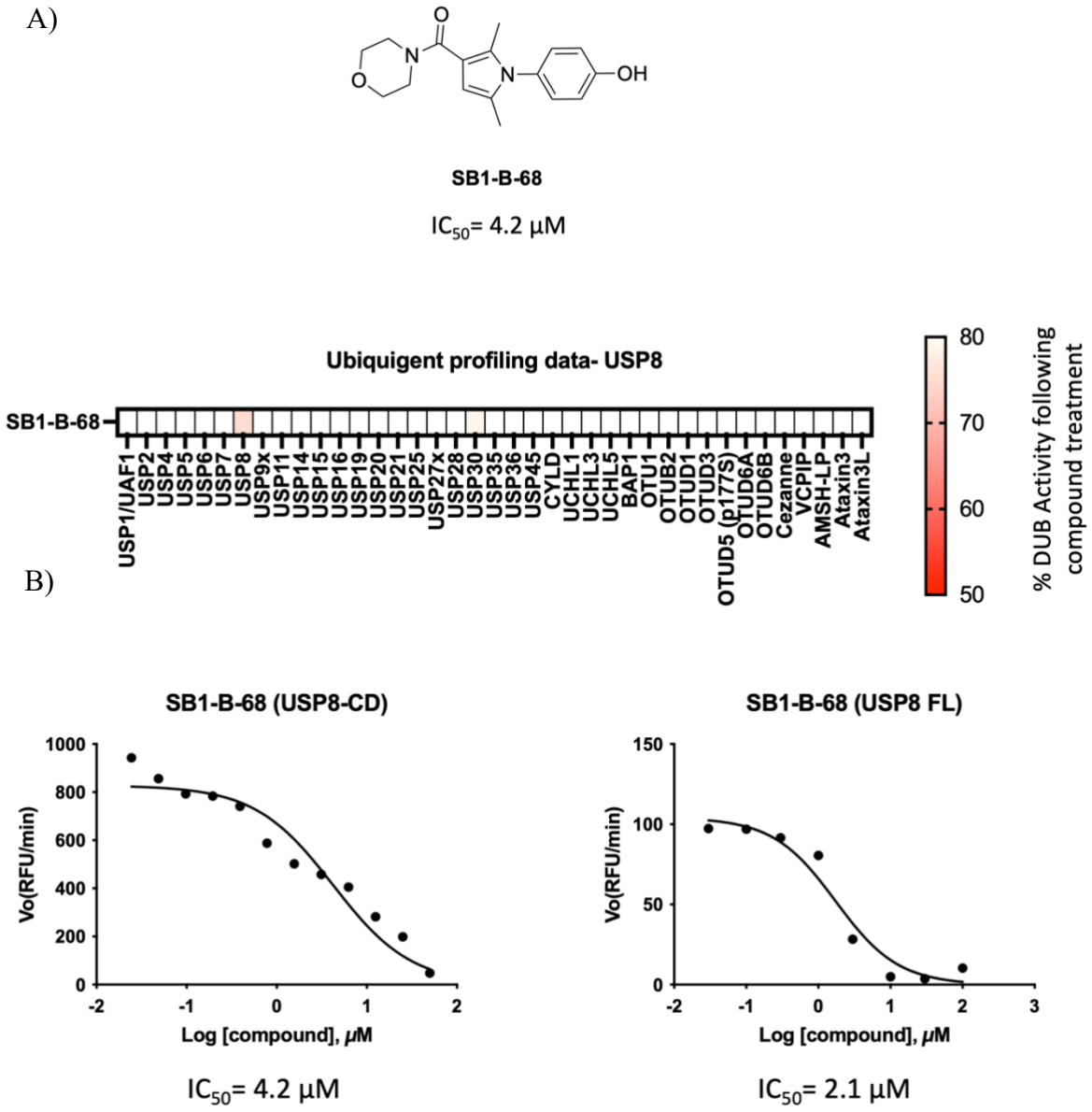


Figure 2.6. Validation of SB1-B-58 with biochemistry and Ubiquigent profiling.
A) SB1-B-68 is selective for USP8 in a panel of 41 DUBs.
B) SB1-B-68 inhibits both USP8 CD and FL USP8.

2.2.7 Orthogonal validation of SB1-B-68 by Microscale Thermophoresis (MST)

To instill confidence that SB1-B-68 is a bonafide inhibitor of USP8, I carried out MST experiments under the guidance of Dr. Kelly Arnett at the Center for Macromolecular Interactions at Harvard Medical School. The MST instrument detects the motion of fluorescent molecules along a microscopic temperature gradient, which reflects changes in the molecular hydration shell, charge, or size. Since one or all these parameters will change with virtually every binding event, a wide range of biomolecules can be measured, from ions and small

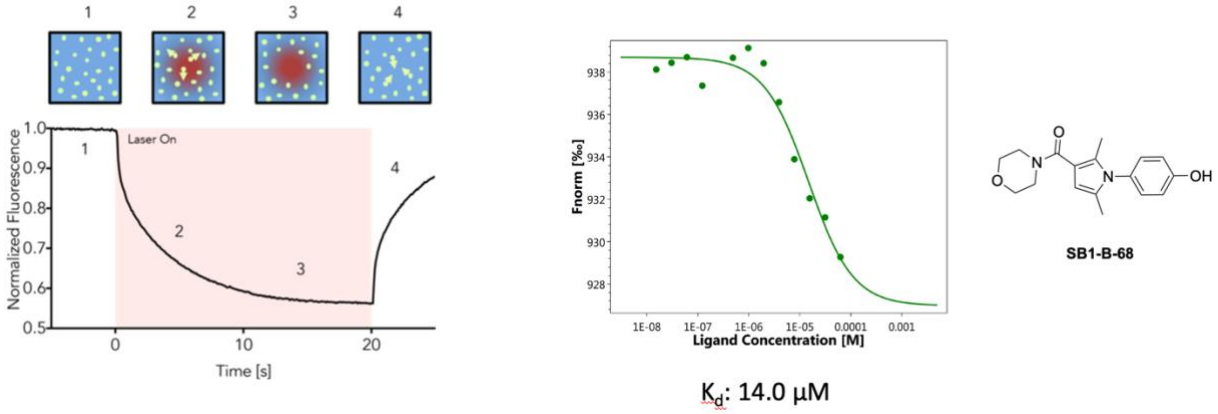


Figure 2.7. MST confirms binding of SB1-B-68 to USP14 with a K_d value of 14.0 µM.

molecule fragments to large macromolecular complexes, in small volumes (~20 µl), in a wide range of standard buffers and complex mixtures such as liposomes, detergent, serum, and cell lysates. A prerequisite for this experiment is fluorescent labeling of either the small molecule ligand or substrate. For this experiment, I used a His reactive RED-tris-NTA dye to label my 6xHis tagged USP8. SB1-B-68 showed direct binding to USP8 with a K_d value of 14 µM (**Figure 2.7**), providing additional validation that SB1-B-68 provides on-target inhibition of UPS8CD.

2.2.8 Computational docking studies with SB1-B-68 series

We used the x-ray co-crystal structure of IU1 bound to USP14 to inform the design of SB1-B-68 analogs. The x-ray structure of apo USP8 was first reported by Dr. Sirano Dhe-Paganon and coworkers.[66] The initial USP8-SB-B-68 complex was obtained by structural alignment of USP8 (3N3K) with USP14-IU1 co-crystal structure (6IIK) and placement of SB-B-68 on the similar binding pocket as IU1 at USP14 (**Figure 2.8**). The complex was further optimized before applying the induced fit docking, allowing the protein side chain to move freely. The highest ranked poses suggested that potentially SB1-B-68 represents the binding mode analogous to USP14-IU1. A detailed analysis of the model revealed the key interactions including the π–π stacking between the pyrrole core with PHE1014 and the phenol ring with TYR1068 and HID1059. These interactions are analogous with those observed in the USP14-IU1 co-crystal structure, where the π–π stacking interactions on the benzene ring and dimethyl pyrrole are essential for the proper binding. Additionally, consistent with our preliminary-SAR studies, the oxygen group on the morpholine ring plays a key role by accepting hydrogens from the proximate residues GLN867 and GLN860. During preliminary SAR studies, we observed that replacing the oxygen atom in the morpholine ring with a carbon killed the compound's activity, which further supports the model. Using this model, I developed an SAR plan which includes replacing the morpholine oxygen with other hydrogen bonding groups, introducing larger hydrophobic functional groups to the dimethyl pyrrole to pick up additional hydrophobic interactions with nearby residues, ring expansion of the phenyl ring to take advantage of additional π–π stacking interactions, and replacing the phenol -OH with other hydrogen accepting and donating groups. I generated robust and reliable synthetic routes for accessing these chemical modifications, and using these routes I generated a small library of SB1-B-68 analogs.

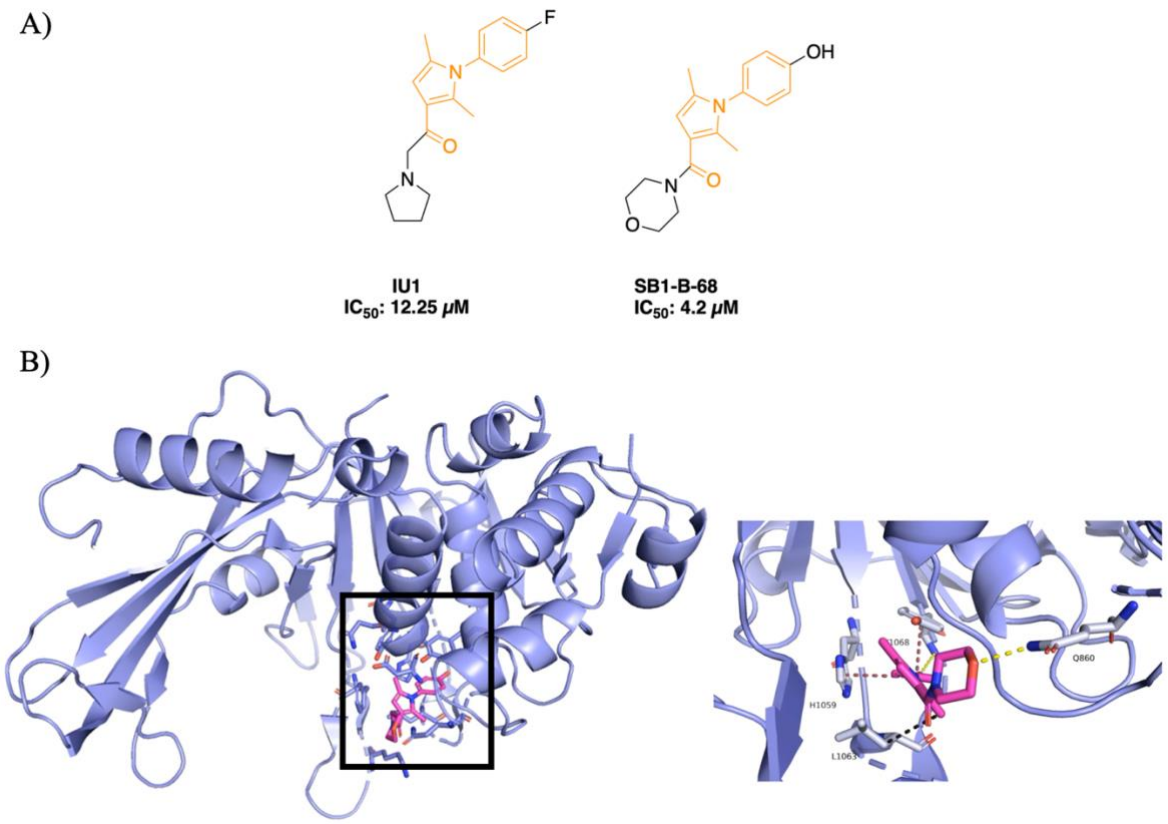


Figure 2.8. Computational model of SB1-B-68 bound to USP8
A) The USP14 inhibitor IU1 and the USP8 'hit' compound SB1-B-68 feature the same pyrrole core. Given these structural similarities, we assumed that SB1-B-68 binds in the distal pocket of USP8. We overlapped the crystal structures of USP8 and USP14 to generate a predicted binding mode of SB1-B-68 in the USP8 distal pocket and to guide our chemistry efforts with structural information. B) The left panel shows a docked pose of SB1-B-68 in the USP8 distal pocket. The right panel is zoomed in, and key residues and interactions are shown.

2.2.9 SB1-B-68 structure activity relationship (SAR) data

Based on the synthetic route and accessibility for derivatization at various points, three regions of the molecule were identified for SAR studies. The first was the left-hand side of the molecule arising from the final step of the synthesis which was the coupling of different amines to the dimethyl pyrrole acid intermediate. The initial screening hit featured a morpholine ring attached directly to the dimethyl pyrrole core via an amide bond. The initial step was to assess various substitutions to the dimethyl pyrrole core by coupling on different saturated cyclic and heterocyclic amines. AXA-03-075 was synthesized with just a piperidine, removing the oxygen from the morpholine ring of SB1-B-68 to assess its importance. AXA-03-075 was effectively inactive, highlighting the importance of the oxygen in engaging in hydrogen bonding interactions. Other derivatives were synthesized installing different substituents at the core amide position to yield the following compounds: AXA-03-079 (pyrrolidine), AXA-03-085 (methyl piperazine), AXA-03-081 (piperidine-4-ol), and AXA-03-083 (thiomorpholine). AXA-03-081 had a weaker IC_{50} of 64 μM representing an over 10-fold loss in activity. The other derivatives were much weaker with IC_{50} values of all > 100 μM. There were no clear improvements to compound activity with the cyclic saturated substituents, I selected alternate amines. AXA-03-157 contains a phenyl ring in place of the morpholine which resulted in an IC_{50} of > 100 μM. Likewise, increasing the spacing from a direct attachment to the amide bond to a methylene spacer (AXA-03-157) resulted in a very weak compound. Increasing the spacer to two methylene groups and adding two electron-withdrawing methoxy groups to the phenyl ring resulted in a completely dead compound (AXA-03-161). These results suggest that the USP8 binding pocket around the left-side of the compound is tight, allowing for a narrow SAR window.

Table 2.3. SAR studies of SB1-B-68 series analogs focused on the amide position. Table showing compound ID, structure, and IC_{50} determined in the Ub-Rho assay. This set focused on derivatizing at the amide position of the dimethyl pyrrole core (the left-hand side).

Table 2.3 (Continued)

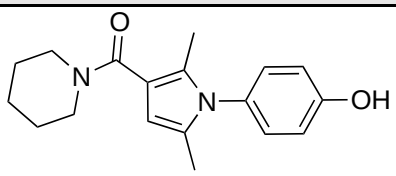
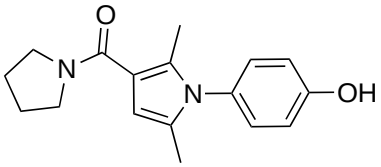
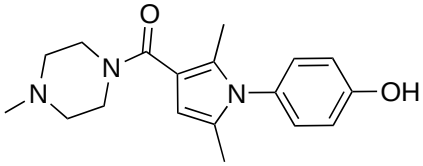
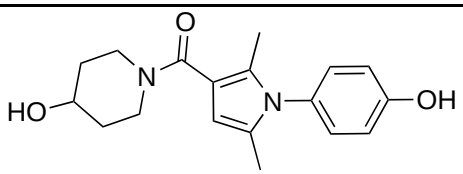
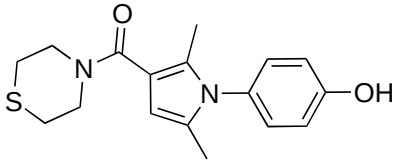
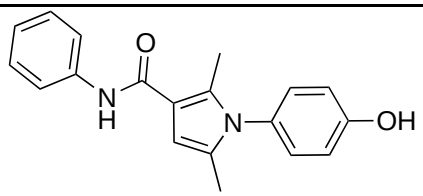
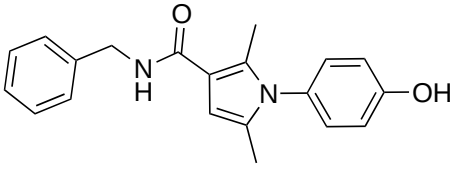
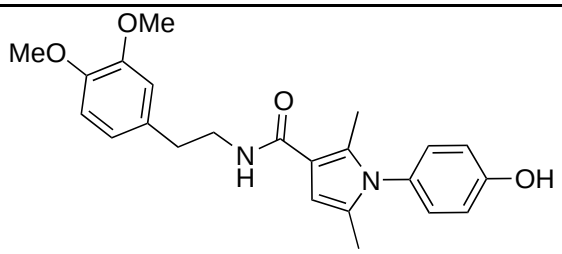
Compound	Structure	IC50 (μM)
AXA-03-075		>100
AXA-03-079		>100
AXA-03-085		>100
AXA-03-081		64
AXA-03-083		>100
AXA-03-157		>100
AXA-03-159		>100

Table 2.3 (Continued)

AXA-03-161		> 100

The phenyl ring in the SB1-B-68 compound contained a hydroxy group para to the pyrrole nitrogen. Alterations to this hydroxy group were made to determine the importance of this position and toleration for change. All derivatives from this series were synthesized keeping the morpholine group consistent to enable direct comparison. In AXA-03-129 hydroxyl group was swapped with an electron-withdrawing cyano group resulting in a comparably weaker compound compared to the parent (IC50 = 26 μM). Next the hydroxyl group was switched to a sulfonyl group (AXA-03-143) which resulted in a further reduction in compound potency (IC50 = 54 μM). Changing the functionality to a free amine as in AXA-03-173 resulting in a complete loss of activity. Similar results were observed when we moved the hydroxyl group from the para position to the meta position (AXA-04-001) and when we introduced a pyridine ring (AXA-03-207).

Table 2.4. SAR studies of SB1-B-68 series analogs focused on the phenyl region. Table showing compound ID, structure, and IC_{50} determined in the Ub-Rho assay. This set focused on derivatizing at the hydroxy position of the hit compound phenyl group (the right-hand side).

Table 2.4 (Continued)

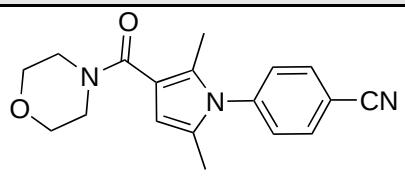
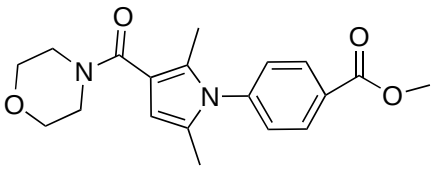
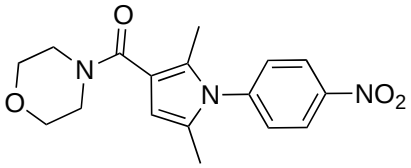
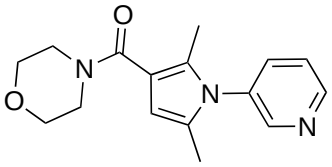
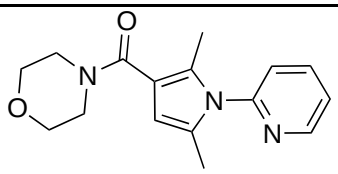
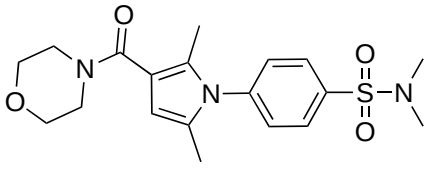
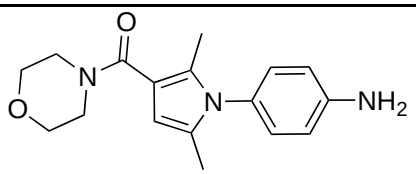
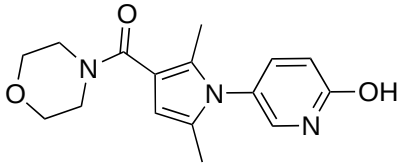
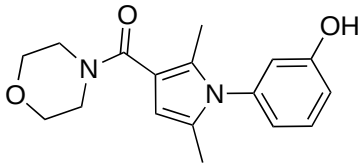
Compound	Structure	IC50 (μM)
AXA-03-129		26
AXA-03-133		N/A
AXA-03-135		44
AXA-03-137		N/A
AXA-03-141		N/A
AXA-03-143		54

Table 2.4 (Continued)

AXA-03-173		>100
AXA-03-207		>100
AXA-04-001		>100

2.2.10 Ubiquigent profiling for SB1-B-68 series

We assessed the selectivity of SB1-B-68 analogs against a panel of 41 purified DUBs (Ubiquigent). In addition to inhibiting USP8, the goal of this work is the establish chemical starting points to further develop reversible compound libraries that target DUB S3-S5 and distal pockets. Towards this goal, we identified the analog AXA-03-131, which features an oxazole in place of the pyrrole. Interestingly, this compound showed highly selective inhibition of USP16, with no activity observed against other DUBs in the panel (**Figure 2.9)**. In a mouse model of Alzheimer's disease, inhibition of USP16 rescued stem cell aging and improved long-term and spatial memory. [67] Despite its therapeutic relevance, there are not reported USP16 inhibitors in the literature. AXA-03-131 represents a promising starting point for the development of potent and selective USP16 compounds.

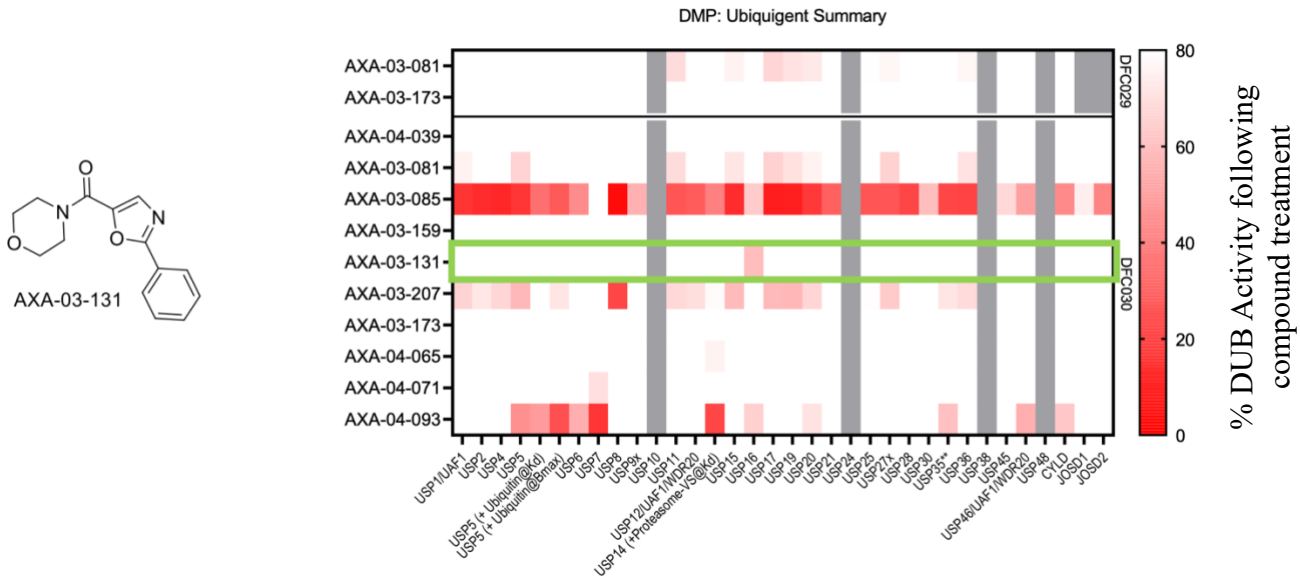


Figure 2.9. Ubiquigent profiling of SB1-B-68 analogs revealed a highly selective USP16 inhibitor, AXA-03-131.

2.2.11 SB1-B-68 readily oxidizes, confounding the "hit" result

The parent dimethyl pyrrole compound, SB1-B-68, reacts with oxygen under ambient conditions over a timespan of ~ three weeks. Specifically, the 10mM DMSO stock readily oxidizes, and changes color from pale yellow to progressively darker brown. Oxidized products, corresponding to m/z +16 and m/z +32 of the parent compound, were observed by LCMS. Following this observation, fresh SB1-B-68 was synthesized and tested against USP8 in Ub-Rho. We did not observe inhibition of USP8 with the fresh stock of SB1-B-68. However, when the fresh DMSO stock of SB1-B-68 was allowed to oxidize, over the course of ~ three weeks (under ambient conditions) and re-tested against USP8, inhibitory activity **was** observed. Moreover, we observed that only trace amounts of the oxidized SB1-B-68 product is sufficient to inhibit USP8CD in the low, single-digit micro molar range, as evidenced by NMR and LCMS studies.

While the potential for oxidation is potentially confounding, SB1-B-68 appeared as a highly selective hit for USP8 against a panel of USPs in the Ubiquigent screen. Future follow-up medicinal

chemistry efforts around the dimethyl-pyrrole series could focus on installing a carbonyl group on the pyrrole or phenol groups to try to replicate the inhibitory activity of the oxidized B68.

2.2.12 USP8 confirmatory biochemistry with M058-0519

In parallel with our follow-up work around XL-9872-040 and M058-0519, we went back to the Novartis HTS to credential a third scaffold. From this, we identified the bicylic pyrrolo-pyridine M058-0519. Currently, no bicylclic pyrrolo -pyridine has been reported as a DUB inhibitor. However, Takeda investigated a pyrrolo -pyridine analog as a Smoothened inhibitor.[68] The molecule made it to phase 1 trials, where it was investigated in solid cancer indications. The efficacy and safety signals were promising , but the program was later discontinued due to portfolio prioritization. However, this suggests that the scaffold has favorable drug-like properties and makes a promising starting point for the development of a DUB-targeted chemical probe.

M058-0519 appeared in the screen as a 2.2 μM hit for USP8. We resynthesized the compound in-house and observed a slightly weaker IC50 of ~30 μM. The compound was profiled at Ubiquigent, where it showed good selectivity for USP8 and little to no off-target inhibition of other DUBs in the panel (**Figure 2.10**) We synthesized analogs of this compound with two goals: improve the potency of this series against USP8, but also profile the analogs against a panel of cellular DUBs to build our in house library and access related pockets on other DUBs of interest. This is a logical approach given that USPs belong to the same family and that binding pockets are generally conserved.

2.2.13 M058-0519 structure activity relationship (SAR) data

Following the identification of M058-0519 from the high throughput screen, a chemistry campaign was initiated to establish structure activity relationship trends. M058-0519 contains a bicyclic core consisting of two fused rings (pyrrole-pyridinone) with a few substituents in different regions of the molecule (**Figure 2.10**). Further interrogation of this scaffold was performed, and

multiple derivatives were synthesized to assess each position on the molecule. The first area of the molecule that was explored was the 4-methyl on the phenyl group. Based on the synthetic route established in the resynthesis of the screening hit, the core intermediate for the M058-0519 scaffold contains a carboxylic acid on the pyrrole ring that provides a convenient handle for the introduction of various amines. The ideal position of the 4-methyl was assessed by synthesizing derivatives where the methyl was either moved or removed while keeping the phenyl ring the same. Removing the methyl (YL-12826-95) reduced the compound's potency against USP8CD. Moving the methyl to the meta position (AXA-05-007) also reduced the activity, while an ortho substitution (AXA-05-009) was very weakly inhibitory (100 μM). Similarly, analogs that featured a 2,6-dimethyl substitution or a 2,4-dimethyl pattern were weak.

In the next round of chemistry, we continued to focus on the 4-methyl group on the phenyl ring but we switched the methyl group for a diversity of electron withdrawing, electron donating, and bulky groups. Dichloro (YL-12826-96), methoxy (AXA-05-019), tertbutyl (AXA-05-017), cyano (AXA-05-021), and naphtyl (AXA-05-015) analogs were synthesized. All these derivatives were inactive, suggesting that the that the SAR window for this scaffold against USP8 is quite narrow. Alternate cyclic groups were tested to further interrogate this area of the scaffold. Interestingly, a morpholine analog (AXA-05-135) showed a 2x fold improvement with an IC50 value of 13 uM. Cyclopentyl (AXA-05-065) and cyclohexyl (AXA-05-027) were inactive. An analog containing a piperazine spacer between the core and the 4-methyl group (M058-0638, purchased from ChemDiv) was weakly active with an IC_{50} of ~100 uM.

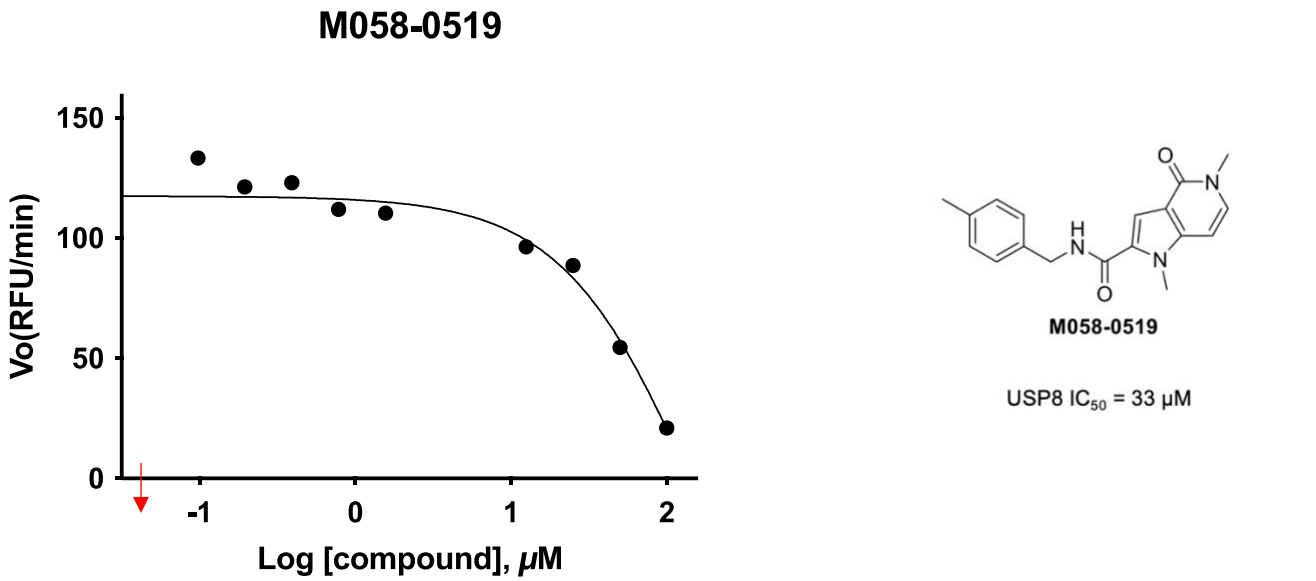
Next, substituents on the core nitrogens were assessed. For comparison, the 4-methyl phenyl tail of the parent compound was kept consistent. Derivatives were synthesized to determine the importance of the methyl groups on the pyrrole and pyridinone rings. Removing both methyl groups (AXA-05-067, IC_{50} ~ 100 μM) resulted in a loss of activity. Extending the pyridinone nitrogen from

a methyl to an ethyl group (YL-12826-99) killed the compound's activity. An isobutyl analog (M058-0930, IC_{50} =13 μM) resulted in a ~3x fold improvement in affinity. Similarly, fusing a phenyl group to the pyridinone ring (C593-0555, IC_{50} =12 μM) seemingly improved the potency. A butyl substitution ablated the compounds activity (AXA-05-179, dead), while a propyl-phenyl analog (AXA-05-093, IC_{50} =100 μM) was very weak. A summary of the SAR data is included below.

2.2.14 Redox activity of select M058-0519 analogs

A routine experiment that is performed in the lab is a redox activity assay to rule out false positives.[69] Small molecules can generate reactive oxygen species (ROS) that can lead to oxidation of the catalytic cysteine residue and ablation of DUB catalytic activity. The redox assay utilizes resazurin, which is a blue-purple phenoxazine dye that can be irreversibly reduced to a highly fluorescent pink compound (resorufin). This assay was carried out during three previous HTS screening campaigns at GlaxoSmithKline as a simple approach to ruling out "hit" compounds that generate ROS, rather than bind to the target protein directly. One compound identified from the original paper that reliably generates redox activity is SB1-B-62.

A)



B)

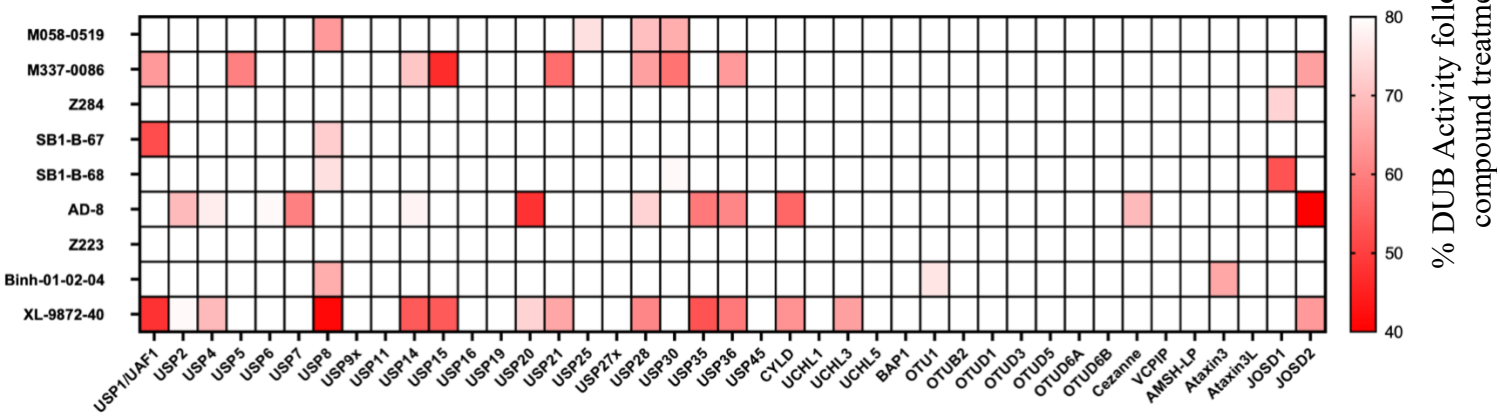
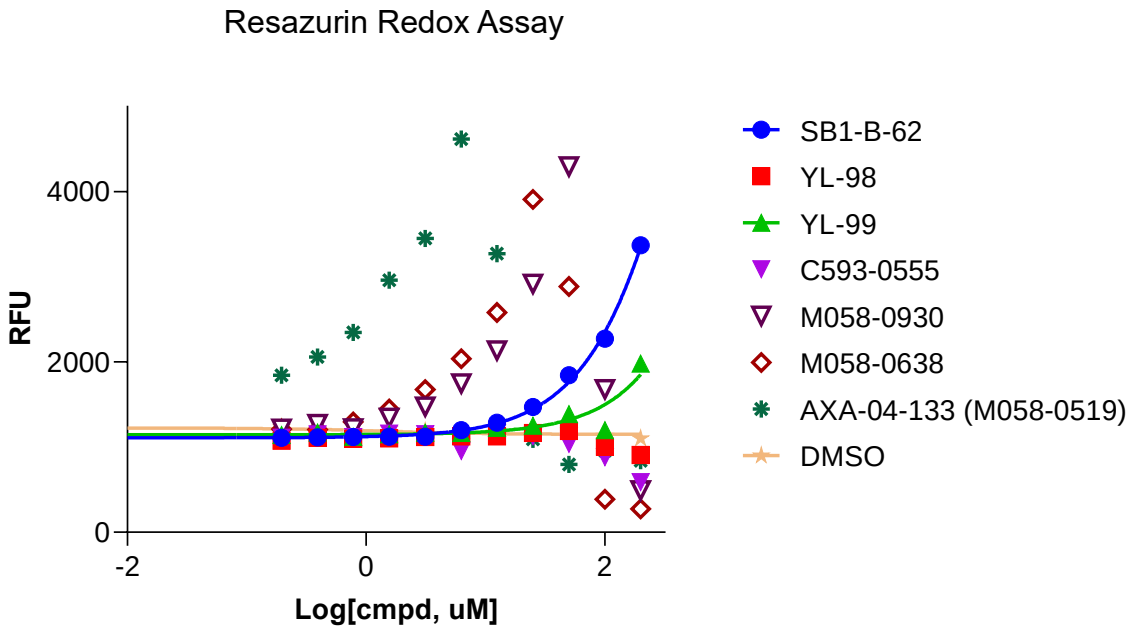


Figure 2.10. Validation of USP8 inhibition by M058-0519 with biochemistry and Ubiquigent profiling.
A) M058-0519 was resynthesized in-house and tested against USP8CD, where it showed an IC_{50} of 33 μM.
B) M058-0519 shows good selectivity for USP8 when profiled against a panel of cellular DUBs.

As this compound had already been synthesized during Dr. Anthony Varca's high throughput screen, we used it as a positive control for our own experiments. M058-0519 series compounds were incubated in dose-response, where an increase in fluorescence corresponds to the compound's redox activity. The morpholine analog AXA-04-135 (USP8 IC_{50} = 13 μM) demonstrated a significant increase in fluorescence signal at lower concentrations than the positive control itself (**Figure 2.11**). One compound purchased from the third-party, CRO ChemDiv (M058-0930, IC_{50} = 100 μM) produced a bell-shaped curve. Other groups have identified similar curves in the literature. A bell-shaped curve may be the result of compound trapping some of the radical species in solution, but points to the potential redox activity of this compound.[69] Additional derivatives did not show redox activity, suggesting that this property can be engineered out of the molecule with specific substitution patterns. For example, the fused phenyl analog C593-0555 (IC_{50} = 12 μM) did not demonstrate redox activity. Similarly, decorating the pyridine nitrogen with larger alkyl and aromatic groups (AXA-05-079 and AXA-05-093) also ablated the redox signal. On the left-hand side of the parent compound, we changed the 4-methyl for a dimethyl (AXA-05-77), napthyl (AXA-05-015), or dicholoro (YL-12826-98). These analogs did not demonstrate redox activity. Thus, we observed that not all compounds from the M058 series are redox active, and that certain substitutions can be made to remove this property. Our chemistry efforts resulted in a small, unique library of M058-0519 series analogs, which we profiled against a broader panel of cellular DUBs with Ubiquigent. From these screening efforts, we successfully generated lead inhibitors of the therapeutically relevant DUBs USP4 and USP28, which will be the focus of Chapter 3 of this work.

A)



B)

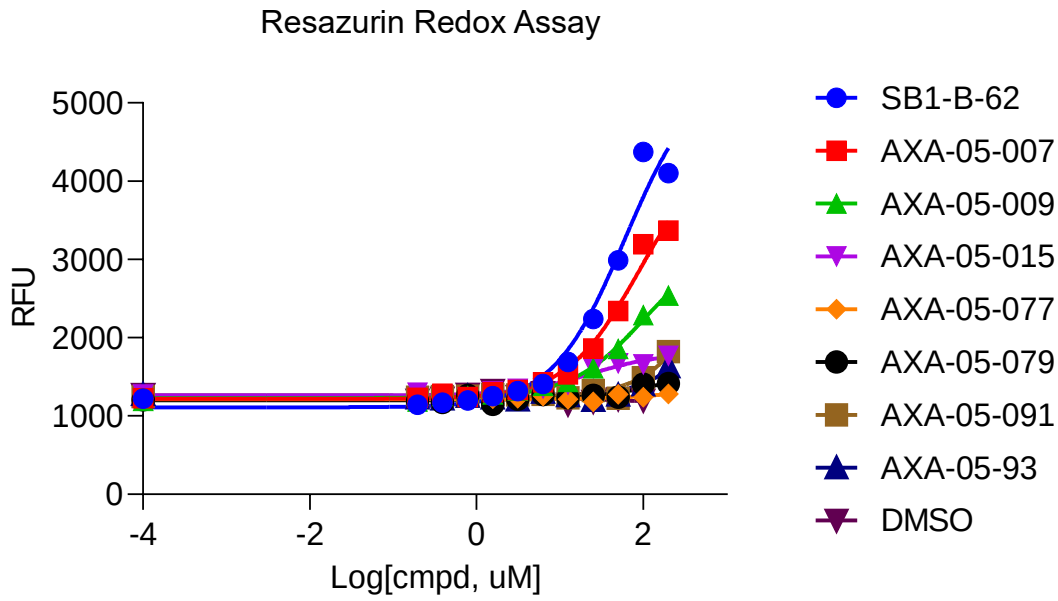


Figure 2.11. Resazurin redox assay results

A) Resazurin redox assay results for select compounds. SB1-B-62 represents a positive control compound that was previously reported as being a redox-active compound (Lor et al., 2007). Data are represented as mean ± SEM (n = 2).

B) Resazurin redox assay data for M058-0519 series (USP8 screening hit) analogs shows redoxactivity for only some of the compounds synthesized.

Table 2.5. SAR studies of M058-0519 analogs against USP8. Table showing compound ID, structure, and IC_{50} determined in the Ub-Rho assay.

Table 2.5 (Continued)

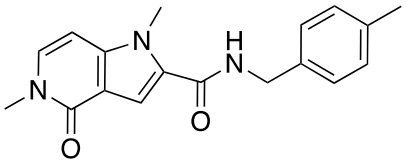
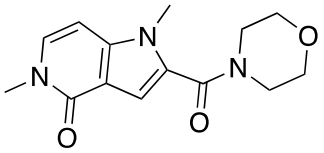
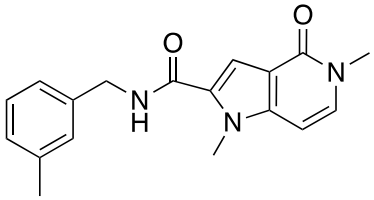
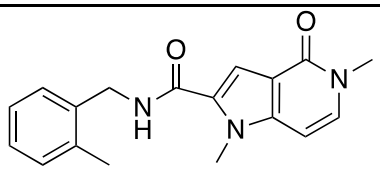
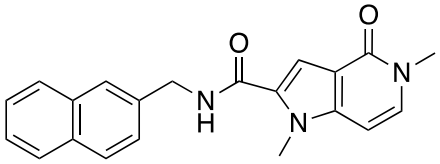
Compound	Structure	IC50 (μM)
AXA-04-133		33
AXA-04-135		13
AXA-05-007		> 100
AXA-05-009		~100
AXA-05-015		> 100

Table 2.5 (Continued)

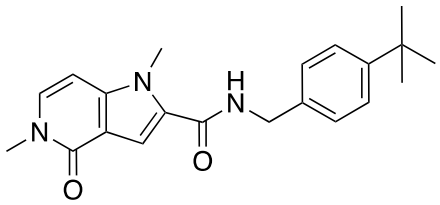
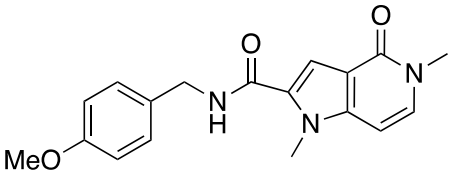
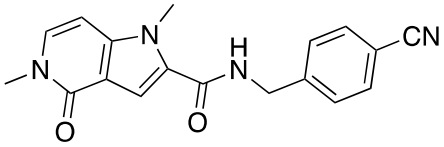
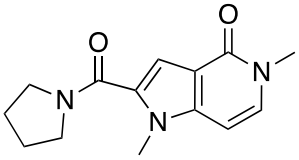
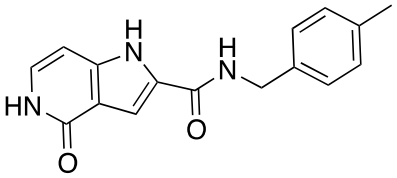
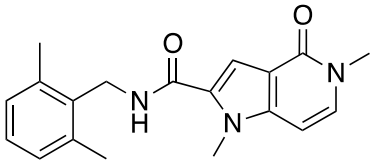
AXA-05-017		> 100
AXA-05-019		> 100
AXA-05-021		> 100
AXA-05-065		> 100
AXA-05-067		~100
AXA-05-077		> 100

Table 2.5 (Continued)

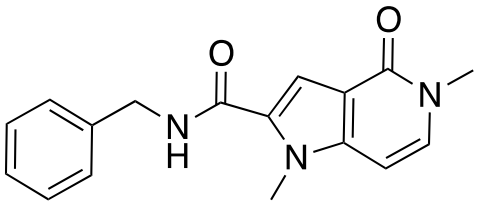
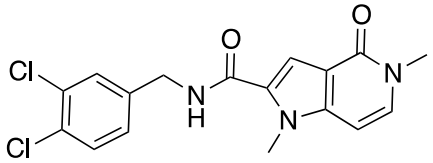
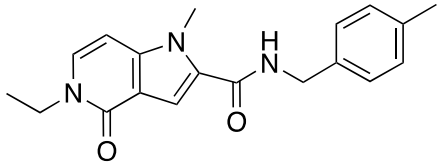
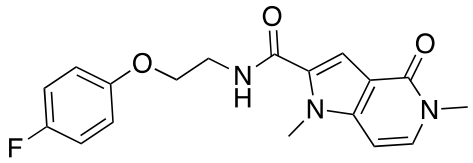
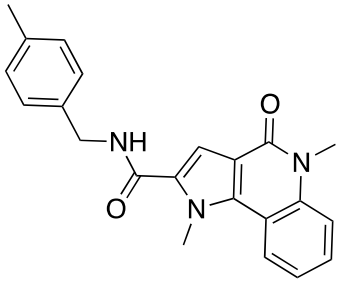
YL-12826-95		> 100
YL-12826-96		> 100
YL-12826-99		> 100
MS-1337-13		> 100
C593-0555		12

Table 2.5 (Continued)

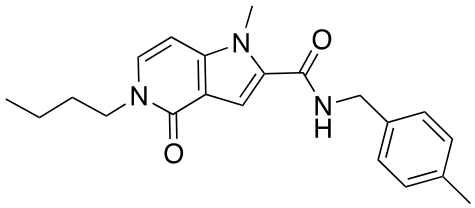
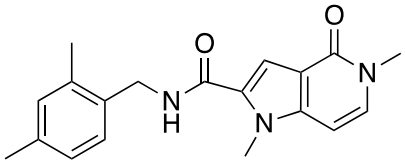
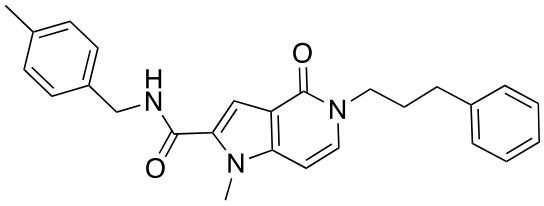
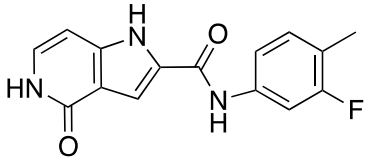
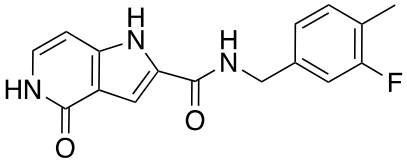
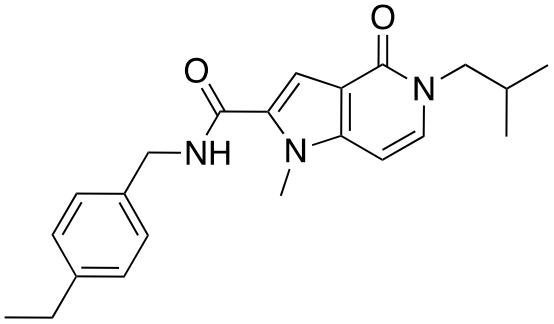
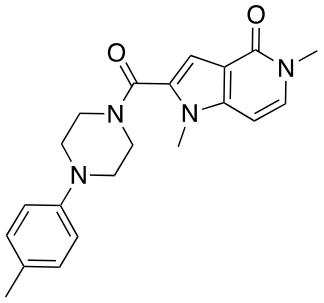
AXA-05-079		> 100
AXA-05-091		> 100
AXA-05-093		~100
AXA-05-101		~100
AXA-05-103		~100

Table 2.5 (Continued)

M058-0930		~100
M058-0638		~100

2.3 Discussion

Chemistry efforts on these USP8 scaffolds have resulted in the generation of selective analogs and some preliminary SAR to guide future efforts. For both series, multiple locations on the molecule were derivatized to develop a better understanding of the molecule. Excitingly, each series demonstrated both positive and negative SAR trends for different regions of the molecule indicating that further work is warranted to continue to optimize each scaffold. There are still areas that can be explored to further improve compound potency, particularly in the case of XL-9872-040, where the SAR window appears to be larger. Medicinal chemistry efforts around these series are on going to assess other regions of the compound that have not yet been investigated and to assess difficult to derivatize sections. For example, we are pursuing analogs of XL-9872-040 with the goal of removing the carbonyl group at the 7-position of the core. This modification is aimed at chemically stabilizing

the compound and will allow us to more fully explore the upper-right hand region of the scaffold (similar to how installing a quaternary center at the 3a-position stabilized the scaffold sufficiently to allows us to make changes to the piperazine position on the left-hand side of the compound). Since our SAR taught us that a saturated cyclic group at that position is required for activity against USP8, we believe these changes will be productive and provide additional insights into the requirements for activity. While we focused on understanding the activity of XL-9872-040 series analogs against USP8, we are also interested in gaining insight into the scaffold's broader activity against other cellular DUBs. Towards this, we are mixing and matching features of this scaffold with other promising hits from the Novartis HTS to generate "fusion compounds." This approach allows us to combine properties of hit compounds to generate SAR insights quickly and efficiently. For example, a thienopyridine series was identified as potent and selective USP28 hits, while a bicylic pyrrole-pyridine was identified as a selective USP8 hit. We are synthesizing XL-9872-040/thienopyridine fusions and XL-9872-040/bicyclic pyridone fusions and submitting these for profiling to gain insights into broader activity. Given that the S3-S5 and distal pockets are largely conserved across DUBs, these efforts will allow us to further credential "foundational chemotypes." Later in this work, I will further detail that led to the discovery of novel USP4 and USP28 inhibitors.

In this work, we established a pyrrole series (represented by SB1-B-68) as a "foundational chemotype" for the development of DUB inhibitors. We define a foundational chemotype as a DUB binding scaffold that: i) contains at least one exemplar compound that inhibits its primary DUB target with an IC50 < 10 μM and 20-fold selectivity relative to 90% of 50+ other DUBs, ii) binds in one of two non-catalytic pockets conserved across many DUB enzymes and iii) is preferentially represented by multiple analogs which exhibit disparate DUB selectivity patterns. In line with this definition, the pyrrole analog IU1 inhibits USP14 with good selectivity against other DUBs. We confirmed that a different pyrrole-based compound, SB1-B-68 (identified from the Novartis HTS), inhibits USP8 with

a IC_{50} of ~ 4 μM. Follow-up SAR studies suggests that the morpholine on the left-hand side of the compound is required for activity (changing that ring for a cyclohexyl or piperazine ablated the activity). Removing the hydroxyl group on the right-hand side of the molecule also penalized the activity of the compound. Replacing with the hydroxyl group with electron withdrawing moieties (such as cyano or nitro) generated weakly active compounds. Follow-up SAR studies continue to focus on this region. Replacing the pyrrole with an oxazole generated a selective hit for USP16. Chemistry efforts around this compound are so far generating low-micromolar inhibitors of this DUB.

Starting with the selective USP8 hit, M059-0519, we looked at this scaffold closely to develop a potent USP8 inhibitor. We took advantage of the scaffold's modularity and explored many different regions. Our efforts resulted in a small library of analogs that we assayed against USP8 specifically, and against other cellular DUBs more broadly. Against USP8, we discovered analogs that showed modest improvements in potency, as shown by Ub-Rho. We also observed that a handful of analogs from this series appeared to be redox active, although the redox activity is not an inherent property of the scaffold. We synthesized several analogs where we successfully engineered out the redox signal. While we are still determining the SAR rules for what determines redox activity, we observed that modifications to both the 4-methyl ring and additions of larger alkyl groups to the core resulted in compounds that were not redox active. In broader profiling experiments with Ubiquigent, M058-0519 analogs exhibited activity against the DUBs USP4 and USP28, which are both well validated therapeutic targets in the oncology literature. The final chapter of this work will focus on our medicinal chemistry, biochemistry, computational, and crystallographic efforts in developing novel inhibitors of these two proteins.

2.4 Materials and methods

Recombinant protein expression

DUB enzymes utilized in the screening campaign and subsequent validation experiments were either purchased directly from Boston Biochem/R&D Systems or expressed and purified from DUB plasmids. USP8 was expressed in E. coli BL21(DE3) bacteria and purified via affinity column chromatography using Ni-NTA. The construct encoding USP8 catalytic domain (AA 743-1110), was cloned into pET28 expression vector with an Nterminal 6xHis tag in NEB® 10-beta Competent E. coli (High Efficiency) cells. The NEB® 10-beta Competent E. coli (High Efficiency) cells were then inoculated into Luria Broth (LB) media (10 g tryptone, 10 g sodium chloride, 5 g yeast extract per 1 L) and incubated at 37°C with 200 rpm orbital rotation for 16 hours. Cultures were then centrifuged at 13000 rpm to pellet the cells. Plasmids containing the desired construct were then isolated from the cell pellets by QIAprep Spin Miniprep kit following the manufacturer's instructions. Plasmids were sequenced to confirm the correct amino acid sequence for the desired protein construct.

Plasmids were then transfected into E. coli BL21 (DE3) cells and grown on LB plates supplemented with antibiotics (either 100 µg/mL ampicillin or 50 µg/mL kanamycin depending on the plasmid resistance). Single colonies from the LB plates were then picked and inoculated into 5 mL of LB media supplemented with the specific antibiotic for the plasmid and grown at 37°C with 200 rpm orbital rotation overnight. The 5 mL starter cultures were then added to 1 L of LB media supplemented with antibiotics and incubated at 37°C with 200 rpm orbital rotation until the optical density at 600 nM (OD600) was between 0.6 and 1.0 for the culture. The cultures were then cooled to 16 °C and protein expression was then induced via addition of 1M (final concentration of 500 µM) isopropyl-1-thio-D-galactopyranoside (IPTG). Cultures were incubated overnight at 18 °C with 200 rpm orbital rotation. The 1 L cultures were then pelleted by centrifugation at 4,540 x g at 4°C for 20 minutes. Pellets were stored at -80 °C pending lysis. The supernatant was decanted, and cell pellets

were resuspended in 100 mL of lysis buffer (50 mM Tris pH 7.5, 500 nM NaCl, 5% glycerol, 20mM imidazole, 500 µM TCEP, made up to 400 mL with 312 mL of Milli-Q^{TM} water). The cultures were then sonicated (20% of total sonicator power) on ice alternating 15s of sonication with 45 s of rest for a total of 3 minutes of sonication. The resulting lysate was centrifuged at 30,000 x g for 20 min at 4°C and the supernatant containing the expressed proteins was collected and filtered with a 1.1 µM filter into a fresh tube.

Given that USP8 is a 6xHis tagged protein, 1 mL of 5% Ni-NTA Agarose resin (Qiagen) per 1 L culture was mixed with lysate supernatant in a gravity flow column and incubated for 2 hours at 4°C with gentle agitation. The solution was then drained via gravity flow and the resin was washed with lysis buffer supplemented with 25 mM imidazole. Protein was eluted by addition of elution buffer (lysis buffer supplemented with 300 mM imidazole) to the resin. An SDS-PAGE gel was performed to confirm elution of protein of interest. Protein was subsequently dialyzed into exchange buffer (2L of 50nM Tris pH 7.5, 500 mM NaCl, 500 µM TCEP). The eluent from the HisTrap purification was collected and concentrated to < 1 mL via centrifugation using a 30 kDa concentrator (Amicon Ultra, Millipore). Protein sample was then purified via fast protein liquid chromatography using a Superdex 200 (GE healthcare) size exclusion column in SEC buffer (500 uL of 50 mM Tris pH 7.5, 0.5 mM TCEP, 5% glycerol was added to the concentrated protein, which brought the final NaCl concentration to 250 mM). Fractions were eluted with 50 mM Tris pH 7.5, 500 mM NaCl, 0.5 mM TCEP, 5% glycerol, 20 mM imidazole). Fractions containing desired protein of interest were identified by SDS-PAGE gel and Coomassie staining. Fractions that contained contaminants (that are ~25 kDa from the desired product bands) were additionally purified by size exclusion chromatography (if the contaminants are within 25 kDa size exclusion will not work). Fractions were then pooled together and concentrated to < 1 mL via centrifugation using a 30 kDa concentrator (Amicon Ultra, Millipore).

Protein concentration was determined by recording tyrosine/tryptophan fluorescence at 280 nm on a NanoDrop along with the calculated extinction coefficient of the protein construct.

Cell lines

HEK293T (female human origin) cell lines were used for target engagement experiments. HEK293T cells (ATCC, Cat# CRL-3216) are a clonal isolate of HEK293 cells transformed with the SV40 large T antigen. For growth, HEK293T cells were maintained in DMEM containing 4 mM L-glutamine (Gibco) supplemented with 10% (v/v) 10% heat inactivated fetal bovine serum (FBS) (Gibco), and penicillin/streptomycin (100 U/mL penicillin and 0.1 mg/mL streptomycin) (Gibco). Cells were grown at 37°C with 5% CO2 in a water-saturated incubator. For passaging, cells were incubated with trypsin/EDTA at 37°C to detach cells.

Ubiquitin-rhodamine110 kinetic assay

DUBs from the high-throughput screen were tested for their respective activity in the Ub-Rho110 assay in the presence or absence of inhibitors using Nunc™ 384-well plates (Thermo Scientific™ catalog number: 2262260). Individual DUBs were pre-incubated with different concentrations of inhibitors in assay buffer (50 mM Tris pH 8, 50 mM NaCl, 0.002% Tween-20, 5 mM DTT). Compounds and protein were incubated for 30 minutes at room temperature prior to the addition of Ub-Rho110 (Boston Biochem) substrate. The initial rate of the reaction was measured by collecting fluorescence data at one-minute intervals over 30-minute period using a Clariostar fluorescence spectrometer at excitation and emission wavelengths of 485 nm and 535 nm, respectively. The calculated initial rate values (V0) were normalized to plate control wells and were plotted as a function of inhibitor concentrations to determine IC50s. All experimental data were plotted using GraphPad Prism (log(inhibitor) vs. normalized response – Variable slope, least squares fit).

In-vitro DUB selectivity profiling

Compounds were screened using the Ubiquigent DUBProfilerTM SPT system (www.ubiquigent.com/drug-discovery-services/dubprofiler/). Each of 41 purified DUBs was incubated with compound for 15 minutes, then Ub-Rho110 added, and fluorescence recorded. Percent inhibition was determined based on fluorescence relative to a DMSO control. An autofluorescence control experiment determines the fluorescence signal generated by the compound at screening concentration in absence of enzyme relative to the enzyme and no enzyme control for each of the DUBs in the panel. A product signal modulation (PSM) control experiment determines the fluorescence signal generated by the compound (at screening concentration) in the presence of synthetic rhodamine 110 glycine (the product of enzymatic cleavage of the DUBProfilerTM Ub-Rho substrate) and DUBProfilerTM substrate (at standard assay concentration) expressed as a percentage relative to the fluorescence signal of synthetic rhodamine 110 glycine and DUBProfilerTM substrate (at standard assay concentration). Autofluorescence and PSM data can indicate autofluorescence (positive %) or quenching (negative %) of background signal and/or assay signal.

Target Engagement

HEK293T cells were pelleted, washed with PBS, lysed on ice with lysis buffer (20 mM Tris pH 8, 150 mM NaCl, 1% NP-40, 10% glycerol, 1 mM TCEP, phosphatase inhibitor cocktails (Sigma P5726 and Calbiochem 524624), and protease inhibitors (pepstatin, leupeptin, PMSF, and aprotinin), and clarified by centrifugation. Protein content was quantified by BCA and the clarified cell lysate was then diluted to 2 mg/mL in lysis buffer. 40 µL samples of lysate were incubated with compounds or DMSO at desired concentrations and incubated at room temperature for 15 minutes. Samples were then supplemented with 1:1 Ub-PA/Ub-VME probe at a final concentration in the sample of 2 µM and incubated at room temperature with shaking for 10-30 minutes depending on DUB being

assessed. Reactions were quenched with 4x LDS sample buffer (Thermo Fisher B0007) supplemented with 10% BME, vortexed vigorously, and heated to 95°C for 5 minutes. Samples were resolved by SDS-PAGE and analyzed by Western blot with the indicated antibodies (Primary antibodies used: USP28 rabbit monoclonal antibody from Abcam, catalog number: ab126604. UBPY mouse monoclonal antibody from Santa Cruz Biotechnology Inc, catalog number: sc-376130. GAPDH rabbit monoclonal antibody from Cell Signaling, catalog number: 2118S. GAPDH (D4C6R) mouse monoclonal antibody from Cell Signaling, catalog number: 97166S. Secondary antibodies used: IRDye® 800CW Goat anti-Rabbit IgG Secondary Antibody from LI-COR, catalog number: 926-32211, IRDye® 680LT Goat anti-Mouse IgG Secondary Antibody from LI-COR, catalog number: 926-68020

Redox Assay

50 µL of redox assay buffer (50 mM Tris pH 7.5, 50 mM NaCl, 5 mM DTT, and 25 µM resazurin) was added to column 1 of an Axygen® 96-well Polypropylene PCR Microplate (product number: PCR-96-FS-C). 25 µL of redox assay buffer was added to remaining wells in columns 2-11. Column 12 received25 µL of redox assay buffer with 0.5 µL DMSO. 0.5 µL of 10 mM compound was then added to each row in column 1 for an initial concentration of 100 µM. A serial two-fold dilution of each compound was then performed down each row, omitting column 12. The plate was then incubated for 30 minutes in darkness, transferred to a NUNC™ 384-well plate (Thermo Scientific™ catalog number: 2262260) and then read ona Clariostar fluorescence spectrometer at excitation and emission wavelengths of 545 nm and 600 nm respectively. The baseline signal of the averaged DMSO control wells was then subtracted from all data points. Fluorescence values for each compound were plotted as a function of compound dose usingGraphPad Prism (log(agonist) vs. response - Variable slope (four parameters), least squares fit).

Microscale Thermophoresis

USP8CD was initially labeled with the commercially available tris-NTA dye, using NanoTemper's Protein Labeling Kit RED. The concentration of labeled protein was kept constant at ~100 nM. The ligand to protein concentration ratio was tested in the range of 0.01 to 100. Samples were loaded into K025 Monolith™ Premium Capillaries. After a short incubation period, MST analysis was performed using the Monolith NT.115 (NanoTemper Technologies). All numerical models were fitted to experimental data using the NT Analysis 1.5.41 software (NanoTemper Technologies). Presented results are weighted-averages of at least 2 independent experiments.

Chemical Synthesis General Methods and Materials

All commercially available starting materials were purchased from Sigma Aldrich, Fisher Scientific, Oakwood Chemical, and Combi Block. All reagents were used as received without further purification. Anhydrous solvents, such as tetrahydrofuran (THF), dichloromethane (DCM), diethyl ether (Et2O), dimethyl formamide (DMF), dimethylsulfoxide (DMSO), 1,4-dioxane, and toluene were purchased from Fisher Scientific, and used as received. If necessary, air or moisture sensitive reactions were carried out under an inert atmosphere of nitrogen. Removal of solvents was accomplished on a Büchi R-300 rotary evaporator and further concentration was done under a Welch 1400B-01 vacuum line, and/or Labconco FreeZone 6 plus system. Purification of compounds was performed by normal phase column chromatography using Teledyne CombiFlash chromatography system, and/or reversed phase chromatography on Waters Micromass ZQ preparative system with SunFire® Prep C18 OBD™ 5µM column. The purity was analyzed on Waters Acquity UPLC system. Analytical thin layer chromatography (TLC) plates were purchased

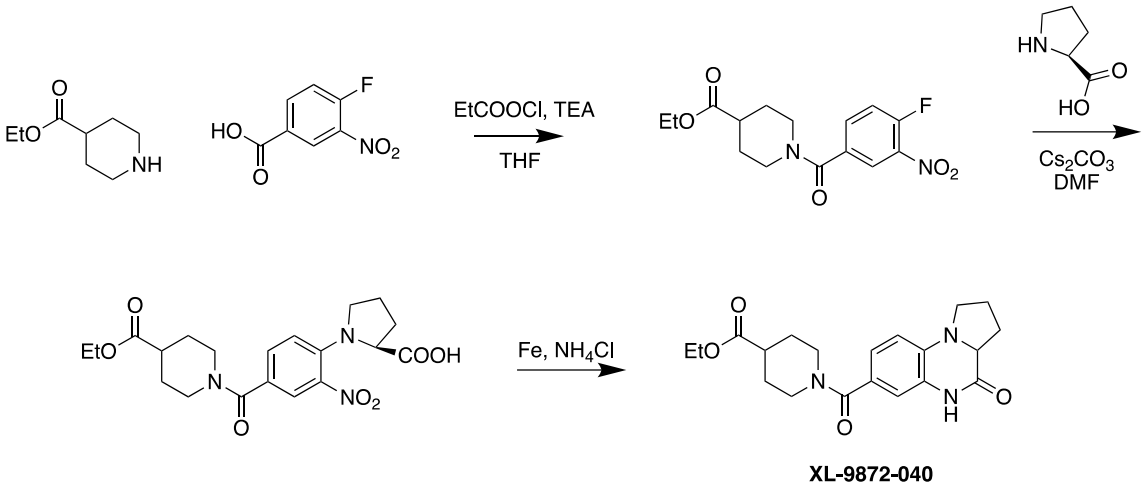
from Fisher Scientific (EMD Millipore TLC Silica Gel60 F254). Visualization was accomplished by irradiation under UV light (254 nm).

All 1H-NMR spectra were recorded at 298K on a Bruker ARX 500 (500 MHz) spectrometer. Samples were dissolved in CDCl3, DMSO-d6, or Methanol-d4 obtained from Cambridge Isotope Laboratories. The spectra were referenced to the residual solvent peak (CDCl3: 7.26 ppm for 1H-NMR and 77.16 ppm for 13C-NMR; DMSO-d6: 2.50 ppm for 1H-NMR and 39.25 ppm for 13C-NMR, CD3OD: 3.31 ppm for 1H NMR and 49.00 ppm for 13C NMR or tetramethylsilane (TMS) as the internal standard. Chemical shift, multiplicity (s=singlet, d=doublet, t=triplet, q=quartet, m=multiplet, br=broad peak), coupling constants (Hz), and number of protons were assigned using MestReNova software. Mass spectrometry (LCMS) data were obtained on Waters Acquity UPLC system in positive ESI mode.

Final compounds submitted for testing were prepared and stored as 10 mM stock solutions in DMSO. Stocks were stored at -20°C and aliquoted as needed for specific experiments to reduce the number of freeze thaw cycles. Unless otherwise noted for specific compounds, no apparent solubility issues were observed with the compounds either in DMSO or aqueous buffer conditions at the concentrations used.

USP8 hit resynthesis

Ethyl 1-(4-oxo-1,2,3,3a,4,5-hexahydropyrrolo[1,2-*a*]quinoxaline-7-carbonyl)piperidine-4 carboxylate (XL-9872-040)



XL-9872-040

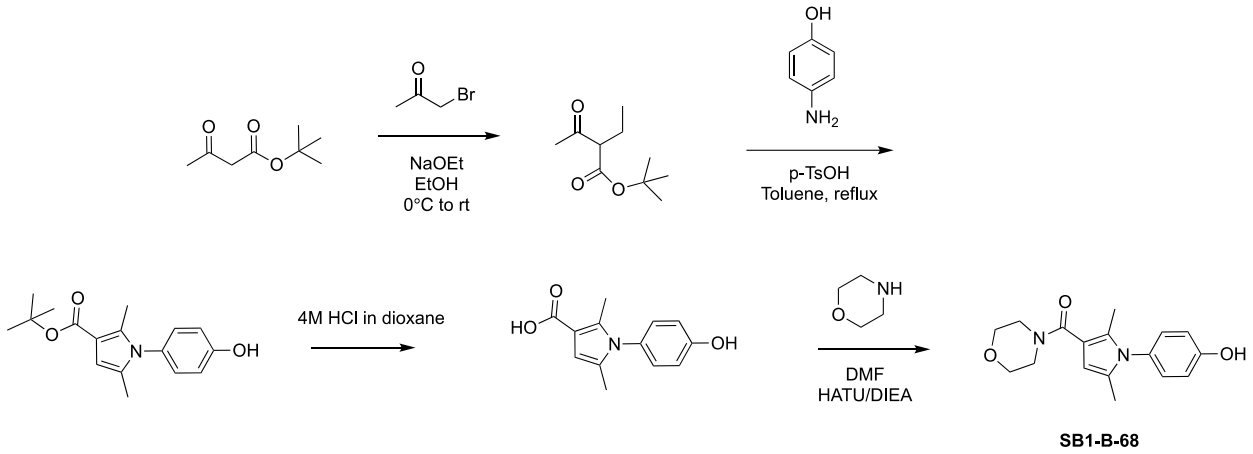
The synthesis of this hit compound was carried out through a multi-step synthetic route.

Step 1: 4-fluoro-3-nitrobenzoic acid (250 mg, 1.35 mmol) was dissolved in THF (9 mL) with TEA (273 mg, 2.70 mmol) and cooled to 0°C. EtCOOCl was added to the reaction mixture, and the reaction was allowed to warm to RT and stirred for 30 min. The reaction was cooled again to 0°C, after which ethyl piperidine-4-carboxylate (234 mg, 1.49 mmol) was added to the reaction mixture. The reaction was warmed to RT and stirred overnight. The reaction was diluted with $NaHCO_3$ and extracted with EtOAc (2x). The organics were washed with brine, dried, filtered, and evaporated. The crude was purified by silica gel chromatography (0-50% Hexanes/EtoAc) to afford product as a yellow oil (221 mg, 51%). LCMS (ESI) [M+H]+ calcd for $C_{15}H_{17}FN_2O_5^+$: 324.11, found m/z 324.12.

Step 2: Ethyl 1-(4-fluoro-3-nitrobenzoyl)piperidine-4-carboxylate (50 mg, 0.15 mmol), L-proline (45 mg, 0.19 mmol), and Cs_2CO_3 (151 mg, 0.46 mmol) were stirred in DMF (2 mL) at 60°C for 2 hr. The reaction was diluted with 20% citric acid, and extracted with EtOAc (2x). The organics were washed with brine, dried, filtered, and evaporated. The crude was purified by silica gel chromatography (50-100% Hexanes/EtoAc) to afford product as a yellow-oil (62 mg, 93%). LCMS (ESI) [M+H]+ calcd for $C_{20}H_{25}N_3O_7^+$: 419.17, found m/z 419.19.

Step 3: (4-(4-(ethoxycarbonyl)piperidine-1-carbonyl)-2-nitrophenyl)-*L*-proline (62 mg, 0.144 mmol) was dissolved in EtoAc, to which a scoop of Pd/C was added. The reaction was sealed with a rubber stopper, and purged with H_2 for 2 min. The reaction was stirred at RT for 3 hr. The reaction was filtered with a silica plug, diluted with water, and extracted with EtoAc (2x). The organics were washed with brine, dried, filtered, and evaporated. The crude was purified by silica gel chromatography (50-100% Hexanes/EtoAc) to afford product as a white powder. The final was further purified by HPLC (23.4 mg, 42%).

(1-(4-hydroxyphenyl)-2,5-dimethyl-1*H*-pyrrol-3-yl)(morpholino)methanone (SB1-B-68)



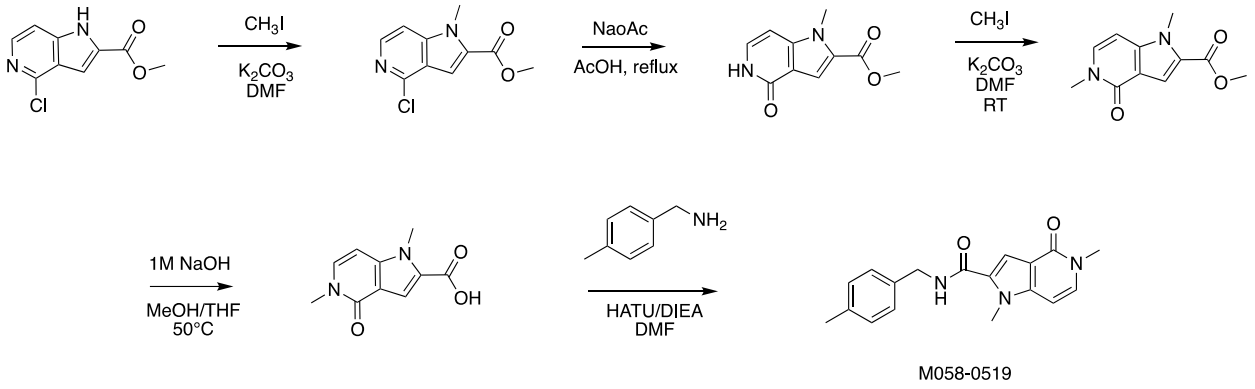
Step 1: A solution of tert-butyl acetoacetate (5 mL, 30.6 mmol) in ethanol was cooled to 0°C in an ice bath. Sodium ethoxide (12.3 mL, 30.6 mmol) was added dropwise for 15 min while stirring. The mixture was added dropwise to a solution of bromopropanone (2.2 mL, 25.4 mmol) in ethanol/toluene (30 mL 2:1) at 0°C with continuous stirring for 4 hours. The reaction pH was adjusted to 7.0 with 1M HCl. The solvent was removed under reduced pressure. 200 mL of EtOAc was added to the mixture and the solid was precipitated. The filtrate was washed with water to neutral pH. The mixture was dried over Na_2SO_4 and purified by silica gel chromatography (0-20%

Hexanes/Ethyl acetate) to afford tert-butyl 2-acetyl-4-oxopentanoate. LCMS (ESI) [M+H]+ calcd for $C_{10}H_{18}O_3^+$: 186.25, found m/z 185.19.

Step 2:Tert-butyl 2-acetyl-4-oxopentanoate (0.47 mmol) in toluene (2.5 mL) was dissolved with 4-aminophenol (0.47 mmol) and p-toluenesulfonic acid monohydrate (0.11 mmol) and stirred under reflux overnight. The reaction was dissolved in water and extracted with EtOAc (3x). Organics were washed with brine, dried, filtered, and evaporated under reduced pressure. The crude was purified by silica gel chromatography to afford *tert*-butyl 1-(4-hydroxyphenyl)-2,5-dimethyl-1*H*-pyrrole-3-carboxylate. LCMS (ESI) [M+H]+ calcd for $C_{17}H_{21}NO_3^+$: 287.15, found m/z 286.14.

Step 3: *Tert*-butyl 1-(4-hydroxyphenyl)-2,5-dimethyl-1*H*-pyrrole-3-carboxylate was stirred in neat 4M HCl in dioxane (5 mL) for 1 hour. The reaction was evaporated under reduced pressure to afford 1-(4-hydroxyphenyl)-2,5-dimethyl-1*H*-pyrrole-3-carboxylic acid. LCMS (ESI) [M+H]+ calcd for $C_{13}H_{13}NO_3^+$: 231.09, found m/z 230.90.

Step 4: 1-(4-hydroxyphenyl)-2,5-dimethyl-1*H*-pyrrole-3-carboxylic acid was dissolved in DMF with morpholine, HATU, and triethylamine. The reaction was stirred at RT for 3 hours. The reaction was dissolved in water and extracted with EtOAc (3x). Organics were washed with brine, dried, filtered, and evaporated under reduced pressure. The crude was purified by silica gel chromatography (50-100% Hexanes/EtoAc) to afford product as a white powder. The final was further purified by HPLC (22.4 mg, 52%). LCMS (ESI) [M+H]+ calcd for $C_{17}H_{20}N_2O_3^+$: 300.09, found m/z 299.15.



Step 1: Methyl 4-chloro-1*H*-pyrrolo[3,2-*c*]pyridine-2-carboxylate and K_2CO_3 were dissolved in DMF. CH_3I was added, and the reaction was stirred at RT for 3 hours. The reaction was diluted in water and extracted with EtOAc (3x). Organics were washed with brine, dried, filtered, and evaporated under reduced pressure. The crude was purified by silica gel chromatography (50-100% Hexanes/EtoAc) to afford product as a white powder. LCMS (ESI) [M+H]+ calcd for $C_{10}H_9ClN_2O_2^+$: 224.04, found m/z 223.04.

Step 2: Methyl 4-chloro-1-methyl-1*H*-pyrrolo[3,2-*c*] pyridine-2-carboxylate and NaOAc were dissolved in AcOH and stirred under reflux overnight. The reaction was poured into ice-cold water, and the product was filtered off as a while solid. LCMS (ESI) [M+H]+ calcd for $C_{10}H_{10}N_2O_3^+$: 206.07, found m/z 206.04.

Step 3: Methyl 1-methyl-4-oxo-4,5-dihydro-1*H*-pyrrolo[3,2-*c*] pyridine-2-carboxylate and K_2CO_3 were dissolved in DMF. CH_3I was added, and the reaction was stirred at RT overnight. The reaction was diluted in water and extracted with EtOAc (3x). Organics were washed with brine, dried, filtered, and evaporated under reduced pressure. The crude was purified by silica gel chromatography (50-100% Hexanes/EtoAc) to afford product as a white powder. LCMS (ESI) [M+H]+ calcd for $C_{11}H_{12}N_2O_3^+$: 220.08, found m/z 219.06.

Step 4: Methyl 1,5-dimethyl-4-oxo-4,5-dihydro-1*H*-pyrrolo[3,2-*c*]pyridine-2-carboxylate was dissolved in 1:1 MeOH/Water. 1M NaOH was added to the reaction, which was stirred at 50°C

overnight. The reaction was acidified with 1M HCl, then diluted in water and extracted with EtOAc (3x). Organics were washed with brine, dried, filtered, and evaporated under reduced pressure to afford product as a white solid. LCMS (ESI) [M+H]+ calcd for $C_{10}H_{10}N_2O_3^+$: 206.20, found m/z 205.07.

Step 5: 1,5-dimethyl-4-oxo-4,5-dihydro-1*H*-pyrrolo[3,2-*c*]pyridine-2-carboxylic acid was dissolved in DMF with *p*-tolylmethanamine, HATU, and triethylamine. The reaction was stirred at RT for 3 hours. The reaction was dissolved in water and extracted with EtOAc (3x). Organics were washed with brine, dried, filtered, and evaporated under reduced pressure. The crude was purified by silica gel chromatography (50-100% Hexanes/EtoAc) to afford product as a white powder. The final was further purified by HPLC (22.4 mg, 52%). LCMS (ESI) [M+H]+ calcd for $C_{18}H_{19}N_3O_2^+$: 309.15, found m/z 308.25.

Compounds were synthesized based on the synthetic routes established above for hit compounds. LCMS and NMR data for derivatives can be found below.

XL-9872-040 series derivatives

XL-9872-040: ^{1}H NMR (500 MHz, DMSO) δ 10.39 (s, 1H), 6.97 (dd, *J* = 8.0, 1.9 Hz, 1H), 6.90 (d, *J* = 1.8 Hz, 1H), 4.09 (q, *J* = 7.1 Hz, 2H), 3.72 (s, 9H), 3.45 – 3.34 (m, 2H), 2.20 – 2.02 (m, 2H), 1.86 (d, *J* = 13.1 Hz, 2H), 1.57 – 1.45 (m, 2H), 1.19 (td, *J* = 7.1, 0.9 Hz, 3H). LCMS (ESI) $[M+H]^+$ calcd for $C_{20}H_{25}N_3O_4^+$ m/z 371.44, found m/z 370.01.

AXA-01-103: ^{1}H NMR (500 MHz, DMSO) δ 10.39 (s, 1H), 6.97 (dd, *J* = 8.0, 1.9 Hz, 1H), 6.90 (d, *J* = 1.8 Hz, 1H), 6.56 (d, *J* = 8.1 Hz, 1H), 4.09 (q, *J* = 7.1 Hz, 2H), 3.72 (s, 9H), 3.45 – 3.34 (m, 2H), 2.68 – 2.59 (m, 1H), 2.20 – 2.02 (m, 2H), 2.04 – 1.95 (m, 1H), 1.86 (d, *J* = 13.1 Hz, 2H),

1.57 – 1.45 (m, 2H), 1.19 (td, *J* = 7.1, 0.9 Hz, 3H). LCMS (ESI) $[M+H]^+$ calcd for $C_{21}H_{27}N_3O_4^+$ m/z 385.46, found m/z 384.26.

AXA-01-117: ^{1}H NMR (500 MHz, DMSO) δ 10.39 (s, 1H), 6.97 (dd, *J* = 8.1, 1.8 Hz, 1H), 6.90 (d, *J* = 1.8 Hz, 1H), 6.56 (d, *J* = 8.1 Hz, 1H), 4.09 (q, *J* = 7.1 Hz, 2H), 4.01 (s, 2H), 3.45 – 3.34 (m, 2H), 2.99 (s, 2H), 2.63 (tt, *J* = 11.0, 3.9 Hz, 1H), 2.20 – 1.86 (m, 6H), 1.57 – 1.45 (m, 2H), 1.19 (t, *J* = 7.1 Hz, 3H), 1.01 (s, 3H). LCMS (ESI) $[M+H]^+$ calcd for $C_{21}H_{27}N_3O_4^+$ m/z 385.46, found m/z 384.26.

AXA-01-157: LCMS (ESI) $[M+H]^+$ calcd for $C_{19}H_{23}N_3O_4^+$ m/z 357.17, found m/z 356.26.

AXA-01-189: ^{1}H NMR (500 MHz, DMSO) δ 10.39 (s, 1H), 6.88 (dd, *J* = 8.1, 1.8 Hz, 1H), 6.81 (d, *J* = 1.9 Hz, 1H), 6.63 (d, *J* = 8.0 Hz, 1H), 4.18 (td, *J* = 7.7, 6.0 Hz, 1H), 4.08 (q, *J* = 7.1 Hz, 3H), 3.80 (dt, *J* = 9.7, 7.2 Hz, 1H), 2.98 (s, 3H), 2.78 (dddd, *J* = 21.4, 11.4, 6.2, 2.6 Hz, 2H), 2.63 (tt, *J* = 11.1, 4.0 Hz, 1H), 1.84 (s, 2H), 1.50 (dtd, *J* = 13.2, 11.4, 4.2 Hz, 2H), 1.19 (t, *J* = 7.1 Hz, 4H). LCMS (ESI) $[M+H]^+$ calcd for $C_{19}H_{23}N_3O_4^+$ m/z 372.19, found m/z 371.26.

AXA-01-203: ^{1}H NMR (500 MHz, DMSO) δ 10.25 (s, 1H), 6.88 – 6.80 (m, 2H), 6.66 (d, *J* = 8.0 Hz, 1H), 6.36 (s, 1H), 4.12 – 4.00 (m, 2H), 2.98 (s, 2H), 2.78 (dddd, *J* = 21.4, 11.4, 6.2, 2.6 Hz, 2H), 2.62 (tt, *J* = 11.1, 4.0 Hz, 1H), 1.86 (d, *J* = 12.9 Hz, 2H), 1.50 (dtd, *J* = 13.1, 11.4, 4.1 Hz, 2H), 1.25 (s, 6H), 1.19 (t, *J* = 7.1 Hz, 3H). LCMS (ESI) $[M+H]^+$ calcd for $C_{20}H_{25}N_3O_4^+$ m/z 387.18, found m/z 386.26.

AXA-02-003: ^{1}H NMR (500 MHz, DMSO) δ 11.27 (s, 1H), 10.47 (s, 1H), 8.05 – 7.99 (m, 2H), 7.29 (d, *J* = 1.8 Hz, 1H), 7.24 – 7.11 (m, 2H), 6.48 (d, *J* = 8.1 Hz, 1H), 4.09 (qd, *J* = 7.2, 4.0 Hz, 8H), 1.89 (dt, *J* = 12.2, 6.1 Hz, 2H), 1.54 (dt, *J* = 21.4, 11.1 Hz, 9H). LCMS (ESI) $[M+H]^+$ calcd for $C_{22}H_{27}N_3O_4^+$ m/z 397.20, found m/z 396.26.

AXA-03-161: LCMS (ESI) $[M+H]^+$ calcd for $C_{23}H_{26}N_2O_4^+$ m/z 394.47, found m/z 393.52.

AXA-02-007: ^{1}H NMR (500 MHz, DMSO) δ 10.25 (s, 1H), 6.88 – 6.80 (m, 2H), 6.66 (d, *J* = 8.0 Hz, 1H), 6.36 (s, 1H), 4.12 – 4.00 (m, 4H), 2.98 (s, 2H), 2.62 (tt, *J* = 11.1, 4.0 Hz, 1H), 1.86 (d, *J* = 12.9 Hz, 2H), 1.50 (dtd, *J* = 13.1, 11.4, 4.1 Hz, 2H), 1.25 (s, 6H), 1.19 (t, *J* = 7.1 Hz, 3H). LCMS (ESI) $[M+H]^+$ calcd for $C_{19}H_{25}N_3O_4^+$ m/z 359.18, found m/z 358.26.

AXA-02-197: LCMS (ESI) $[M+H]^+$ calcd for $C_{27}H_{31}N_3O_4^+$ m/z 461.56, found m/z 460.26.

AV-51: LCMS (ESI) $[M+H]^+$ calcd for $C_{20}H_{21}N_3O_4^+$ m/z 367.56, found m/z 366.26.

AXA-02-153: ^{1}H NMR (500 MHz, DMSO) δ 10.40 (s, 1H), 7.66 (d, *J* = 7.6 Hz, 1H), 6.96 (dd, *J* = 8.0, 1.9 Hz, 1H), 6.90 (d, *J* = 1.9 Hz, 2H), 6.56 (d, *J* = 8.2 Hz, 2H), 3.83 (dt, *J* = 13.7, 6.8 Hz, 2H), 2.87 (s, 2H), 2.18 – 2.04 (m, 1H), 2.00 (s, 2H), 1.97 – 1.89 (m, 1H), 1.66 (s, 2H), 1.51 (t, *J* = 12.4 Hz, 2H), 1.25 (s, 1H), 1.06 – 0.99 (m, 9H). LCMS (ESI) $[M+H]^+$ calcd for $C_{22}H_{30}N_3O_4^+$ m/z 398.51, found m/z 397.24.

AXA-02-151: LCMS (ESI) $[M+H]^+$ calcd for $C_{21}H_{28}N_3O_4^+$ m/z 384.48, found m/z 397.24.

AXA-02-155: ^{1}H NMR (500 MHz, DMSO) δ 10.40 (s, 1H), 8.53 (t, *J* = 6.3 Hz, 1H), 6.97 (dd, *J* = 8.1, 1.9 Hz, 1H), 6.91 (d, *J* = 1.9 Hz, 2H), 6.56 (d, *J* = 8.1 Hz, 2H), 3.89 (td, *J* = 9.9, 6.3 Hz, 2H), 3.39 (dt, *J* = 8.3, 6.0 Hz, 2H), 2.91 (s, 2H), 2.20 – 1.89 (m, 4H), 1.73 (d, *J* = 12.9 Hz, 2H), 1.52 (q, *J* = 12.2 Hz, 2H), 1.25 (s, 1H), 1.01 (s, 3H). LCMS (ESI) $[M+H]^+$ calcd for $C_{21}H_{25}F_3N_3O_4^+$ m/z 438.45, found m/z 437.54.

AXA-02-173: LCMS (ESI) $[M+H]^+$ calcd for $C_{25}H_{27}ClN_4O_3^+$ m/z 466.59, found m/z 465.18

AXA-02-157: ^{1}H NMR (500 MHz, DMSO) δ 10.39 (s, 1H), 7.66 (d, *J* = 7.9 Hz, 1H), 6.96 (dd, *J* = 8.1, 1.9 Hz, 1H), 6.56 (d, *J* = 8.1 Hz, 1H), 4.09 (s, 3H), 3.50 (d, *J* = 8.1 Hz, 1H), 2.86 (s, 3H), 2.41 – 2.31 (m, 2H), 2.17 – 1.91 (m, 5H), 1.69 (t, *J* = 15.0 Hz, 8H), 1.56 – 1.45 (m, 2H), 1.24 (t, *J*

= 12.5 Hz, 2H), 1.13 (q, *J* = 11.3 Hz, 4H), 1.01 (s, 4H).LCMS (ESI) $[M+H]^+$ calcd for $C_{25}H_{34}N_3O_4^+$ m/z 438.57, found m/z 437.54.

AXA-03-001: LCMS (ESI) $[M+H]^+$ calcd for $C_{20}H_{25}N_3O_4^+$ m/z 371.18, found m/z 370.36

AXA-02-159: ^{1}H NMR (500 MHz, DMSO) δ 10.40 (s, 1H), 7.87 (d, *J* = 4.3 Hz, 1H), 6.96 (dd, *J* = 8.1, 1.9 Hz, 1H), 6.90 (d, *J* = 1.8 Hz, 1H), 6.56 (d, *J* = 8.1 Hz, 1H), 3.39 (dt, *J* = 8.3, 6.0 Hz, 2H), 2.86 (s, 2H), 2.65 – 2.57 (m, 3H), 2.30 (ddt, *J* = 11.5, 7.8, 3.9 Hz, 1H), 2.20 – 1.89 (m, 4H), 1.67 (d, *J* = 12.9 Hz, 2H), 1.49 (q, *J* = 12.2 Hz, 2H), 1.01 (s, 3H), 0.60 (td, *J* = 6.9, 4.8 Hz, 2H), 0.40 – 0.34 (m, 2H). LCMS (ESI) $[M+H]^+$ calcd for $C_{22}H_{28}N_3O_4^+$ m/z 396.22, found m/z 395.54.

AXA-02-167: LCMS (ESI) $[M+H]^+$ calcd for $C_{25}H_{28}N_3O_4^+$ m/z 432.52, found m/z 431.51.

AXA-02-161: ^{1}H NMR (500 MHz, DMSO) δ 10.41 (s, 1H), 9.67 (s, 1H), 8.13 (t, *J* = 5.7 Hz, 1H), 6.96 (dd, *J* = 8.1, 1.9 Hz, 1H), 6.90 (d, *J* = 1.8 Hz, 1H), 6.56 (d, *J* = 8.1 Hz, 1H), 3.97 (dd, *J* = 22.5, 10.1 Hz, 2H), 3.64 (t, *J* = 12.2 Hz, 2H), 3.14 (d, *J* = 29.7 Hz, 3H), 2.92 (s, 2H), 2.45 – 2.36 (m, 1H), 2.19 – 1.90 (m, 4H), 1.75 (d, *J* = 13.1 Hz, 2H), 1.01 (s, 3H). LCMS (ESI) $[M+H]^+$ calcd for $C_{25}H_{25}N_3O_4^+$ m/z 469.27, found m/z 468.51

AXA-02-163: ^{1}H NMR (500 MHz, DMSO) δ 10.40 (s, 1H), 7.87 (s, 1H), 6.96 (dd, *J* = 8.1, 1.9 Hz, 1H), 6.90 (d, *J* = 1.9 Hz, 1H), 6.56 (d, *J* = 8.2 Hz, 1H), 3.44 – 3.35 (m, 1H), 3.23 (d, *J* = 6.3 Hz, 2H), 2.96 (d, *J* = 45.1 Hz, 3H), 2.76 (s, 3H), 2.55 (s, 11H), 2.43 – 2.34 (m, 1H), 2.18 – 1.90 (m, 3H), 1.71 (d, *J* = 12.9 Hz, 2H), 1.50 (q, *J* = 12.1 Hz, 2H), 1.01 (s, 3H). LCMS (ESI) $[M+H]^+$ calcd for $C_{26}H_{36}N_6O_3^+$ m/z 482.63, found m/z 481.47

AXA-02-171: LCMS (ESI) $[M+H]^+$ calcd for $C_{22}H_{25}N_5O_3S^+$ m/z 439.17, found m/z 438.47

AXA-02-165: ^{1}H NMR (500 MHz, DMSO) δ 10.41 (s, 1H), 9.41 (s, 1H), 8.10 (t, *J* = 5.7 Hz, 1H), 6.96 (dd, *J* = 8.1, 1.9 Hz, 1H), 6.90 (d, *J* = 1.9 Hz, 1H), 6.56 (d, *J* = 8.1 Hz, 1H), 3.20 (q, *J* = 6.1 Hz, 2H), 3.02 (t, *J* = 9.2 Hz, 2H), 2.92 (s, 2H), 2.55 (s, 11H), 2.45 – 2.37 (m, 1H), 2.20 – 2.04 (m,

2H), 2.02 (t, *J* = 7.3 Hz, 2H), 1.97 – 1.90 (m, 1H), 1.90 – 1.82 (m, 1H), 1.75 (d, *J* = 13.0 Hz, 2H), 1.51 (q, *J* = 12.3 Hz, 2H), 1.01 (s, 3H). LCMS (ESI) $[M+H]^+$ calcd for $C_{25}H_{35}N_5O_3^+$ m/z 453.59, found m/z 452.17

AXA-02-175: ^{1}H NMR (500 MHz, DMSO) δ 10.40 (s, 1H), 7.87 (s, 1H), 6.96 (dd, *J* = 8.1, 1.9 Hz, 1H), 6.90 (d, *J* = 1.9 Hz, 1H), 6.56 (d, *J* = 8.2 Hz, 2H), 3.44 – 3.35 (m, 2H), 3.23 (d, *J* = 6.3 Hz, 2H), 2.96 (d, *J* = 45.1 Hz, 3H), 2.76 (s, 3H), 2.43 – 2.34 (m, 2H), 2.18 – 1.90 (m, 3H), 1.71 (d, *J* = 12.9 Hz, 2H), 1.50 (q, *J* = 12.1 Hz, 2H), 1.01 (s, 3H). LCMS (ESI) $[M+H]^+$ calcd for $C_{28}H_{29}N_5O_3^+$ m/z 483.23, found m/z 482.28

AXA-03-013: LCMS (ESI) $[M+H]^+$ calcd for $C_{18}H_{21}N_3O_4^+$ m/z 343.15, found m/z 342.16

AXA-02-203: LCMS (ESI) $[M+H]^+$ calcd for $C_{21}H_{28}N_3O_4^+$ m/z 384.22, found m/z 342.16

AXA-02-145: ^{1}H NMR (500 MHz, DMSO) δ 10.42 (s, 1H), 6.95 (dd, *J* = 8.1, 1.9 Hz, 1H), 6.86 (d, *J* = 1.8 Hz, 1H), 6.56 (d, *J* = 8.1 Hz, 1H), 4.09 (q, *J* = 7.1 Hz, 2H), 3.50 (dt, *J* = 8.8, 4.9 Hz, 1H), 3.39 (td, *J* = 9.1, 5.2 Hz, 2H), 2.99 (s, 3H), 2.63 (tt, *J* = 11.1, 4.0 Hz, 1H), 2.15 – 1.90 (m, 3H), 1.86 (d, *J* = 13.1 Hz, 2H), 1.57 – 1.35 (m, 4H), 1.19 (t, *J* = 7.1 Hz, 4H), 0.76 (t, *J* = 7.5 Hz, 3H). LCMS (ESI) $[M+H]^+$ calcd for $C_{22}H_{29}N_3O_4^+$ m/z 399.49, found m/z 398.38

AXA-02-149: LCMS (ESI) $[M+H]^+$ calcd for $C_{19}H_{23}N_3O_4^+$ m/z 357.17, found m/z 356.27

AXA-03-023: ^{1}H NMR (500 MHz, DMSO) δ 10.41 (s, 1H), 7.00 (dd, *J* = 8.1, 1.9 Hz, 1H), 6.92 (d, *J* = 1.9 Hz, 2H), 6.59 – 6.51 (m, 2H), 3.45 (s, 4H), 3.10 – 3.01 (m, 4H), 2.20 – 2.10 (m, 3H), 1.97 – 1.90 (m, 2H), 1.24 (s, 2H), 1.05 – 0.98 (m, 6H). LCMS (ESI) $[M+H]^+$ calcd for $C_{20}H_{27}N_5O_3^+$ m/z 386.49, found m/z 385.38

AXA-03-025: LCMS (ESI) $[M+H]^+$ calcd for $C_{20}H_{23}N_5O_4S^+$ m/z 397.16, found m/z 396.39

AXA-03-033: LCMS (ESI) $[M+H]^+$ calcd for $C_{22}H_{29}N_3O_4^+$ m/z 399.49, found m/z 398.24

AXA-03-031: ^{1}H NMR (500 MHz, DMSO) δ 10.39 (s, 1H), 7.13 (ddd, *J* = 8.1, 1.9, 1.1 Hz, 1H), 7.05 (dd, *J* = 3.7, 1.9 Hz, 1H), 6.55 (d, *J* = 8.2 Hz, 2H), 4.10 (s, 3H), 3.66 (t, *J* = 6.7 Hz, 2H), 3.54 (s, 2H), 3.46 – 3.35 (m, 2H), 3.16 (s, 2H), 2.20 – 2.02 (m, 2H), 2.00 (dd, *J* = 9.4, 4.9 Hz, 2H), 1.97 – 1.89 (m, 2H), 1.01 (d, *J* = 1.3 Hz, 3H). LCMS (ESI) $[M+H]^+$ calcd for $C_{20}H_{25}N_3O_4^+$ m/z 371.44, found m/z 370.39

AXA-03-035: LCMS (ESI) $[M+H]^+$ calcd for $C_{21}H_{28}N_4O_3^+$ m/z 384.48, found m/z 383.44

AXA-03-029: ^{1}H NMR (500 MHz, DMSO) δ 10.39 (s, 1H), 6.96 (dd, *J* = 8.1, 1.8 Hz, 1H), 6.90 (d, *J* = 1.8 Hz, 1H), 6.55 (d, *J* = 8.1 Hz, 1H), 3.78 (s, 2H), 3.57 – 3.35 (m, 5H), 3.17 (ddt, *J* = 13.6, 8.8, 3.8 Hz, 2H), 2.19 – 2.09 (m, 2H), 2.06 – 1.89 (m, 2H), 1.84 (d, *J* = 12.7 Hz, 2H), 1.40 (d, *J* = 9.9 Hz, 2H), 1.12 (t, *J* = 7.0 Hz, 3H), 1.01 (s, 3H). LCMS (ESI) $[M+H]^+$ calcd for $C_{20}H_{27}N_3O_3^+$ m/z 357.44, found m/z 356.49.

SB1-B-68 Derivatives

AXA-03-075: ^{1}H NMR (500 MHz, DMSO) δ 9.77 (s, 1H), 7.11 – 7.04 (m, 2H), 6.90 – 6.84 (m, 2H), 5.88 (d, *J* = 1.1 Hz, 1H), 3.51 (t, *J* = 5.5 Hz, 4H), 1.94 (d, *J* = 16.0 Hz, 6H), 1.63 – 1.57 (m, 2H), 1.49 (d, *J* = 4.6 Hz, 3H). LCMS (ESI) $[M+H]^+$ calcd for $C_{17}H_{20}N_2O_2^+$ m/z 284.36, found m/z 283.17.

AXA-03-079: ^{1}H NMR (500 MHz, DMSO) δ 9.78 (s, 1H), 7.09 – 7.03 (m, 2H), 6.91 – 6.84 (m, 2H), 6.10 (d, *J* = 1.0 Hz, 1H), 2.51 (p, *J* = 1.9 Hz, 6H), 2.06 (s, 3H), 1.92 (s, 3H), 1.86 – 1.79 (m, 4H). LCMS (ESI) $[M+H]^+$ calcd for $C_{18}H_{22}N_2O_2^+$ m/z 298.17, found m/z 297.27.

AXA-03-173: LCMS (ESI) $[M+H]^+$ calcd for $C_{17}H_{21}N_3O_2^+$ m/z 299.37, found m/z 298.31.

AXA-03-085: ^{1}H NMR (500 MHz, DMSO) δ 9.78 (s, 1H), 7.11 – 7.04 (m, 2H), 6.91 – 6.84 (m, 2H), 5.90 (d, *J* = 1.1 Hz, 1H), 3.54 (d, *J* = 5.3 Hz, 4H), 2.30 (t, *J* = 5.1 Hz, 5H), 2.20 (s, 3H), 1.97 (s, 3H), 1.92 (s, 3H). LCMS (ESI) $[M+H]^+$ calcd for $C_{18}H_{23}N_3O_2^+$ m/z 313.40, found m/z 312.38.

AXA-03-159: LCMS (ESI) $[M+H]^+$ calcd for $C_{20}H_{20}N_2O_2^+$ m/z 320.39, found m/z 319.25.

AXA-03-081: ^{1}H NMR (500 MHz, DMSO) δ 9.77 (s, 1H), 7.11 – 7.04 (m, 2H), 6.91 – 6.84 (m, 2H), 5.89 (d, *J* = 1.0 Hz, 1H), 4.73 (d, *J* = 4.2 Hz, 1H), 3.13 (s, 2H), 1.94 (d, *J* = 16.7 Hz, 6H), 1.75 (d, *J* = 12.2 Hz, 2H), 1.36 – 1.23 (m, 3H). LCMS (ESI) $[M+H]^+$ calcd for $C_{18}H_{22}N_2O_3^+$ m/z 314.16, found m/z 313.18.

AXA-03-083: ^{1}H NMR (500 MHz, DMSO) δ 9.81 (s, 1H), 7.11 – 7.04 (m, 2H), 6.91 – 6.84 (m, 2H), 5.91 (d, *J* = 1.0 Hz, 1H), 3.83 – 3.77 (m, 4H), 2.64 – 2.58 (m, 4H), 1.96 (s, 3H), 1.93 (s, 3H). LCMS (ESI) $[M+H]^+$ calcd for $C_{17}H_{20}N_2O_2^+$ m/z 316.12, found m/z 315.21.

AXA-04-001: LCMS (ESI) $[M+H]^+$ calcd for $C_{17}H_{20}N_2O_3^+$ m/z 300.35, found m/z 299.32.

AXA-03-131: ^{1}H NMR (500 MHz, DMSO) δ 8.05 (dq, *J* = 7.6, 2.4 Hz, 1H), 7.87 (s, 2H), 7.64 – 7.55 (m, 2H), 3.73 (s, 3H), 3.68 (td, *J* = 3.6, 1.7 Hz, 2H), 2.51 (p, *J* = 1.9 Hz, 3H). LCMS (ESI) $[M+H]^+$ calcd for $C_{14}H_{14}N_2O_3^+$ m/z 258.28, found m/z 257.82.

AXA-03-049: ^{1}H NMR (500 MHz, DMSO) δ 7.59 – 7.51 (s, 1H), 7.35 – 7.29 (m, 2H), 5.98 (d, *J* = 1.0 Hz, 1H), 3.63 – 3.53 (m, 8H), 2.51 (p, *J* = 1.9 Hz, 2H), 2.01 (s, 3H), 1.95 (s, 3H). LCMS (ESI) $[M+H]^+$ calcd for $C_{17}H_{20}N_2O_2^+$ m/z 284.36, found m/z 283.63.

AXA-03-207: LCMS (ESI) $[M+H]^+$ calcd for $C_{16}H_{19}N_3O_3^+$ m/z 301.35, found m/z 300.52.

AXA-03-129: ^{1}H NMR (500 MHz, DMSO) δ 8.07 – 8.00 (m, 1H), 7.64 – 7.56 (m, 2H), 6.03 (d, *J* = 1.1 Hz, 2H), 3.62 – 3.53 (m, 5H), 2.51 (p, *J* = 1.9 Hz, 6H), 2.01 (d, *J* = 22.8 Hz, 3H). LCMS (ESI) $[M+H]^+$ calcd for $C_{18}H_{19}N_3O_2^+$ m/z 309.37, found m/z 308.73.

AXA-03-143: ^{1}H NMR (500 MHz, DMSO) δ 7.93 – 7.86 (m, 1H), 7.66 – 7.60 (m, 1H), 6.04 (s, 2H), 3.63 – 3.56 (m, 6H), 3.50 (q, *J* = 5.2 Hz, 2H), 2.68 (s, 3H), 2.62 (s, 1H), 2.18 (s, 1H), 2.10 (s,

1H), 2.02 (d, *J* = 23.2 Hz, 3H), 1.24 (s, 2H). LCMS (ESI) $[M+H]^+$ calcd for $C_{19}H_{25}N_3O_4^+$ m/z 391.17, found m/z 390.54.

AXA-03-135: ^{1}H NMR (500 MHz, DMSO) δ 8.41 – 8.34 (m, 2H), 7.71 – 7.64 (m, 2H), 6.06 (d, *J* = 1.1 Hz, 1H), 3.63 – 3.53 (m, 9H), 2.04 (d, *J* = 21.6 Hz, 5H). LCMS (ESI) $[M+H]^+$ calcd for $C_{17}H_{19}N_3O_4^+$ m/z 329.14, found m/z 328.41.

AXA-03-157: ^{1}H NMR (500 MHz, DMSO) δ 9.83 (s, 1H), 9.33 (s, 1H), 7.77 – 7.71 (m, 2H), 7.33 – 7.26 (m, 2H), 7.12 – 7.05 (m, 2H), 7.05 – 6.98 (m, 1H), 6.93 – 6.87 (m, 2H), 6.56 (d, *J* = 1.1 Hz, 1H), 2.23 (s, 3H), 1.96 (s, 3H). LCMS (ESI) $[M+H]^+$ calcd for $C_{19}H_{18}N_2O_2^+$ m/z 306.37, found m/z 305.75.

M058-0519 Derivatives

AXA-04-133: ^{1}H NMR (500 MHz, DMSO) δ 7.46 (d, *J* = 7.5 Hz, 1H), 7.34 (d, *J* = 0.8 Hz, 1H), 7.21 (d, *J* = 8.1 Hz, 2H), 7.14 (d, *J* = 8.0 Hz, 2H), 6.61 (dd, *J* = 7.5, 0.8 Hz, 2H), 4.39 (d, *J* = 6.1 Hz, 2H), 3.92 (s, 3H), 3.46 (s, 3H), 2.28 (s, 3H). LCMS (ESI) $[M+H]^+$ calcd for $C_{18}H_{19}N_3O_2^+$ m/z 309.37, found m/z 308.72.

AXA-04-135: ^{1}H NMR (500 MHz, DMSO) δ 2.18 (d, *J* = 7.4 Hz, 1H), 1.48 (s, 1H), 1.33 (d, *J* = 7.4 Hz, 1H), 1.57 (s, 3H), 1.64 (s, 8H), 2.77 (p, *J* = 1.9 Hz, 3H). LCMS (ESI) $[M+H]^+$ calcd for $C_{14}H_{17}N_3O_3^+$ m/z 275.13, found m/z 274.21.

AXA-05-007: ^{1}H NMR (500 MHz, DMSO) δ 8.93 (t, *J* = 6.1 Hz, 1H), 7.46 (d, *J* = 7.5 Hz, 1H), 7.36 (s, 1H), 7.22 (t, *J* = 7.5 Hz, 1H), 7.15 – 7.09 (m, 2H), 7.06 (d, *J* = 7.5 Hz, 1H), 6.61 (d, *J* = 7.3 Hz, 1H), 4.40 (d, *J* = 6.1 Hz, 2H), 3.92 (s, 3H), 3.46 (s, 3H), 2.30 (s, 3H). LCMS (ESI) $[M+H]^+$ calcd for $C_{18}H_{19}N_3O_2^+$ m/z 309.15, found m/z 308.20.

AXA-05-009: ^{1}H NMR (500 MHz, DMSO) δ 8.85 (t, *J* = 5.9 Hz, 1H), 7.46 (d, *J* = 7.5 Hz, 1H), 7.39 (s, 1H), 7.29 – 7.23 (m, 1H), 7.21 – 7.12 (m, 3H), 6.61 (d, *J* = 7.4 Hz, 1H), 4.41 (d, *J* = 5.8

Hz, 2H), 3.92 (s, 3H), 3.47 (s, 3H), 2.55 (s, 1H), 2.33 (s, 2H). LCMS (ESI) $[M+H]^+$ calcd for $C_{18}H_{19}N_3O_2^+$ m/z 309.15, found m/z 308.20.

AXA-05-015: ^{1}H NMR (500 MHz, DMSO) δ 9.07 (t, *J* = 6.1 Hz, 1H), 7.90 (dd, *J* = 8.0, 2.0 Hz, 2H), 7.81 (s, 1H), 7.54 – 7.44 (m, 5H), 7.40 (s, 1H), 6.62 (d, *J* = 7.5 Hz, 1H), 4.61 (d, *J* = 6.0 Hz, 2H), 3.94 (s, 3H), 3.47 (s, 3H). LCMS (ESI) $[M+H]^+$ calcd for $C_{21}H_{19}N_3O_2^+$ m/z 345.15, found m/z 344.20.

AXA-05-017: ^{1}H NMR (500 MHz, DMSO) δ 8.92 (t, *J* = 6.0 Hz, 1H), 7.46 (d, *J* = 7.5 Hz, 1H), 7.35 (dd, *J* = 6.5, 1.9 Hz, 3H), 7.25 (d, *J* = 8.2 Hz, 2H), 6.61 (d, *J* = 7.5 Hz, 1H), 4.39 (d, *J* = 6.0 Hz, 2H), 3.92 (s, 3H), 3.46 (s, 3H), 1.27 (s, 9H). LCMS (ESI) $[M+H]^+$ calcd for $C_{21}H_{25}N_3O_2^+$ m/z 351.19, found m/z 350.21.

AXA-05-019: ^{1}H NMR (500 MHz, DMSO) δ 8.90 (t, *J* = 6.1 Hz, 1H), 7.46 (d, *J* = 7.5 Hz, 1H), 7.33 (s, 1H), 7.28 – 7.22 (m, 2H), 6.93 – 6.86 (m, 2H), 6.60 (d, *J* = 7.4 Hz, 1H), 4.36 (d, *J* = 6.0 Hz, 2H), 3.92 (s, 3H), 3.73 (s, 3H), 3.46 (s, 3H). LCMS (ESI) $[M+H]^+$ calcd for $C_{18}H_{19}N_3O_3^+$ m/z 325.14, found m/z 324.15.

AXA-05-021: ^{1}H NMR (500 MHz, DMSO) δ 9.06 (t, *J* = 6.0 Hz, 1H), 7.81 (d, *J* = 8.2 Hz, 2H), 7.50 (dd, *J* = 22.8, 7.8 Hz, 3H), 7.39 (s, 1H), 6.61 (d, *J* = 7.4 Hz, 1H), 4.51 (d, *J* = 6.1 Hz, 2H), 3.91 (s, 3H), 3.47 (s, 3H). LCMS (ESI) $[M+H]^+$ calcd for $C_{18}H_{16}N_4O_2^+$ m/z 320.13, found m/z 319.13.

AXA-05-065: ^{1}H NMR (500 MHz, DMSO) δ 7.45 (d, *J* = 7.4 Hz, 1H), 6.67 (s, 1H), 6.60 (d, *J* = 7.5 Hz, 1H), 3.68 (s, 3H), 3.58 (t, *J* = 5.5 Hz, 3H), 3.46 (s, 3H), 1.64 (d, *J* = 5.6 Hz, 2H), 1.55 (s, 3H). LCMS (ESI) $[M+H]^+$ calcd for $C_{14}H_{17}N_3O_2^+$ m/z 259.13, found m/z 258.11.

AXA-05-103: ^{1}H NMR (500 MHz, DMSO) δ 8.90 (t, *J* = 6.1 Hz, 1H), 7.46 (d, *J* = 7.5 Hz, 1H), 7.33 (s, 1H), 7.28 – 7.22 (m, 1H), 6.93 – 6.86 (m, 2H), 6.60 (d, *J* = 7.4 Hz, 1H), 4.36 (d, *J* = 6.0

Hz, 2H), 3.92 (s, 3H). LCMS (ESI) $[M+H]^+$ calcd for $C_{15}H_{12}FN_3O_2^+$ m/z 299.11, found m/z 298.18.

AXA-05-077: ^{1}H NMR (500 MHz, DMSO) δ 8.92 (t, *J* = 6.1 Hz, 1H), 7.46 (d, *J* = 7.5 Hz, 1H), 7.34 (s, 1H), 7.21 (d, *J* = 8.0 Hz, 2H), 7.14 (d, *J* = 7.8 Hz, 2H), 6.61 (d, *J* = 7.4 Hz, 1H), 4.39 (d, *J* = 6.0 Hz, 2H), 3.92 (s, 3H), 2.28 (s, 3H), 2.28 (s, 3H). LCMS (ESI) $[M+H]^+$ calcd for $C_{19}H_{21}N_3O_2^+$ m/z 323.16, found m/z 322.23.

AXA-05-079: LCMS (ESI) $[M+H]^+$ calcd for $C_{21}H_{25}N_3O_2^+$ m/z 351.19, found m/z 350.26.

AXA-05-091: ^{1}H NMR (500 MHz, DMSO) δ 8.92 (t, *J* = 6.1 Hz, 1H), 7.46 (d, *J* = 7.5 Hz, 1H), 7.34 (s, 1H), 7.21 (d, *J* = 8.0 Hz, 2H), 7.14 (d, *J* = 7.8 Hz, 2H), 6.61 (d, *J* = 7.4 Hz, 2H), 4.39 (d, *J* = 6.0 Hz, 2H), 3.92 (s, 3H), 2.28 (s, 3H), 2.28 (s, 3H). LCMS (ESI) $[M+H]^+$ calcd for $C_{19}H_{21}N_3O_2^+$ m/z 323.16, found m/z 322.23.

AXA-05-093: LCMS (ESI) $[M+H]^+$ calcd for $C_{26}H_{27}N_3O_2^+$ m/z 413.21, found m/z 412.20.

YL-12826-95: ^{1}H NMR (500 MHz, DMSO) δ 8.92 (t, *J* = 6.1 Hz, 1H), 7.46 (d, *J* = 7.5 Hz, 1H), 7.34 (s, 1H), 7.21 (d, *J* = 8.0 Hz, 2H), 7.14 (d, *J* = 7.8 Hz, 2H), 6.61 (d, *J* = 7.4 Hz, 4H), 4.39 (d, *J* = 6.0 Hz, 2H), 3.92 (s, 3H). LCMS (ESI) $[M+H]^+$ calcd for $C_{17}H_{17}N_3O_2^+$ m/z 295.13, found m/z 294.32.

YL-12826-96: ^{1}H NMR (500 MHz, DMSO) δ 8.97 (t, *J* = 6.1 Hz, 1H), 8.11 (s, 1H), 7.46 (d, *J* = 7.5 Hz, 1H), 7.40 – 7.34 (m, 4H), 7.25 (qd, *J* = 7.1, 4.2 Hz, 1H), 6.61 (d, *J* = 7.5 Hz, 1H), 4.44 (d, *J* = 6.1 Hz, 2H), 4.36 (d, *J* = 5.3 Hz, 1H), 3.93 (s, 3H). LCMS (ESI) $[M+H]^+$ calcd for $C_{17}H_{15}Cl_2N_3O_2^+$ m/z 363.05, found m/z 362.12.

YL-12826-99: ^{1}H NMR (500 MHz, DMSO) δ 8.92 (t, *J* = 6.1 Hz, 1H), 7.47 (d, *J* = 7.4 Hz, 1H), 7.35 (s, 1H), 7.21 (d, *J* = 7.8 Hz, 2H), 7.14 (d, *J* = 7.8 Hz, 2H), 6.62 (d, *J* = 7.4 Hz, 2H), 4.39 (d,

J = 6.0 Hz, 2H), 3.99 – 3.91 (m, 5H), 2.51 (p, *J* = 1.9 Hz, 2H), 1.21 (t, *J* = 7.1 Hz, 3H). LCMS (ESI) $[M+H]^+$ calcd for $C_{19}H_{21}N_3O_2^+$ m/z 323.16, found m/z 322.18.

MS-1337-13: LCMS (ESI) $[M+H]^+$ calcd for $C_{18}H_{18}FN_3O_2^+$ m/z 343.36, found m/z 342.28.

C593-0555: LCMS (ESI) $[M+H]^+$ calcd for $C_{18}H_{18}FN_3O_2^+$ m/z 343.36, found m/z 342.68.

M058-0930: LCMS (ESI) $[M+H]^+$ calcd for $C_{22}H_{21}N_3O_2^+$ m/z 359.16, found m/z 358.18.

M058-0638: LCMS (ESI) $[M+H]^+$ calcd for $C_{21}H_{24}N_4O_2^+$ m/z 364.16, found m/z 363.61.

2.5 Author contributions

I synthesized the XL-9872-040 and SB1-B-68 analogs. Dr. Yanran Liu and I synthesized M058-0519 analogs. I purified and titrated USP8CD. Isabella Jaen-Maisonet and I ran the ubiquitin rhodamine assays and the redox assays. I performed the MST experiments with USP8CD. The target engagement experiments were done by Dr. Anthony Varca.

Chapter 3: A pyrrolo-pyridine motif is a foundational chemotype for DUB inhibition.

3.1. Introduction

We executed a HTS with Novartis against a library of DUBs that are associated with interesting biology and/or had a lack of well validated chemical probes. This led to the development of novel, selective inhibitors of USP25, USP28, and USP30.[70,71] For my thesis work, I focused on the hit-to-lead validation of USP8 targeting compounds. These efforts led to the identification of M058-0519, a compound which features a bicyclic pyrrolo-pyridine as its core scaffold and appeared as a 33μM hit of USP8. A subsequent medicinal chemistry campaign around this pyrrolo-pyridine scaffold led to a modest ~3x fold improvement in potency against USP8. In addition to testing these compounds against USP8, we profiled our compound library against a larger panel of DUBs with an emphasis on USPs, given that the ligandable -pockets are largely conserved in this family and represent promising sites for inhibitor development against the gene family. [72,73]

Based on the results of our screening efforts, we discovered M058-0519 analogs (with disparate structural features) that selectively inhibit USP25/28 and USP4/15. These hits exhibited no redox activity or other apparent compound artifacts (such as autofluorescence or fluorescence quenching). We followed these up with the goal of further improving compound potency as well understanding the SAR trends for each of these DUBs. We used structural information and biochemistry to gain insights into where the compounds bind on each of these proteins. In a panel against 41 other cellular DUBs, YL-12826-4 demonstrated inhibition of USP28 (IC_{50} = 2 μM) values here), while AXA-05-047 demonstrated inhibition of USP4 (IC_{50} = 70 μM).

The hit compound YL-12826-4 was active against both USP28 and USP25. Follow-up compounds were also active against both DUBs. This was not surprising given that USP28 and USP25 share high structural and sequence homology among the entire USP family.[74, 73,75] Both

DUBs contain a large, conserved insertion within their catalytic domains which support distal ubiquitin binding and serve the mediate formation of polymeric forms for each protein,[73,75] making them unique amongst the USP family. Despite sharing an identical overall domain structure, USP25 and USP28 have distinct functions in the cell. USP25 is localized to the cytosol where it has been shown to regulate inflammation pathway and antiviral immune response. USP25 deubiqutinates TRAF3 and TRAF6 regulating downstream effects in both TLR4 and IL-7 signaling pathways.[76, 77, 78] USP25 exerts control over Wnt signaling through interaction with takyrases.[79] USP25 is also found in the endoplasmic reticulum where it plays a role in regulating degradation of misfolded proteins.[80]

USP28 is localized to the nucleus where it regulates DNA damage response and cell cycle progression.[81,82] Genetic knockdown studies have proposed a number of substrates for USP28's activity.[83,84, 85] USP28 was found to stabilize F-box/WD repeat-containing protein 7 (FBW7) and FBW-7 substrates. FBW-7 is an important component of the SKP1-CUL1-F-BOX (SCF)-type E3 ubiquitin ligase complex that targets key transcriptional factors to ubiquitin directed proteosome degradation. Through this activity FBW7 recruits multiple transcription factors including LSD1[86], HIF1α,[40], and c-Myc,[83] which results in their ubiqutination and degradation.[87,88] The role of USP28 in regulating the stability of c-Myc, a historically "difficult-to-drug" protein, makes it a promising drug target. Accordingly, USP28 has been implicated in multiple cancers including intestinal cancer [83,89] and breast cancer.[86] Despite the important biological functions associated with both USP25 and USP28, only a handful of probes have been reported in the literature. Multiple groups including ours, converged on a series of thieonpyridines [90,91,84] which will be discussed in more detail later in this chapter.

The hit compound AXA-05-047 was active against both USP4 and USP15. Follow-up compounds were also active against both DUBs. USP4 and USP15 are identified as paralogs and both share a common domain organization which consists of a DUSP (domain in USP), two UBL (ubiquitin-like), and a bi-part catalytic domain (USP domain)[92]. However, both DUBs have distinct functions in the cell. Depending on the context, USP4 can be localized to the nucleus, cytoplasm, or throughout. In HCC cells, USP4 is expressed only in the cytoplasm, while in Saos-2 cells it is found exclusively in the nucleus.[93] Moreover, USP4 exists as two isoforms which have distinct subcellular localizations. The short isoform is distributed throughout the cell and the long isoform is localized to the cytoplasm. USP4 can activate the WNT/β-catenin signaling pathway by increasing the stability of beta-catenin and promoting its accumulation in the nucleus.[94] USP4 been shown to stabilize ARF-BP1 leading to the reduction of p53 levels.[95] USP4 can also regulate the NF-$\kappa\beta$ signaling pathway by deubiquitinating and stabilizing HDAC2.[96] Given the data suggesting that USP4 can regulate various oncoproteins and signaling pathways, it has been proposed as a therapeutic target in hepatocellular carcinoma and other cancers.

USP15 is localized in both the nucleus and cytoplasm and engages in diverse biological functions. USP15 regulates numerous cellular processes such as spliceosomal regulation, T cell activation, neuroinflammation, antiviral immune response, and DNA repair. [36,97–104] It is also implicated in different cancer-associated mechanism, such as regulating TGF-B dependent oncogenesis in glioblastoma, [36] and promoting breast and ovarian cancer progression by stabilizing ERα and mutant p53. [105–107] Despite the important therapeutic relevance of USP4 and USP15 progress on the development of inhibitors remains slow. Specific and potent probe compounds need to be developed to fully-uncover the therapeutic potential of these DUBs.

I synthesized derivatives following the general protocols established for the resynthesis of the screening hits toward the goal of further improving compound activity to create better probes as well as better understanding the components of each hit important for inhibitory activity. As established earlier in this work, the M058-0519 scaffold is highly chemically accessible. We identified several points of derivatization to assess the importance of each region of the molecule on the observed compound activity. Following the synthetic efforts, compounds were tested in dose-response in a ubiquitin-rhodamine assay to determine IC_{50} values. Compounds were also studied in-house via target engagement and ABPP experiments. The full chemistry efforts and SAR trends are reported below for each DUB hit.

Despite the important roles of USP28 in physiology and disease, the development of potent inhibitors against the enzyme is still in early days. Currently only a handful of USP28 inhibitors have been reported. The first USP28 inhibitor was the benzylic amino ethanol AZ1 (USP28 IC50= 0.7 μM), discovered by AstraZeneca via high throughput screen.[108] In 2021, a team at Forma Therapeutics reported a more potent USP28 inhibitor, FT206 (USP28 IC_{50} in the low nM range). Forma's compounds all share a thienopyridine carboxmidie chemical scaffold with a high degree of selectivity for both USP25 and USP28. Forma Therapeutics also reported a series of closely related thienopyrazines. [109] Peng and colleagues reported a very similar thienopyridine compound, CT1113.[91] Dr. Anthony Varca and Dr. Bin Hu from our own research group reported additional thienopyridine analogs, represented by bin-01-07. Earlier this year, Dr. Xiong and co-workers used a structure-guided approach to synthesize an analog of Vismodegib that showed inhibition of USP28 in the tens of μM range.[110] In our work, screening efforts lead to the identification of new series of USP28 inhibitors based on a previously undisclosed bicyclic pyrrole-pyridine chemical scaffold. In collaboration with the DFCI crystallography core, we previously solved an x-ray

crystal structure of USP28 catalytic domain bound to the literature compound SB1-B-55. We used this structural information to guide our optimization efforts around the M058-0519 bicyclic pyrrole-pyridine core, leading to the rapid development of exquisitely selective, nM range compounds represented by AXA-05-189 and related analogs. Computational docking experiments suggest that AXA-05-189 binds to the distal pocket of USP28, located about 10Å from the catalytic pocket. This pocket is largely unexplored by previously disclosed USP28 inhibitors. Our results also provide valuable proof-of-concept for our DUB targeting approach, wherein the derivatization of a single scaffold can lead to the selective inhibition of disparate DUBs.

3.2. Results

3.2.1 Ubiquigent profiling revealed selective M058-0519 series hits of USP28 and USP25

The hit compound, YL-12826-4 was discovered during a screen of our in-house library of M058 analogs synthesized by Dr. Yanran Liu and myself (Figure 3.1). This compound is a bicyclic pyrrolo-pyridine, with ethyl groups coming off the nitrogens, and a benzo dioxol group at the carboxamide position. That dioxy group was attached to the core to increase the solubility, polarity, and molecular weight of the parent compound. YL-12826-4 showed no inhibition of other DUBs in the panel. Following the screen, the compound was tested in Ub-Rho where it showed a modest IC_{50} of 2.2 uM.

3.2.2 Computational docking studies of YL-12826 and USP28

A co-crystal structure of the USP28 was discovered because of a close collaboration between our group and the crystallography core at the Dana Farber. Studying SB1-B-55, the carboxmide bears a strong resemblance to the carboxamide on YL-12826-4. Given this structural resemblance, we used the available structural information to guide a computational docking study of YL-12826-4 binding to the same pocket in USP28 (the distal pocket is several angstroms from

the catalytic site). There is remarkable overlap between the YL-4 and SB1-B-55 in our predicted model (Figure 3.3A). The bicyclic pyrrolo-pyridine and thienopyridines overlap almost perfectly, and both engage in π-π stacking interactions. The amide nitrogen on both cores make a key H-bonding interaction with a nearby Glu366. Both the thienopyrazine and the bicylic pyrdinone make van der Waals interactions with Val176, Leu180, Thr260, His261, Leu264, Met288, Phe292, Leu590, Cys644, and Met646. The phenyl-8-azabicyclo[3.2.1]octane group is making contacts with Val256, Ser257, Phe370, Lys381, His592, Ala596, and Tyr601, as well as a T-π interaction with Tyr643. Given that, we hypothesized that extending the tail on YL-4 to an ethyl dimethoxy would allow for better π-π stacking interactions with Tyr601 and Tyr64.

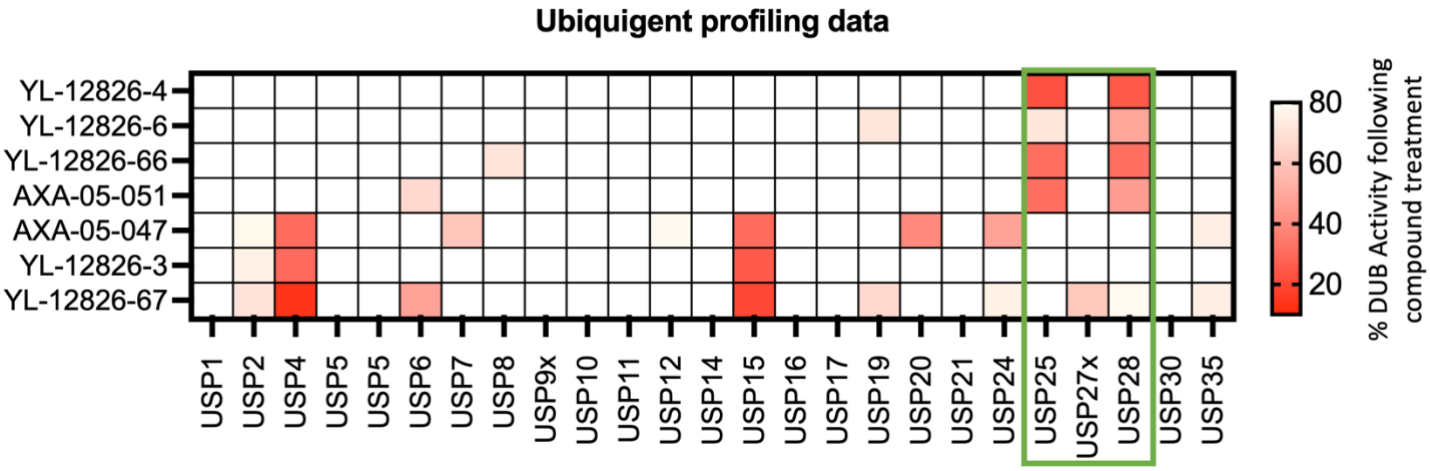


Figure 3.1. Ubiquigent profiling reveals M058-0519 analogs that are selective USP28 and USP25 hits.

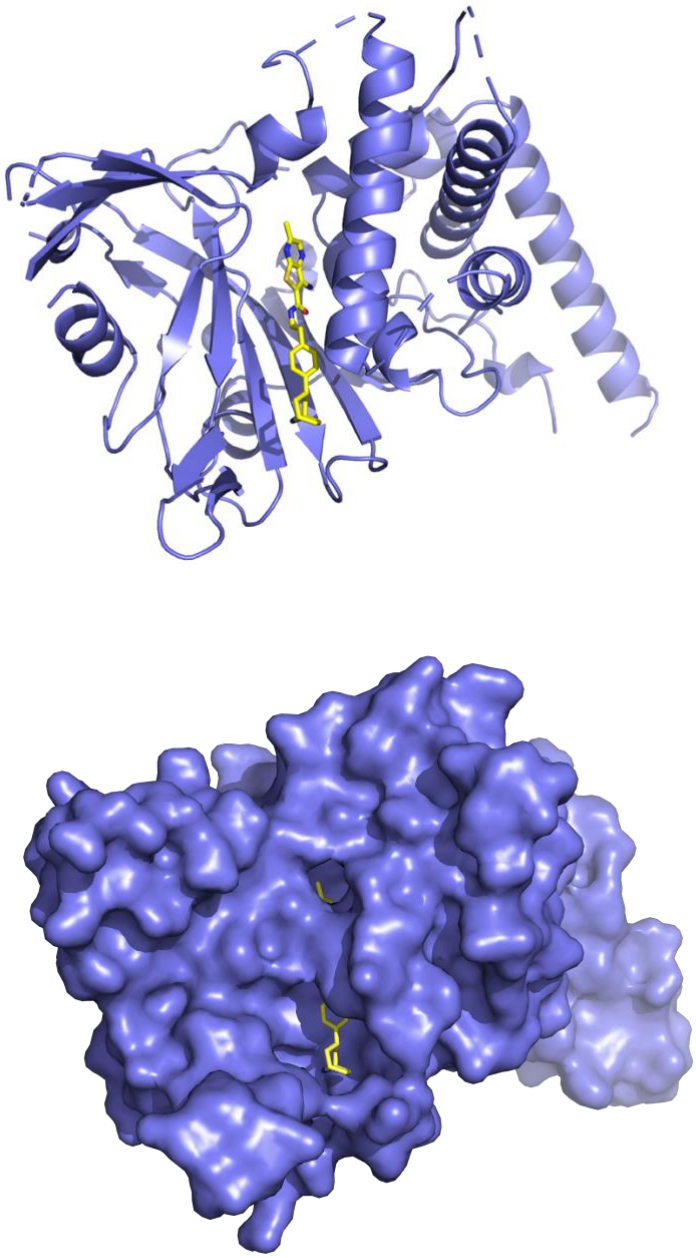
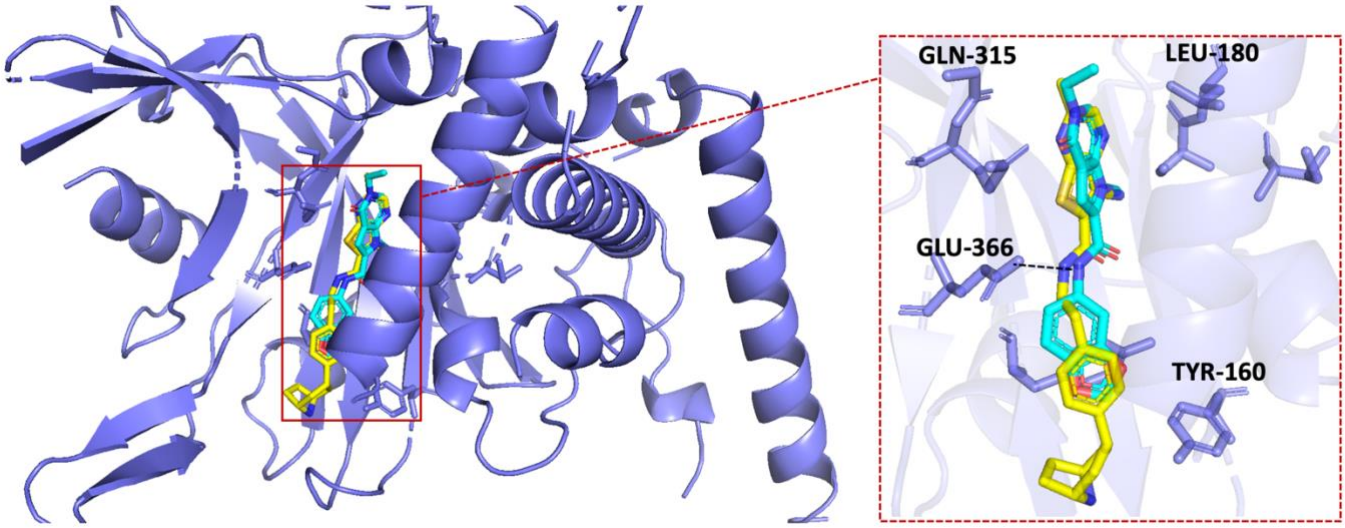


Figure 3.2. USP28 crystallography. Crystal structure of USP28 (blue) with Forma Therapeutic's compound SB1-B-55 (Yellow), obtained by the DFCI Crystallography Core. We used this structure to guide our follow-up chemistry efforts around the YL-12826-4 hit compound (PDB:7TUO).

A)



B)

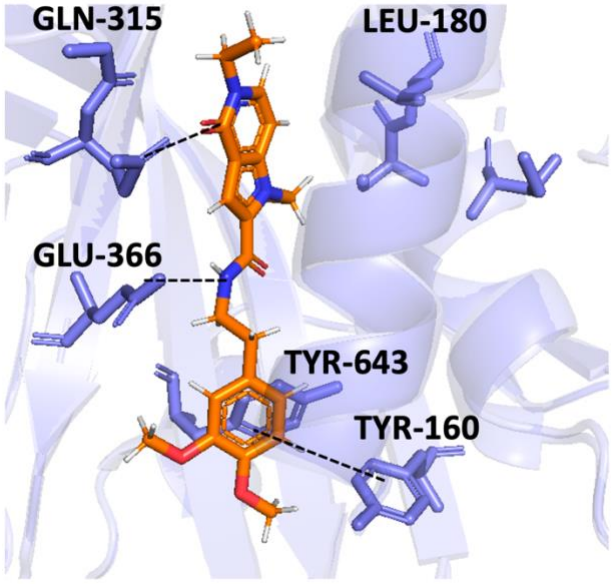


Figure 3.3. Computational insights from the USP28 co-crystal structure.
A) Our computational model predicts that YL-12826-4 and SB1-B-55 bind in the same (distal) pocket of USP28. The bicylic cores from both scaffolds assumed almost identical poses in the binding pocket. The amide nitrogens from both scaffolds are predicted to engage in strong H-bonding interactions with a GLU-366.
B) Changing the cyclic acetal to a dimethoxyphenethylamine improved potency ~120 fold. Our model suggests that this improvement is driven by the fact that the phenyl on the tail end of the molecule is able to engage in pi-pi stacking interactions with tyrosines -160 and -643.

3.2.3 YL-12826-4 structure activity relationship (SAR) data

In addition to the modeling data, we used examples from the literature and our own in-house SAR to guide our chemistry efforts towards understanding the determinants of potency for YL-12826-4. The dimethoxyphenethylamine analog AXA-05-189 inhibited USP28 with an IC50 of 18 nM, which represented ~200-fold increase in potency relative to the parent compound. Methylation of the amide nitrogen (AXA-06-001, IC50= 485 nM) reduced the potency ~26-fold. This provides experimental validation of our YL-4:USP28 model, which predicted that the amide nitrogen engages in important hydrogen-bonding interactions. Interestingly, a closed-ring analog (AXA-05-191) was weaker by about 10-fold. A close look at the docked structure of AXA-05-189 indicates that the methoxy -CH_3 groups engage in favorable CH_3- π interactions, which become unavailable in the closed-ring analog. Introducing a methoxy piperazine AXA-06-015, improved the potency even further, demonstrating an IC50 of 10 nM in USP28 Ub-Rho experiments. The methoxy functional group provides a convenient handle for the installation of linkers towards making small-molecule degraders of USP25 and USP28. Efforts to degrade these proteins are ongoing in the Buhrlage lab. AXA-06-015 is among the most potent USP28 inhibitors reported to date. A full summary of the SAR trends can be found below.

3.2.4 Additional Ubiquigent profiling of select USP28-active analogs

The compounds AXA-05-189 and AXA-06-015 demonstrated exquisite selectivity for USP28 over the entire panel of DUBs. Following compound treatment at 100 μM of AA-05-189, only 1% of USP28 activity remained. For AXA-06-015, 11% of USP28 activity remained. Aside from the potency observed, the compounds also demonstrated a high degree of selectivity for USP28. Within the entire panel of DUBs at Ubiquigent, only one other DUB, USP25, showed significant inhibition following treatment with USP28 compounds. This result is consistent with

other groups that have reported USP28 inhibitors . As mentioned above, USP25 and USP28 share high sequence homology within their DUB domain and identical domain organization, characterized by a long insertion found only in these two DUBs .[73] USP25 and USP28 branch from the same node on the DUB family tree owing to the high degree of overlap in the amino acid sequence of their catalytic domains. Based on the results of the Ubiquigent profiling, AXA-05-189 and AXA-06-015 show comparable activity for USP25. Despite the lack

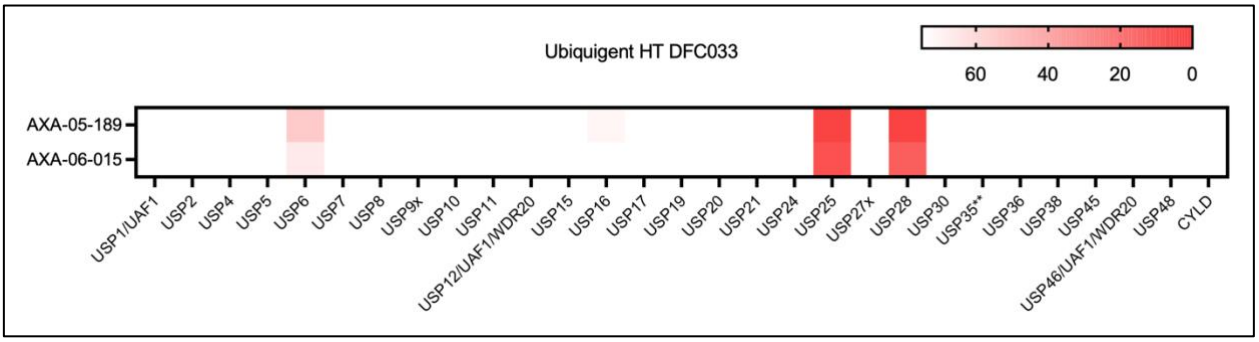


Figure 3.4. **Select analogs are highly selective for USP25/28**. Select hit compounds were assessed for selectivity against an expanded panel of purified recombinant DUBs using DUBProfiler (Ubiquigent). Com pounds were tested at 100 μM. The percent activity of each DUB remaining following compound treatment is reported for each compound.

of selectivity for a single DUB, these dual USP25/28 represent highly potent and selective compounds based on scaffold that is distinct from those previously reported in the literature.

3.2.5 Orthogonal validation of USP28 inhibitors by Activity-Based Protein Profiling (ABPP)

As a next step in the characterization of these compounds, competitive activity-based protein profiling (ABPP) coupled with quantitative mass spectrometry was used to confirm target binding to native enzyme in a cellular environment and further assess probe selectivity (**Figure 3.4**).[111] In these experiments, HEK293T lysates were treated with inhibitor at 250 μM or DMSO as a control. Following compound incubation, the lysates were co-incubated with ubiquitin-based probes which irreversibly label the catalytic cysteine reside of DUBs. A 1:1 mixture of biotinylated ubiquitin-propargylamine (Ub-PA) and biotinylated ubiquitin-vinyl methyl ester (Ub-VME) was

used. A signal is observed when compound inhibition prevents the probes from labeling the catalytic cysteine, resulting in unlabeled DUBs. A biotin tag attached to the probe enables affinity purification with streptavidin beads and enrichment of DUBs in lysate that are bound by activity-based probes. Samples are further processed by tryptic digest, TMT labeling, and peptide sequencing by liquid-chromatography-tandem mass spectrometry resulting in identification of all DUBs contained within the sample.

Table 3.1. SAR studies of M058-0519 analogs against USP28. Table showing compound ID, structure, and IC_{50} determined in the USP28 Ub-Rho assay.

Table 3.1 (Continued)

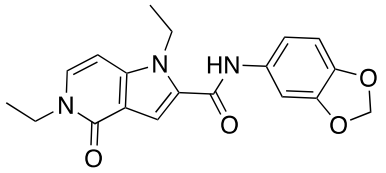
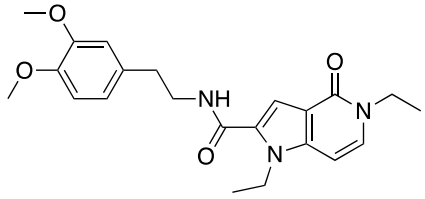
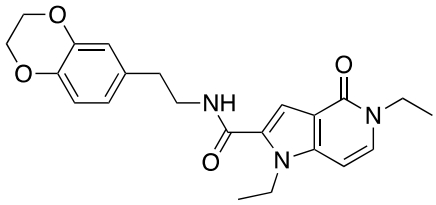
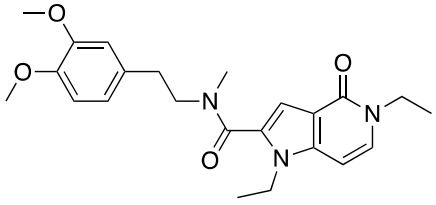
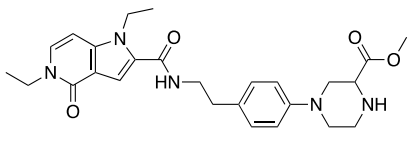
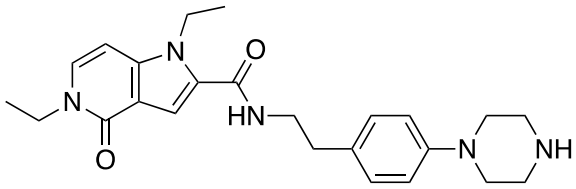
Compound	Structure	USP28 IC50 (nM)
YL-12826-4		2200
AXA-05-189		18
AXA-05-191		150
AXA-06-001		485
AXA-06-015		10

Table 3.1 (Continued)

AXA-06-017		12.6

DMSO control samples are compared to inhibitor treated samples. DUBs that are present in the DMSO control sample but not in the compound treated sample sampled indicates that compounds prevented labeling by the activity-based probes. Comparison of the compound and DMSO treated samples also allows for the calculation of the percent blockage (of probe labeling) value, which is reported for each compound against each DUB detected using the specific activity-based probe mixture. A higher percent blockage of probe labeling means that the compound is better able to block the binding of the activity-based probe to the DUB. The activity-based probes are not able to label all cellular DUBs thus a complete picture of selectivity cannot be obtained from this experiment. In this ABPP experiment, we detected ~60 DUBs distributed across most of the DUB families, which provided us with sufficient coverage to broadly assess activity and selectivity. SB1-B-55 (a potent, noncovalent USP28 inhibitor discovered by Forma Therapeutics) was used as a positive control for the experiment. **Figure 3.5** shows a heatmap of the results of the ABPP experiment for specific compounds.

The original hit compound, YL-12826-4, showed no activity against USP25 or USP28 in the experiment despite these DUBs being detected by ABPP. YL-12826-4 did in fact show inhibition of USP28 in our in-house Ub-Rho assays and at Ubiquigent. The discrepancy could be contributed to multiple factors. As the ABPP assay takes place in cellular lysate, compounds maybe be subject to degradation by other activity enzymes in within the lysate.

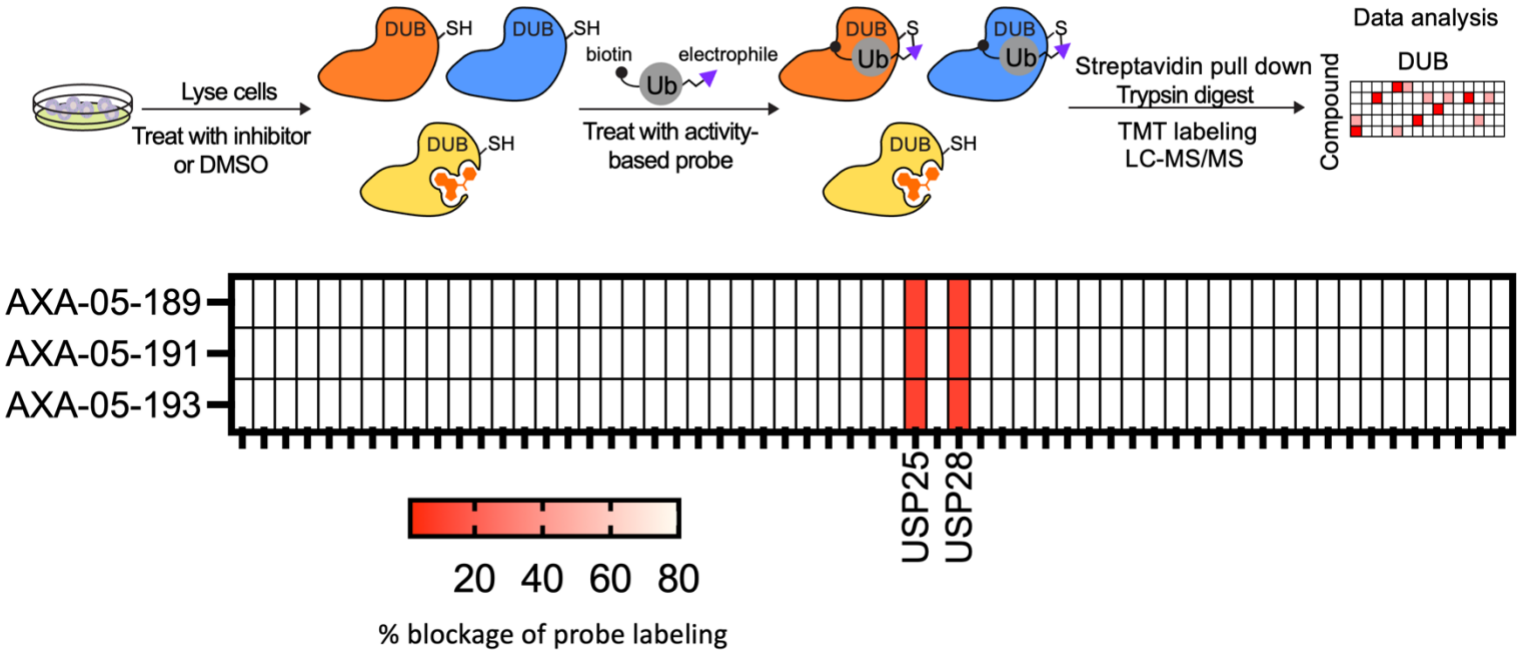


Figure 3.5. ABPP studies with AXA-05-189, -191, and -193. This lysate-based experiment detects over 60 DUBs. For each DUB detected, comparison of inhibitor treated samples to DMSO results in a differential percentage of DUB detected between both cases. This is expressed as % blockage of probe labeling. The darker red means the compound is binding to that DUB preventing the probe from binding. The USP28 inhibitors profiled in this experiment show exquisite selectivity among all the DUBs profiled.

Nonspecific binding of YL-12826-04 to other proteins may prevent it from being available in high enough concentrations to bind and inhibit its target DUB. Another reason for the lack of on-target inhibition could be attributed to ABPP's reliance on covalent bond formation between DUBs and activity-based probes, in which case non-covalent inhibitors (such as YL-12826-04) would need to be very potent to compete with the covalent labeling event. A likely scenario is that YL-4 can bind to and dissociate from USP28 in lysate, whereas the activity-based probes can irreversibility label the catalytic cysteine, resulting in little to no blockage. Thus, it is possible that the lack of activity against any DUBs demonstrated by YL-4 could be due to multiple different factors, despite the results seen in purified DUB assays.

The dual USP25/28 inhibitors AXA-05-189 and AXA-05-191 showed robust on-target inhibition with very little off-target effects. Consistent with the results from out ubiquitin-rhodamine assays, AXA-05-189 showed a higher percent blockage compared to the closed-ring analog AXA-05-191. SB1-B-55 represent a dual USP25/28 inhibitor reported in the patent literature by Forma Therapeutics. In our kinetic ubiquitin-rhodamine assay it has a IC_{50} value of 65 nM against USP28, which is in-line with reported values for the compound. SB1-B-55 was included in the ABPP experiment to benchmark AXA-05-189 and AXA-05-191. SB1-B-55 showed roughly equipotent blockage of USP25 and USP28. AXA-05-189 showed more efficient blockage, which highlights that the bicyclic pyrdinone scaffold demonstrates more potent activity in purified enzyme biochemical assays as well as stronger cellular target engagement than SB1-B-55.

3.2.4 M058-0519 analogs selectively inhibit USP4 and USP15

In addition to USP25/28, we identified hit compounds from the M058-0519 series that demonstrate inhibitory activity of USP4 and USP15. Analogs from this series were tested against USP28, as well as profiled against a larger panel of DUBs to as part of our efforts to develop a library of small molecules that targeting DUB S3-S5 and distal pockets. The goal of these screening efforts is to identify new chemotypes for reversible binders to provide starting points for new compounds that target these pockets. As described below, this approach provided strong data and validation of our platform's approach to inhibitor development.

3.2.6 Ubiquigent profiling revealed selective M058-0519 series hits of USP4 and USP15

After YL-12826-67 and other closely related analogs were tested against USP28 in-house, these compounds were sent for broader selectivity profiling at Ubiquigent. Despite their inactivity against USP28, the goal of these efforts was to identify selective scaffolds for interesting cellular DUBs more broadly. As mentioned previously, DUBs are particularly amenable to this approach given that their distal and S3-S5 pocket are largely conserved across families. Compounds were assayed at a single concentration of 100 μM against a panel of 41 DUBs. The percent activity remaining following compound treatment is reported for each compound against each DUB in the panel. The heat map shown in **Figure 3.7** shows the results of the Ubiquigent selectivity profiling.

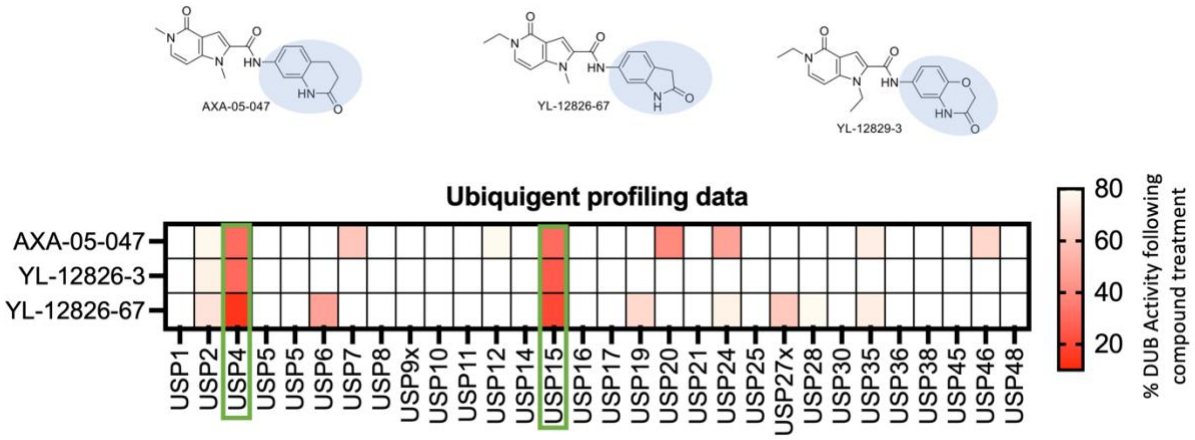


Figure 3.6. Ubiquigent DUBProfiler selectivity profiling revealed selective hits for USP4/15. Compounds were assessed for selectivity against an expanded panel of purified recombinant DUBs using DUBProfiler (Ubiquigent) at 100 μM. The percent activity of each DUB remaining following compound treatment is reported for each compound.

Three of the compounds included in this profiling experiment, AXA-05-047, YL-12826-3, and YL-12826-67 demonstrated high selectivity for USP4 and USP15. Following compound treatment at 100 μM, AXA-05-047 showed 14% of USP4 activity remaining. The close analogs YL-12826-3 and YL-12826-67 showed 29% and 13% USP4 activity remaining, respectively. All three analogs featured a lactam derivative attached directly to the bicylic pyrdinone core via an amide bond. Given this pattern, we observed that these hit compounds represented a good starting point for the development of USP4 inhibitors. In follow-up kinetic ubiquitin-rhodamine experiments, these compounds showed relatively weak IC_{50} values of 60-70 μM. We embarked on a medicinal chemistry campaign with the goal of further improving the potencies by 10-fold. We synthesized a small library of compounds that feature a diversity of lactam analogs, and we succeeded in identifying SAR trends that improved the potency. A full discussion of these efforts is detailed below.

3.2.7 YL-12826-7 structure activity relationship (SAR) data

Following the identification of USP4 hit compounds from our library screen, a medicinal chemistry campaign to establish structure activity relationship trends were initiated. We selected the YL-12826-67 scaffold for optimization. This compound contained two fused rings (pyridinone-pyrrole) with ethyl groups on the core nitrogen atoms, and a carboxamide coming off the pyrrole group. We focused on the carboxamide position for the first round of chemistry, while keeping the rest of the scaffold the same. The carboxylic acid intermediate is easily synthesized and offers a convenient handle for the attachment of a diversity of commercially available amine building blocks. The dixoxy analogs YL-12826-4 and YL-12826-66 were inactive against USP4. The methyl pyrazole analog, represented by YL-12826-6 was also dead. These results suggest that the lactam is required for the activity against USP4. Following these observations, I focused on

changing to size of the YL-12826-68 lactam. The smaller beta lactam was not commercially available. However, I succeeded in synthesizing six- and seven- membered lactams, represented by AXA-05-047 and AXA-05-049. These compounds were active against USP4 and roughly equipotent to the parent compound, suggesting that the USP4 binding pocket tolerates a range of ring sizes. Changing the lactam to a closely related oxazolone ring (YL-12826-3 and AXA-05-161) did not improve or penalize the potency, which further highlights the binding pocket's tolerance of a diversity of rings, including ones with polar heteroatoms. To further emphasize this point, we made an imidazolone, which has a nitrogen in place of the carbon (AXA-05-163) in the ring. This substitution did not appreciably change the potency in either direction. Methylating the lactam nitrogen (AXA-05-165) and removing the ketone from the ring (AXA-05-169) both decreased the potency slightly, but these changes did not ablate activity in our kinetic ubiquitin-rhodamine assays. It appears that the lactam substitution pattern is preferred for activity against USP4, but the lactam ring is not required. Next, we focused on varying the lactam attachment point. Towards this goal I made AXA-05-177, with the amide bonding coming off the 4-position of the phenyl ring (the parent compound has the amide bond on the 6-position of the phenyl ring). Gratifyingly, this subtle change in this region of the compound improved the potency about ten-fold to 7 μM. We hypothesized that changing the direction of the lactam -NH group allows it to engage in favorable hydrogen bonding interactions more efficiently with the either the residues in the binding pocket or nearby water molecules.

Once we identified a favored lactam analog on the right-hand side of the scaffold, we focused on making changes to the left-hand side of the molecule. The pyridine nitrogen offered a convenient handle for the S_n2 mediated addition of diverse alkyl groups. Bromomethyl benzyl groups are particularly amenable to this chemistry. With this approach, I synthesized the

fluorobenzyl analog AXA-05-193 (IC_{50} = 8 μM). While this derivative is still 10 times more potent than the parent compounds, adding an aromatic group did not improve the potency any further. This piece of data shows that there is room to grow on this side of the scaffold, and that the binding pocket can tolerate bulkier aromatic substituents.

To better understand the effects of adding an aromatic group to the core, we revisited the right-hand side of the scaffold and synthesized the carbamate analog AXA-05-175 (IC_{50} = 8 μM). This result is consistent with our previous observations regarding the identity of the lactam ring, where USP4 tolerates a range of lactam ring sizes and the presence of heteroatoms. Following this result, we decided to continue to focus on the left-hand side by synthesizing a 2,4-difluoro derivative (AXA-06-009, IC_{50} = 6.4 μM), a trifluoro derivative (AXA-06-011, IC_{50} = 23 μM), and by removing the fluoro group all together (AXA-06-021, IC_{50} = 5.2 μM). A full summary of our chemistry efforts are summarized in the table below.

Table 3.2. SAR studies of M058-0519 analogs against USP4. Table showing compound ID, structure, and IC_{50} determined in the USP28 Ub-Rho assay.

Table 3.2 (Continued)

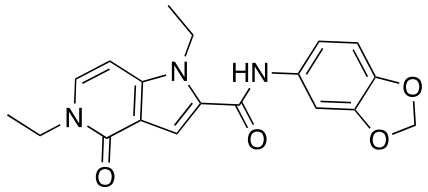
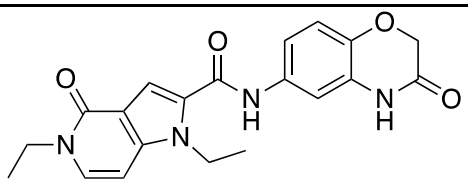
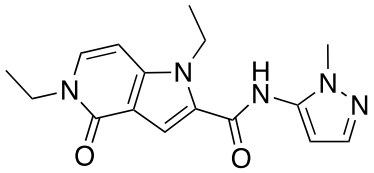
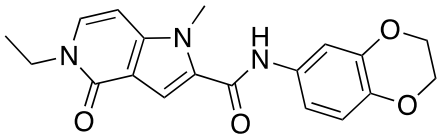
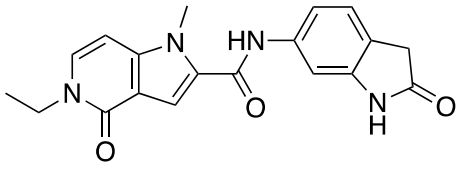
Compound	Structure	USP4 IC50 (μM)
YL-12826-4		> 100
YL-12826-3		69
YL-12826-6		> 100
YL-12826-66		> 100
YL-12826-67		40

Table 3.2 (Continued)

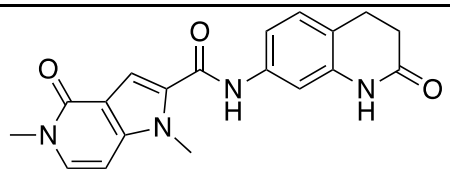
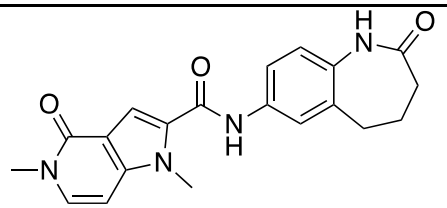
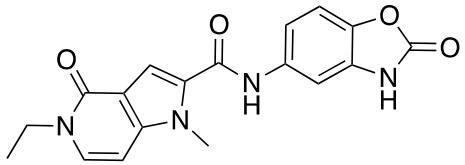
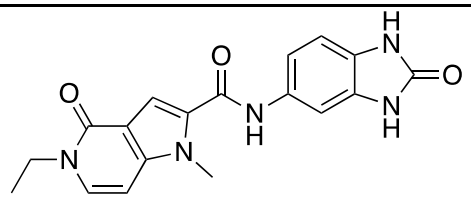
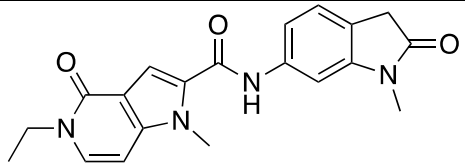
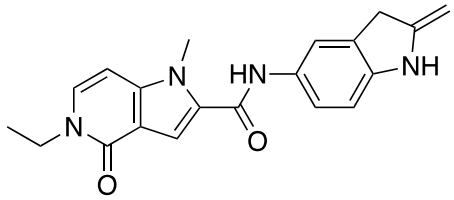
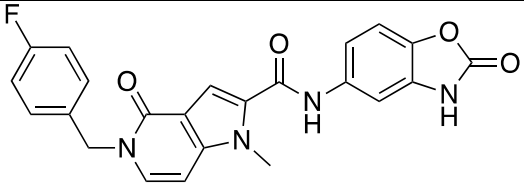
AXA-05-047		70
AXA-05-049		75
AXA-05-161		70
AXA-05-163		70
AXA-05-165		100
AXA-05-169		100
AXA-05-175		8.5

Table 3.2 (Continued)

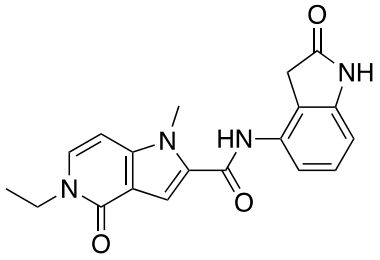
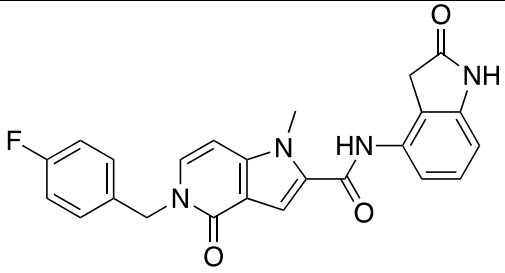
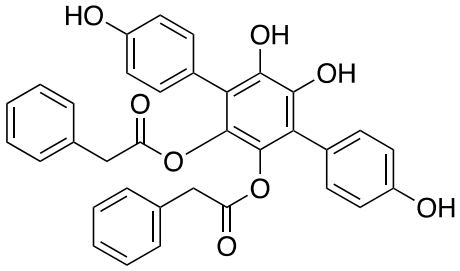
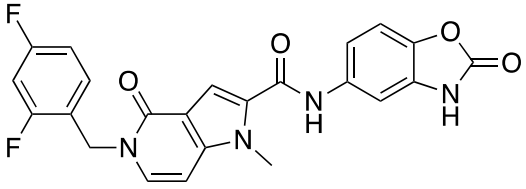
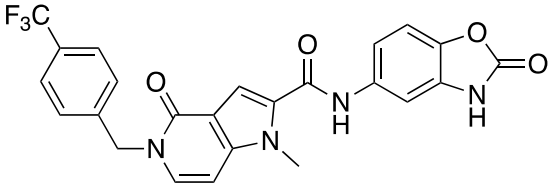
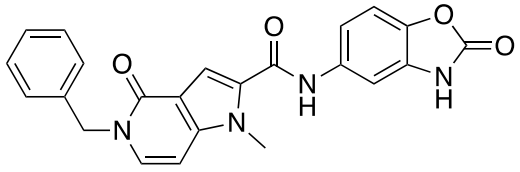
AXA-05-177		7
AXA-05-193		8
Vialinin A		8
AXA-06-009		6.4
AXA-06-011		23

Table 3.2 (Continued)

AXA-06-021		5.2

3.2.7 An alignment of the USP28 and USP4 distal pockets reveals further insights into selectivity.

Using the published crystal structures of USP28 (PDB: 7TUO) and USP4 (PDB: 2Y6E), we performed an alignment of the distal pockets to gain insights into how to further improve the potency and selectivity of the M-series analogs. The pockets are largely conserved (which is unsurprising given that both proteins are both members of the USP family) but we observed some important differences. The basic residue Q315 in USP28 is a tyrosine in USP4. The acidic residue E366 is a basic histidine in USP4. Finally, the basic H261 residue is an alanine in USP4. For the potent M-series analogs that bind to USP28, the E366 provides critical H-bonding with the amide group present on the scaffold (methylating this amide reduces the activity 1,000-fold). This residue is replaced by a basic histidine in USP4. Future medicinal chemistry efforts will focus on replacing the amide moiety with a functional group that is better able to engage in hydrogen-accepting interactions with this histidine, towards making more potent USP4 inhibitors.

3.3 Discussion

Our work led to the discovery of a novel scaffold for the dual inhibition of USP25/28. From a structural point of view, our compounds are distinct from those reported previously reported in the literature. We used the crystal structure of USP28, obtained by the DFCI crystallography core, to gain insights into the binding mode of AXA-05-189. 189 is one of only a handful of structure

of inhibitors bound in this distal pocket found within the USP family of DUBs. Through *in vitro* profiling at Ubiquigent, and ABPP experiments in-house, we observed that 189 and related analogs are exquisitely selective for USP25/28. Cell-based target engagement experiments are in progress in to better characterize target binding. Follow-up efforts also include using USP28 inhibitors as a starting point for the development of proteolysis targeting chimeras (PROTACs).

Medicinal chemistry efforts around the bicylic pyrrolo-pyridine scaffold led to development of a novel chemical series for the inhibition of USP4 and USP15. Progress in the development of USP4 inhibitors remains is in its early stages, with only two compounds reported in the literature so far. Xie et al. isolated the natural product, vialinin A, from Chinese mushroom, and reported the compound as a micromolar inhibitor of USP4. Vialinin A exhibits multiple phenol groups and a highly conjugated ring system that likely makes it a redox-active false positive. Nguyen et al. reported the discovery of neutral red (NR) via a high throughput screen, and reported the compound as a high, double-digit micromolar inhibitor of USP4. NR has not been rigorously profiled against DUBs more broadly to better understand its selectivity. Thus, there remains a considerable need for selective and potent small molecule inhibitors of USP4 to fully elucidate its biology and understand its role in disease.

Our initial hit compound, represented by YL-12826-4, was a selective but relatively weak USP4/15 inhibitor. We successfully improved the potency of this series by over ten-fold, and we generated compounds that inhibit USP4/15 in the low single-digit micromolar range. While selectivity between USP4 and USP15 remains an unresolved issue, the compounds represent the current best in class USP4/15 inhibitors reported in the literature. While generation of USP4 or USP15 selective inhibitors may prove challenging based on their high degree of homology, synthesized derivatives will be tested in dose response against USP15 to confirm inhibitory

activity. At this point, one of the most potent analogs from the series, AXA-05-177, has been submitted for co-crystallization experiments in collaboration with the DFCI crystallography core. Fortunately, USP4 is well-behaved in these experiments, and we have successfully obtained USP4 crystals. Future work involves molecular docking studies and protein crystallography to gain a detailed understanding of how the compounds are binding in the pocket, and how they can be further optimized for potency. From the SAR obtained from these experiments, any model or co-crystal structure can be checked against biochemistry results to provide validation.

In this work, we established the bicylic pyrrolo-pyridine series as a "foundational chemotype" for the development of DUB inhibitors. We define a foundational chemotype as a DUB binding scaffold that: i) contains at least one exemplar compound that inhibits its primary DUB target with an IC50 < 10 μM and 20-fold selectivity relative to 90% of 50+ other DUBs, ii) binds in one of two non-catalytic pockets conserved across many DUB enzymes and iii) is preferentially represented by multiple analogs which exhibit disparate DUB selectivity patterns. In line with this definition, the pyrrolo-pyridine analog M058-0510 inhibits USP8 with good selectivity against other DUBs. When the 4-methylbenzyl group from M058-0510 was changed to a dimethoxy phenethylamine, the compound showed highly potent and selective inhibition of USP25/28. Finally, when a bicyclic lactam was introduced to the amide position, this gave access to a series of USP4/15 inhibitors. Thus, the bicylic pyrrolo-pyridine is a versatile and privileged scaffold for the inhibition of DUBs. While efforts in the lab are focused on improving the potency of compounds against specific DUBs, work is also being done to introduce large and diverse functionalities to the core scaffold. These compounds will be profiled through Ubiquigent and ABPP to determine if other DUBs of interest can be inhibited with this series.

3.4 Materials and methods

Recombinant protein expression and purification

DUB enzymes (USP4 and USP15) utilized in subsequent validation experiments were purchased directly from Boston Biochem/R&D Systems.

Ubiquitin-Rhodamine110 Kinetic Asssay

USP4 was tested for its respective activity in the Ub-Rho110 assay in the presence or absence of inhibitors using Nunc™ 384-well plates (Thermo Scientific™ catalog number: 2262260). USP4 was pre-incubated with different concentrations of inhibitors in assay buffer (50 mM Tris pH 8, 50 mM NaCl, 0.002% Tween-20, 5 mM DTT). Compounds and protein were incubated for 30 minutes at room temperature prior to the addition of Ub-Rho110 (Boston Biochem) substrate. The initial rate of the reaction was measured by collecting fluorescence data at one-minute intervals over 30-minute period using a Clariostar fluorescence spectrometer at excitation and emission wavelengths of 485 nm and 535 nm respectively. The calculated initial rate values (V_0) were normalized to plate control wells and were plotted as a function of inhibitor concentrations to determine IC50s. All the experimental data were plotted using GraphPad Prism (log(inhibitor) vs. normalized response – Variable slope, least squares fit).

In Vitro DUB Selectivity Profiling

Compounds were screened using the Ubiquigent DUBProfilerTM SPT system (www.ubiquigent.com/drug-discovery-services/dubprofiler/). Each of 41 purified DUBs was incubated with compound for 15 minutes, then Ub-Rho110 was added and fluorescence was recorded. Percent inhibition was determined based on fluorescence relative to a DMSO control. An autofluorescence control experiment determines the fluorescence signal generated by the compound at screening concentration in absence of enzyme relative to the enzyme and no enzyme

control for each of the DUBs in the panel. A product signal modulation (PSM) control experiment determines the fluorescence signal generated by the compound (at screening concentration) in the presence of synthetic rhodamine 110 glycine (the product of enzymatic cleavage of the DUBProfilerTM Ub-Rho substrate) and DUBProfilerTM substrate (at standard assay concentration) expressed as a percentage relative to the fluorescence signal of synthetic rhodamine 110 glycine and DUBProfilerTM substrate (at standard assay concentration). Autofluorescence and PSM data can indicate autofluorescence (positive %) or quenching (negative %) of background signal and/or assay signal.

Quantitative Activity-Based Protein Profiling

DUB activity based protein profiling was performed using conditions modified from those in Schauer[49] based on work by Lawson[112]. HEK293T cells were lysed (50 mM Tris pH 8.0, 150 mM NaCl, 5 mM MgCl2, 0.5 mM EDTA, 0.5% NP-40, 10% glycerol, 1 mM TCEP, protease and phosphatase inhibitors) and the lysate was clarified by centrifugation. Clarified lysate was then diluted to 10 mg/mL. 200 mL aliquots were incubated with 250 µM compound or DMSO for 30 minutes at room temperature. Selective USP25/28 inhibitor SB1-B-55 was included in the run as a positive control. Afterwards, the treated lysates were incubated with 1 mM each of Biotin-Ub-PA and Biotin-Ub-VME for 15 minutes at room temperature. 125 mL magnetic streptavidin sepharose slurry was added to each sample, followed by incubation for 30 minutes with end-to-end rotation at room temperature. After immobilizing the beads using a magnetic rack, the beads were washed (3x 0.2% SDS, 3x PBS, 2x ddH2O). After the final wash, supernatant was removed, and the resin was flash frozen and stored at -80°C. Streptavidin beads were resuspended in 95 mL of 100 mM Tris pH 8.0. Each sample was denatured with 0.1% rapigest, reduced (10 mM dithiothreitol), alkylated (22.5 mM iodoacetamide), and digested with

trypsin at 37 °C overnight. The next day, beads were captured using a magnetic rack, and supernatants were acidified with 10% TFA, incubated at 37o C for 30 minutes, and centrifuged at 14,000 rpm for 15 minutes at 4o C to remove rapigest. Peptides were then desalted by C18 and dried by vacuum centrifugation.

Dried peptides were reconstituted in 40mL 50mM pH 8.0 TEAB, 1/4 unit of TMT reagent was then added, and reactions were incubated at room temperature for 1 hour. TMT reactions were pooled and treated with hydroxylamine according to the manufacturer's instructions. Peptide mixtures were then dried, reconstituted in 100 mM ammonium bicarbonate and desalted by SP3114. Eluted TMT labeled peptides were dissolved in 5% acetonitrile with 100 mM ammonium formate, pH 10, and analyzed by a DEEP-SEQ multidimension peptide fractionation platform115–117 built around a NanoAcquity UPLC system (Waters, Milford, MA) and coupled directly to a timsTOF Pro ion mobility mass spectrometer (Bruker, Billerica, MA)118,119. As described in Fu et. al., each of 11 peptide fractions was eluted from the first dimension reversed phase column (5 cm × 150 µm packed with 5 µm XBridge C18, Waters, Milford, MA) and second dimension anion exchange column (5 cm × 150 µm I.D. fused silica packed with 10 µm POROS 10HQ Applied Biosystems, Foster City, CA) using injections of acetonitrile or ammonium formate at pH 10.0120. Peptide fractions were diluted on-line with solvent A (0.1% formic acid in water) to reduce pH and organic concentration and facilitate retention on the third dimension precolumn (5 cm × 100 µm I.D. fused silica packed with 7 µm Symmetry C18, Waters). Peptides were eluted with an HPLC gradient (6.5-35% B in 120 minutes, A = 0.1% formic acid in water, B = 0.1% formic acid in acetonitrile), resolved on an analytical column (30 µm I.D. × 50 cm Monitor C18, Orochem, Naperville, IL) and introduced to the mass spectrometer by electrospray ionization using a captive spray ion source (spray voltage = 1.8 kV). The mass spectrometer

acquired ion mobility MS spectra over a mass range of m/z 100-1700 and 1/k0 of 0.6 to 1.6, and then performed 10 cycles of PASEF MS/MS with a target intensity of 20k, a threshold of 2500 and a quadrupole isolation width of 1 Da. Active exclusion was enabled with a release time of 0.4 minutes. For TMT reporter ion detection, TIMS stepping function (Ogata and Ishihama, 2020) was used. Briefly, the collision energy was ramped stepwise against the ion mobility: 39.88 eV for 1/k0 0.6-0.83, 46.25 eV for 1/k0 0.83-1.0, 52.50 eV for 1/k0 1.0-1.18, 58.75 eV for 1/k0 1.18-1.35, and 64.63 eV for 1/k0 1.35-1.6. The collision energy for the second step is decreased by 20%. Other settings corresponding to the two-step collision energy include collision RF of 500 and 1500, transfer time of 25 μs and 60 μs, and pre pulse storage time of 8 μs and 12 μs, respectively. Raw data files were converted to mgf using multiplierz scripts121, and searched using Mascot 2.6.1 against a forward and reversed human refseq database (NCBI). Search parameters specified a precursor mass tolerance of 20 ppm, a product ion tolerance of 50 mmu, fixed carbamidomethylation of cysteine, TMT 6-plex labeling of lysine and N-termini, and variable oxidation of methionine. For TMT quantitation, identified peptides were filtered to a peptide score no less than 13 and a false discovery rate of 1%. Pep2gene122 was used to reduce the set of peptides to those which mapped to unique gene identifiers, and then aggregated reporter ions were used to derive a protein-level quantification value.

Chemical Synthesis General Methods and Materials

All commercially available starting materials were purchased from Sigma Aldrich, Fisher Scientific, Oakwood Chemical, and Combi Block. All reagents were used as received without further purification. Anhydrous solvents, such as tetrahydrofuran (THF), dichloromethane (DCM), diethyl ether (Et2O), dimethyl formamide (DMF), dimethylsulfoxide (DMSO), 1,4-dioxane, and toluene were purchased from Fisher Scientific, and used as received. If necessary, air or moisture sensitive reactions were carried out under an inert atmosphere of nitrogen. Removal of solvents

was accomplished on a Büchi R-300 rotary evaporator and further concentration was done under a Welch 1400B-01 vacuum line, and/or Labconco FreeZone 6 plus system. Purification of compounds was performed by normal phase column chromatography using Teledyne CombiFlash chromatography system, and/or reversed phase chromatography on Waters Micromass ZQ preparative system with SunFire® Prep C18 OBD™ 5µM column. The purity was analyzed on Waters Acquity UPLC system. Analytical thin layer chromatography (TLC) plates were purchased from Fisher Scientific (EMD Millipore TLC Silica Gel60 F254). Visualization was accomplished by irradiation under UV light (254 nm).

All 1H-NMR spectra were recorded at 298K on a Bruker ARX 500 (500 MHz) spectrometer. Samples were dissolved in CDCl3, DMSO-d6, or Methanol-d4 obtained from Cambridge Isotope Laboratories. The spectra were referenced to the residual solvent peak (CDCl3: 7.26 ppm for 1H-NMR and 77.16 ppm for 13C-NMR; DMSO-d6: 2.50 ppm for 1H-NMR and 39.25 ppm for 13C-NMR, CD3OD: 3.31 ppm for 1H NMR and 49.00 ppm for 13C NMR or tetramethylsilane (TMS) as the internal standard. Chemical shift, multiplicity (s=singlet, d=doublet, t=triplet, q=quartet, m=multiplet, br=broad peak), coupling constants (Hz), and number of protons were assigned using MestReNova software. Mass spectrometry (LCMS) data were obtained on Waters Acquity UPLC system in positive ESI mode.

Final compounds submitted for testing were prepared and stored as 10 mM stock solutions in DMSO. Stocks were stored at -20°C and aliquoted as needed for specific experiments to reduce the number of freeze thaw cycles. Unless otherwise noted for specific compounds, no apparent solubility issues were observed with the compounds either in DMSO or aqueous buffer conditions at the concentrations used.

Compounds were synthesized based on the synthetic routes established in Chapter 2 for hit compounds. LCMS and NMR data for derivatives can be found below.

YL-12826-3: ^{1}H NMR (500 MHz, DMSO) δ 8.08 (d, *J* = 2.6 Hz, 1H), 7.64 (dd, *J* = 7.2, 1.5 Hz, 2H), 7.52 – 7.41 (m, 3H), 7.26 – 7.15 (m, 3H), 5.76 (s, 2H), 4.73 (s, 1H), 3.13 (s, 3H), 3.05 (d, *J* = 6.1 Hz, 2H), 2.88 (s, 3H). LCMS (ESI) $[M+H]^+$ calcd for $C_{20}H_{20}N_4O_4^+$ m/z 380.40, found m/z 379.84.

YL-12826-6: ^{1}H NMR (500 MHz, DMSO) δ 10.16 (s, 1H), 7.52 (d, *J* = 7.5 Hz, 1H), 7.39 (d, *J* = 2.0 Hz, 1H), 6.68 (d, *J* = 7.5 Hz, 1H), 6.24 (d, *J* = 1.9 Hz, 1H), 4.49 (q, *J* = 7.0 Hz, 2H), 3.97 (q, *J* = 7.1 Hz, 2H), 1.25 (dt, *J* = 23.2, 7.1 Hz, 6H). LCMS (ESI) $[M+H]^+$ calcd for $C_{16}H_{19}N_5O_2^+$ m/z 313.15, found m/z 312.14.

AXA-05-047: ^{1}H NMR (500 MHz, DMSO) δ 10.42 (s, 1H), 10.09 (s, 1H), 7.58 (s, 1H), 7.54 – 7.47 (m, 2H), 7.28 (dt, *J* = 8.1, 1.6 Hz, 1H), 7.14 (d, *J* = 8.1 Hz, 1H), 6.66 (d, *J* = 7.5 Hz, 1H), 4.02 – 3.93 (m, 5H), 3.43 (s, 2H), 2.51 (dt, *J* = 3.4, 1.7 Hz, 4H). LCMS (ESI) $[M+H]^+$ calcd for $C_{19}H_{18}N_4O_3^+$ m/z 350.38, found m/z 349.24.

AXA-05-161: ^{1}H NMR (500 MHz, DMSO) δ 10.17 (s, 1H), 7.71 (d, *J* = 2.1 Hz, 1H), 7.58 (s, 1H), 7.52 (d, *J* = 7.5 Hz, 1H), 7.41 (dd, *J* = 8.7, 2.1 Hz, 1H), 7.25 (d, *J* = 8.7 Hz, 1H), 6.67 (d, *J* = 7.5 Hz, 1H), 4.04 – 3.89 (m, 6H), 1.23 (t, *J* = 7.1 Hz, 3H). LCMS (ESI) $[M+H]^+$ calcd for $C_{18}H_{16}N_4O_4^+$ m/z 352.35, found m/z 351.54.

AXA-05-163: ^{1}H NMR (500 MHz, DMSO) δ 10.60 (d, *J* = 1.9 Hz, 1H), 10.52 (d, *J* = 1.9 Hz, 1H), 10.02 (s, 1H), 7.60 – 7.48 (m, 3H), 7.27 (dd, *J* = 8.4, 2.0 Hz, 1H), 6.87 (d, *J* = 8.4 Hz, 1H), 6.66 (d, *J* = 7.5 Hz, 1H), 4.02 – 3.94 (m, 5H), 1.23 (t, *J* = 7.1 Hz, 3H). LCMS (ESI) $[M+H]^+$ calcd for $C_{18}H_{17}N_5O_3^+$ m/z 351.37, found m/z 350.47.

YL-12826-67: ^{1}H NMR (500 MHz, DMSO) δ 10.42 (s, 1H), 10.09 (s, 1H), 7.58 (s, 1H), 7.54 – 7.47 (m, 2H), 7.28 (dt, *J* = 8.1, 1.6 Hz, 1H), 7.14 (d, *J* = 8.1 Hz, 1H), 6.66 (d, *J* = 7.5 Hz, 1H), 4.02

– 3.93 (m, 3H), 2.51 (dt, *J* = 3.4, 1.7 Hz, 4H), 1.26 – 1.20 (m, 3H). LCMS (ESI) $[M+H]^+$ calcd for $C_{19}H_{18}N_4O_3^+$ m/z 350.14, found m/z 349.24.

AXA-05-165: ^{1}H NMR (500 MHz, DMSO) δ 10.16 (s, 1H), 7.61 (s, 1H), 7.52 (dd, *J* = 4.7, 2.8 Hz, 2H), 7.38 (dd, *J* = 8.0, 1.9 Hz, 1H), 7.24 – 7.19 (m, 1H), 6.67 (d, *J* = 7.5 Hz, 1H), 3.98 (d, *J* = 11.8 Hz, 5H), 3.12 (s, 3H), 1.30 – 1.17 (m, 5H). LCMS (ESI) $[M+H]^+$ calcd for $C_{20}H_{20}N_4O_3^+$ m/z 364.15, found m/z 363.57.

AXA-05-169: ^{1}H NMR (500 MHz, DMSO) δ 10.83 (s, 1H), 9.94 (s, 1H), 7.84 (d, *J* = 2.0 Hz, 1H), 7.54 – 7.47 (m, 2H), 7.30 (dd, *J* = 8.6, 2.0 Hz, 1H), 7.21 (d, *J* = 8.6 Hz, 1H), 6.66 (d, *J* = 7.5 Hz, 1H), 6.11 – 6.07 (m, 1H), 3.97 (d, *J* = 6.3 Hz, 4H), 2.38 (s, 3H), 1.25 (dt, *J* = 14.3, 6.9 Hz, 4H). LCMS (ESI) $[M+H]^+$ calcd for $C_{20}H_{20}N_4O_2^+$ m/z 348.16, found m/z 347.67.

AXA-05–049: ^{1}H NMR (500 MHz, DMSO) δ 10.42 (s, 1H), 10.09 (s, 1H), 7.58 (s, 1H), 7.54 – 7.47 (m, 2H), 7.28 (dt, *J* = 8.1, 1.6 Hz, 1H), 7.14 (d, *J* = 8.1 Hz, 1H), 6.66 (d, *J* = 7.5 Hz, 1H), 4.02 – 3.93 (m, 5H), 2.51 (dt, *J* = 3.4, 1.7 Hz, 4H), 1.26 – 1.20 (m, 3H). LCMS (ESI) $[M+H]^+$ calcd for $C_{20}H_{20}N_4O_3^+$ m/z 364.41, found m/z 363.14.

AXA-05-175: ^{1}H NMR (500 MHz, DMSO) δ 11.63 (s, 1H), 10.19 (s, 1H), 7.70 (d, *J* = 2.1 Hz, 1H), 7.64 – 7.56 (m, 2H), 7.40 (dd, *J* = 8.7, 2.1 Hz, 1H), 7.37 – 7.32 (m, 2H), 7.25 (d, *J* = 8.7 Hz, 1H), 7.21 – 7.12 (m, 2H), 6.72 (d, *J* = 7.5 Hz, 1H), 5.17 (s, 2H), 3.96 (s, 3H). LCMS (ESI) $[M+H]^+$ calcd for $C_{23}H_{17}FN_4O_4^+$ m/z 432.12, found m/z 431.15.

AXA-05-177: ^{1}H NMR (500 MHz, DMSO) δ 10.42 (s, 1H), 9.92 (s, 1H), 7.56 – 7.49 (m, 2H), 7.22 – 7.11 (m, 2H), 6.67 (ddd, *J* = 7.5, 4.1, 0.9 Hz, 2H), 3.99 (t, *J* = 7.1 Hz, 2H), 3.94 (s, 3H), 3.52 (s, 2H), 1.23 (t, *J* = 7.1 Hz, 3H). LCMS (ESI) $[M+H]^+$ calcd for $C_{19}H_{18}N_4O_3^+$ m/z 350.14, found m/z 349.10.

AXA-06-009: ^{1}H NMR (500 MHz, DMSO) δ 10.19 (s, 1H), 7.70 (d, *J* = 2.1 Hz, 1H), 7.56 (d, *J* = 6.9 Hz, 2H), 7.40 (dd, *J* = 8.7, 2.1 Hz, 1H), 7.31 – 7.22 (m, 2H), 7.16 (q, *J* = 8.0 Hz, 1H), 7.05 (t, *J* = 8.5 Hz, 1H), 6.75 (d, *J* = 7.6 Hz, 1H), 5.20 (s, 2H), 1.24 (s, 2H), 1.21 (s, 2H). LCMS (ESI) $[M+H]^+$ calcd for $C_{23}H_{16}F_2N_4O_4^+$ m/z 450.11, found m/z 449.40.

AXA-06-011: ^{1}H NMR (500 MHz, DMSO) δ 11.62 (s, 1H), 10.19 (s, 1H), 7.70 (d, *J* = 2.1 Hz, 1H), 7.56 (d, *J* = 6.9 Hz, 2H), 7.40 (dd, *J* = 8.7, 2.1 Hz, 1H), 7.31 – 7.22 (m, 2H), 7.16 (q, *J* = 8.0 Hz, 1H), 7.05 (t, *J* = 8.5 Hz, 1H), 6.75 (d, *J* = 7.6 Hz, 1H), 5.20 (s, 2H), 3.97 (s, 2H), 1.24 (s, 2H).LCMS (ESI) $[M+H]^+$ calcd for $C_{24}H_{17}F_3N_4O_4^+$ m/z 482.12, found m/z 481.14.

AXA-06-021: ^{1}H NMR (500 MHz, DMSO) δ 11.62 (s, 1H), δ 10.19 (s, 1H), 7.70 (d, *J* = 2.1 Hz, 1H), 7.62 – 7.56 (m, 2H), 7.40 (dd, *J* = 8.7, 2.1 Hz, 1H), 7.37 – 7.30 (m, 2H), 7.30 – 7.22 (m, 4H), 6.71 (dd, *J* = 7.6, 0.8 Hz, 1H), 5.19 (s, 2H), 3.96 (s, 3H). LCMS (ESI) $[M+H]^+$ calcd for $C_{23}H_{18}N_4O_4^+$ m/z 414.13, found m/z 413.42.

3.5 Author contributions

M058-0519 analogs were synthesized by Yanran Liu and by myself. ABPP experiments were performed by Ujwal Punyamurtula. USP4 and USP28 computational models were made by Mona Sharafi. I purified USP28 enzyme, and generated all IC_{50} values reported in this section.

Bibliography

(1) Wertz, I. E.; Murray, J. M. Structurally-Defined Deubiquitinase Inhibitors Provide Opportunities to Investigate Disease Mechanisms. *Drug Discov. Today Technol.* **2019**, *31*, 109–123.

(2) Behrends, C.; Harper, J. W. Constructing and Decoding Unconventional Ubiquitin Chains. *Nat. Struct. Mol. Biol.* **2011**, *18* (5), 520–528.

(3) Grou, C. P.; Pinto, M. P.; Mendes, A. V.; Domingues, P.; Azevedo, J. E. The de Novo Synthesis of Ubiquitin: Identification of Deubiquitinases Acting on Ubiquitin Precursors. *Sci. Rep.* **2015**, *5*, 1–16.

(4) Komander, D.; Rape, M. The Ubiquitin Code. *Annu. Rev. Biochem.* **2012**, *81* (1), 203–229.

(5) Akutsu, M.; Dikic, I.; Bremm, A. Ubiquitin Chain Diversity at a Glance. *J. Cell Sci.* **2016**, *129* (5), 875–880.

(6) Swatek, K. N.; Komander, D. Ubiquitin Modifications. *Cell Res.* **2016**, *26* (4), 399–422.

(7) d'Azzo, A.; Bongiovanni, A.; Nastasi, T. E3 Ubiquitin Ligases as Regulators of Membrane Protein Trafficking and Degradation. *Traffic* **2005**, *6* (6), 429–441.

(8) Dang, F.; Nie, L.; Wei, W. Ubiquitin Signaling in Cell Cycle Control and Tumorigenesis. *Cell Death Differ.* **2021**, *28* (2), 427–438.

(9) Pinto-Fernandez, A.; Kessler, B. M. DUBbing Cancer: Deubiquitylating Enzymes Involved in Epigenetics, DNA Damage and the Cell Cycle as Therapeutic Targets. *Front. Genet.* **2016**, *7* (JUL), 1–13.

(10) Wipt, P.; George, K. M. 基因的改变NIH Public Access. *Bone* **2008**, *23* (1), 1–7.

(11) Daulny, A.; Tansey, W. P. Damage Control: DNA Repair, Transcription, and the Ubiquitin-Proteasome System. *DNA Repair (Amst).* **2009**, *8* (4), 444–448.

(12) Chen, Z. J.; Sun, L. J. Nonproteolytic Functions of Ubiquitin in Cell Signaling. *Mol. Cell* **2009**, *33* (3), 275–286.

(13) Das, S.; Ramakrishna, S.; Kim, K. S. Critical Roles of Deubiquitinating Enzymes in the Nervous

System and Neurodegenerative Disorders. *Mol. Cells* **2020**, *43* (3), 1–12.

(14) Leroy, E.; Boyer, R.; Auburger, G.; Leube, B.; Ulm, G.; Mezey, E.; Harta, G.; Brownstein, M. J.; Jonnalagada, S.; Chernova, T.; et al. The Ubiquitin Pathway in Parkinson's Disease [6]. *Nature* **1998**, *395* (6701), 451–452.

(15) Lim, K. H.; Joo, J. Y.; Baek, K. H. The Potential Roles of Deubiquitinating Enzymes in Brain Diseases. *Ageing Res. Rev.* **2020**, *61* (April), 101088.

(16) Hu, H.; Sun, S. C. Ubiquitin Signaling in Immune Responses. *Cell Res.* **2016**, *26* (4), 457–483.

(17) Zinngrebe, J.; Montinaro, A.; Peltzer, N.; Walczak, H. Ubiquitin in the Immune System. *EMBO Rep.* **2014**, *15* (1), 28–45.

(18) D'Arcy, P.; Wang, X.; Linder, S. Deubiquitinase Inhibition as a Cancer Therapeutic Strategy. *Pharmacol. Ther.* **2015**, *147*, 32–54.

(19) Fraile, J. M.; Quesada, V.; Rodríguez, D.; Freije, J. M. P.; López-Otín, C. Deubiquitinases in Cancer: New Functions and Therapeutic Options. *Oncogene* **2012**, *31* (19), 2373–2388.

(20) Schwartz, A. L.; Ciechanover, A. Targeting Proteins for Destruction by the Ubiquitin System: Implications for Human Pathobiology. *Annu. Rev. Pharmacol. Toxicol.* **2009**, *49* (1), 73–96.

(21) Richardson, P. G.; Hideshima, T.; Anderson, K. C. Bortezomib (PS-341): A Novel, First-in-Class Proteasome Inhibitor for the Treatment of Multiple Myeloma and Other Cancers. *Cancer Control* **2003**, *10* (5), 361–369.

(22) A Phase I, Open-Label, Multicenter Study to Investigate the Safety, Tolerability, Pharmacokinetics, and Preliminary Efficacy of ISM3091 in Patients With Advanced Solid Tumors https://clinicaltrials.gov/study/NCT05932862?term=USP1&rank=2.

(23) A Phase 1 Study of KSQ-4279 Alone and in Combination in Patients With Advanced Solid Tumors https://clinicaltrials.gov/study/NCT05240898?term=USP1&rank=1.

(24) Simoneau, A.; Wu, H.-J.; Bandi, M.; Lazarides, K.; Sun, S.; Liu, S.; Meier, S.; Choi, A.; Zhang, H.; Shen, B.; et al. Abstract 4968: Characterization of the Clinical Development Candidate TNG348 as a Potent and Selective Inhibitor of USP1 for the Treatment of BRCA1/2mut Cancers.

Cancer Res. **2023**, *83* (7_Supplement), 4968.

(25) Komander, D.; Clague, M. J.; Urbé, S. Breaking the Chains: Structure and Function of the Deubiquitinases. *Nat. Rev. Mol. Cell Biol.* **2009**, *10* (8), 550–563.

(26) Gopinath, P.; Ohayon, S.; Nawatha, M.; Brik, A. Chemical and Semisynthetic Approaches to Study and Target Deubiquitinases. *Chem. Soc. Rev.* **2016**, *45* (15), 4171–4198.

(27) Haahr, P.; Borgermann, N.; Guo, X.; Typas, D.; Achuthankutty, D.; Hoffmann, S.; Shearer, R.; Sixma, T. K.; Mailand, N. ZUFSP Deubiquitylates K63-Linked Polyubiquitin Chains to Promote Genome Stability. *Mol. Cell* **2018**, *70* (1), 165-174.e6.

(28) Hermanns, T.; Pichlo, C.; Woiwode, I.; Klopffleisch, K.; Witting, K. F.; Ovaa, H.; Baumann, U.; Hofmann, K. A Family of Unconventional Deubiquitinases with Modular Chain Specificity Determinants. *Nat. Commun.* **2018**, *9* (1).

(29) Hewings, D. S.; Heideker, J.; Ma, T. P.; Ahyoung, A. P.; El Oualid, F.; Amore, A.; Costakes, G. T.; Kirchhofer, D.; Brasher, B.; Pillow, T.; et al. Reactive-Site-Centric Chemoproteomics Identifies a Distinct Class of Deubiquitinase Enzymes. *Nat. Commun.* **2018**, *9* (1).

(30) Schauer, N. J.; Magin, R. S.; Liu, X.; Doherty, L. M.; Buhrlage, S. J. Advances in Discovering Deubiquitinating Enzyme (DUB) Inhibitors. *J. Med. Chem.* **2019**.

(31) Oliveira, A. M.; Chou, M. M. USP6-Induced Neoplasms: The Biologic Spectrum of Aneurysmal Bone Cyst and Nodular Fasciitis. *Hum. Pathol.* **2014**, *45* (1), 1–11.

(32) Hao, Y.; Jr, M. D. F.; Tacer, K. F.; Xia, F.; Bi, W.; Kang, S. L.; Patel, A.; Rosenfeld, J. A.; Caignec, C. Le; Krantz, I. D.; et al. HHS Public Access. **2016**, *59* (6), 956–969.

(33) Ma, Z. Y.; Song, Z. J.; Chen, J. H.; Wang, Y. F.; Li, S. Q.; Zhou, L. F.; Mao, Y.; Li, Y. M.; Hu, R. G.; Zhang, Z. Y.; et al. Recurrent Gain-of-Function USP8 Mutations in Cushing's Disease. *Cell Res.* **2015**, *25* (3), 306–317.

(34) Reincke, M.; Sbiera, S.; Hayakawa, A.; Theodoropoulou, M.; Osswald, A.; Beuschlein, F.; Meitinger, T.; Mizuno-Yamasaki, E.; Kawaguchi, K.; Saeki, Y.; et al. Mutations in the Deubiquitinase Gene Usp8 Cause Cushing's Disease. *Nat. Genet.* **2015**, *47* (1), 31–38.

(35) Homan, C. C.; Kumar, R.; Nguyen, L. S.; Haan, E.; Raymond, F. L.; Abidi, F.; Raynaud, M.; Schwartz, C. E.; Wood, S. A.; Gecz, J.; et al. Mutations in USP9X Are Associated with X-Linked Intellectual Disability and Disrupt Neuronal Cell Migration and Growth. *Am. J. Hum. Genet.* **2014**, *94* (3), 470–478.

(36) Eichhorn, P. J. A.; Rodón, L.; Gonzàlez-Juncà, A.; Dirac, A.; Gili, M.; Martínez-Sáez, E.; Aura, C.; Barba, I.; Peg, V.; Prat, A.; et al. USP15 Stabilizes TGF-B2 Receptor I and Promotes Oncogenesis through the Activation of TGF-B2 Signaling in Glioblastoma. *Nat. Med.* **2012**, *18* (3), 429–435.

(37) Magin, R. S.; Liu, X.; Felix, A.; Bratt, A. S.; Chan, W. C.; Buhrlage, S. J. Small Molecules as Tools for Functional Assessment of Deubiquitinating Enzyme Function. *Cell Chem. Biol.* **2021**, *28* (7), 1090–1100.

(38) Lange, S. M.; Armstrong, L. A.; Kulathu, Y. Deubiquitinases: From Mechanisms to Their Inhibition by Small Molecules. *Mol. Cell* **2022**, *82* (1), 15–29.

(39) Popov, N.; Wanzel, M.; Madiredjo, M.; Zhang, D.; Beijersbergen, R.; Bernards, R.; Moll, R.; Elledge, S. J.; Eilers, M. The Ubiquitin-Specific Protease USP28 Is Required for MYC Stability. *Nat. Cell Biol.* **2007**, *9* (7), 765–774.

(40) Flügel, D.; Görlach, A.; Kietzmann, T. GSK-3β Regulates Cell Growth, Migration, and Angiogenesis via Fbw7 and USP28-Dependent Degradation of HIF-1α. *Blood* **2012**, *119* (5), 1292–1301.

(41) Alwan, H. A. J.; Van Leeuwen, J. E. M. UBPY-Mediated Epidermal Growth Factor Receptor (EGFR) de-Ubiquitination Promotes EGFR Degradation. *J. Biol. Chem.* **2007**, *282* (3), 1658–1669.

(42) Wrigley, J. D.; Eckersley, K.; Hardern, I. M.; Millard, L.; Walters, M.; Peters, S. W.; Mott, R.; Nowak, T.; Ward, R. A.; Simpson, P. B.; et al. Enzymatic Characterisation of USP7 Deubiquitinating Activity and Inhibition. *Cell Biochem. Biophys.* **2011**, *60* (1–2), 99–111.

(43) Sahtoe, D. D.; Sixma, T. K. Layers of DUB Regulation. *Trends Biochem. Sci.* **2015**, *40* (8), 456–

467.

(44) Mevissen, T. E. T.; Komander, D. Mechanisms of Deubiquitinase Specificity and Regulation. *Annu. Rev. Biochem.* **2017**, *86* (1), 159–192.

(45) Gavory, G.; O'Dowd, C. R.; Helm, M. D.; Flasz, J.; Arkoudis, E.; Dossang, A.; Hughes, C.; Cassidy, E.; McClelland, K.; Odrzywol, E.; et al. Discovery and Characterization of Highly Potent and Selective Allosteric USP7 Inhibitors. *Nat. Chem. Biol.* **2018**, *14* (2), 118–125.

(46) Kategaya, L.; Di Lello, P.; Rougé, L.; Pastor, R.; Clark, K. R.; Drummond, J.; Kleinheinz, T.; Lin, E.; Upton, J. P.; Prakash, S.; et al. *USP7 Small-Molecule Inhibitors Interfere with Ubiquitin Binding*; Nature Publishing Group, 2017; Vol. 550.

(47) Lamberto, I.; Liu, X.; Seo, H. S.; Schauer, N. J.; Iacob, R. E.; Hu, W.; Das, D.; Mikhailova, T.; Weisberg, E. L.; Engen, J. R.; et al. Structure-Guided Development of a Potent and Selective Non-Covalent Active-Site Inhibitor of USP7. *Cell Chem. Biol.* **2017**, *24* (12), 1490-1500.e11.

(48) Ohol, Y.; Sun, M.; Cutler, G.; Leger, P.; Hu, D.; Biannic, B.; Rana, P.; Cho, C.; Jacobson, S.; Wong, S.; et al. Discovery Of Potent And Selective Inhibitors Of USP7 With Anti-Tumor Activity In Vitro And In Vivo USP7 Inhibitors Inhibit P53-Wild Type Tumors In Vitro and In Vivo USP7 Inhibitors Synergize With DNA- USP7 Inhibitors Are Highly Selective and Potent in Bio. 526.

(49) Schauer, N. J.; Liu, X.; Magin, R. S.; Doherty, L. M.; Chan, W. C.; Ficarro, S. B.; Hu, W.; Roberts, R. M.; Iacob, R. E.; Stolte, B.; et al. Selective USP7 Inhibition Elicits Cancer Cell Killing through a P53-Dependent Mechanism. *Sci. Rep.* **2020**, *10* (1), 1–15.

(50) Turnbull, A. P.; Ioannidis, S.; Krajewski, W. W.; Pinto-Fernandez, A.; Heride, C.; Martin, A. C. L.; Tonkin, L. M.; Townsend, E. C.; Buker, S. M.; Lancia, D. R.; et al. Molecular Basis of USP7 Inhibition by Selective Small-Molecule Inhibitors. *Nature* **2017**, *550* (7677), 481–486.

(51) Ritorto, M. S.; Ewan, R.; Perez-Oliva, A. B.; Knebel, A.; Buhrlage, S. J.; Wightman, M.; Kelly, S. M.; Wood, N. T.; Virdee, S.; Gray, N. S.; et al. Screening of DUB Activity and Specificity by MALDI-TOF Mass Spectrometry. *Nat. Commun.* **2014**, *5*.

(52) Varca, A. C.; Casalena, D.; Chan, W. C.; Hu, B.; Magin, R. S.; Roberts, R. M.; Liu, X.; Zhu, H.;

Seo, H. S.; Dhe-Paganon, S.; et al. Identification and Validation of Selective Deubiquitinase Inhibitors. *Cell Chem. Biol.* **2021**, *28* (12), 1758-1771.e13.

(53) Jeong, C. Inhibition of Ubiquitin-Specific Peptidase 8 Suppresses Growth of Gefitinib-Resistant Non-Small Cell Lung Cancer Cells by Inducing Apoptosis. **2015**, *20* (1), 57–63.

(54) Byun, S.; Lee, S. Y.; Lee, J.; Jeong, C. H.; Farrand, L.; Lim, S.; Reddy, K.; Kim, J. Y.; Lee, M. H.; Lee, H. J.; et al. USP8 Is a Novel Target for Overcoming Gefitinib Resistance in Lung Cancer. *Clin. Cancer Res.* **2013**, *19* (14), 3894–3904.

(55) Durcan, T. M.; Tang, M. Y.; Pérusse, J. R.; Dashti, E. A.; Aguileta, M. A.; McLelland, G.; Gros, P.; Shaler, T. A.; Faubert, D.; Coulombe, B.; et al. USP 8 Regulates Mitophagy by Removing K 6-linked Ubiquitin Conjugates from Parkin . *EMBO J.* **2014**, *33* (21), 2473–2491.

(56) Row, P. E.; Prior, I. A.; McCullough, J.; Clague, M. J.; Urbé, S. The Ubiquitin Isopeptidase UBPY Regulates Endosomal Ubiquitin Dynamics and Is Essential for Receptor Down-Regulation. *J. Biol. Chem.* **2006**, *281* (18), 12618–12624.

(57) Macdonald, E.; Urbé, S.; Clague, M. J. USP8 Controls the Trafficking and Sorting of Lysosomal Enzymes. *Traffic* **2014**, *15* (8), 879–888.

(58) Yan, M.; Zhao, C.; Wei, N.; Wu, X.; Cui, J.; Xing, Y. High Expression of Ubiquitin-Specific Protease 8 (USP8) Is Associated with Poor Prognosis in Patients with Cervical Squamous Cell Carcinoma. *Med. Sci. Monit.* **2018**, *24*, 4934–4943.

(59) Kobayashi, S.; Boggon, T. J.; Dayaram, T.; Jänne, P. A.; Kocher, O.; Meyerson, M.; Johnson, B. E.; Eck, M. J.; Tenen, D. G.; Halmos, B. EGFR Mutation and Resistance of Non-Small-Cell Lung Cancer to Gefitinib. *N. Engl. J. Med.* **2005**, *352* (8), 786–792.

(60) Kosaka, T.; Yatabe, Y.; Endoh, H.; Yoshida, K.; Hida, T.; Tsuboi, M.; Tada, H.; Kuwano, H.; Mitsudomi, T. Analysis of Epidermal Growth Factor Receptor Gene Mutation in Patients with Non-Small Cell Lung Cancer and Acquired Resistance to Gefitinib. *Clin. Cancer Res.* **2006**, *12* (19), 5764–5769.

(61) Jackman, D.; Pao, W.; Riely, G. J.; Engelman, J. A.; Kris, M. G.; Jänne, P. A.; Lynch, T.; Johnson,

B. E.; Miller, V. A. Clinical Definition of Acquired Resistance to Epidermal Growth Factor Receptor Tyrosine Kinase Inhibitors in Non-Small-Cell Lung Cancer. *J. Clin. Oncol.* **2010**, *28* (2), 357–360.

(62) Prevot, T. D.; Li, G.; Vidojevic, A.; Misquitta, K. A.; Fee, C.; Santrac, A.; Knutson, D. E.; Stephen, M. R.; Kodali, R.; Zahn, N. M.; et al. Novel Benzodiazepine-Like Ligands with Various Anxiolytic, Antidepressant, or Pro-Cognitive Profiles. *Mol. Neuropsychiatry* **2019**, *8*, 1–14.

(63) Tang, A. H.; Franklin, S. R.; Himes, C. S.; Ho, P. M. Behavioral Effects of U-78875, a Quinoxalinone Anxiolytic with Potent Benzodiazepine Antagonist Activity. *J. Pharmacol. Exp. Ther.* **1991**, *259* (1), 248–254.

(64) Takahashi, M.; Kohara, A.; Shishikura, J. ichi; Kawasaki-Yatsugi, S.; Ni, J. W.; Yatsugi, S. ichi; Sakamoto, S.; Okada, M.; Shimizu-Sasamata, M.; Yamaguchi, T. YM872: A Selective, Potent and Highly Water-Soluble α-Amino-3-Hydroxy-5-Methylisoxazole-4-Propionic Acid Receptor Antagonist. *CNS Drug Rev.* **2002**, *8* (4), 337–352.

(65) Lee, B. H.; Lee, M. J.; Park, S.; Oh, D. C.; Elsasser, S.; Chen, P. C.; Gartner, C.; Dimova, N.; Hanna, J.; Gygi, S. P.; et al. Enhancement of Proteasome Activity by a Small-Molecule Inhibitor of USP14. *Nature* **2010**, *467* (7312), 179–184.

(66) Avvakumov, G. V.; Walker, J. R.; Xue, S.; Finerty, P. J.; Mackenzie, F.; Newman, E. M.; Dhe-Paganon, S. Amino-Terminal Dimerization, NRDP1-Rhodanese Interaction, and Inhibited Catalytic Domain Conformation of the Ubiquitin-Specific Protease 8 (USP8). *J. Biol. Chem.* **2006**, *281* (49), 38061–38070.

(67) Reinitz, F.; Chen, E. Y.; Di Robilant, B. N.; Chuluun, B.; Antony, J.; Jones, R. C.; Gubbi, N.; Lee, K.; Ho, W. H. D.; Kolluru, S. S.; et al. Inhibiting USP16 Rescues Stem Cell Aging and Memory in an Alzheimer's Model. *Elife* **2022**, *11*, 1–27.

(68) Ishii, T.; Shimizu, Y.; Nakashima, K.; Kondo, S.; Ogawa, K.; Sasaki, S.; Matsui, H. Inhibition Mechanism Exploration of Investigational Drug TAK-441 as Inhibitor against Vismodegib-Resistant Smoothened Mutant. *Eur. J. Pharmacol.* **2014**, *723*, 305–313.

(69) Lor, L. A.; Schneck, J.; McNulty, D. E.; Diaz, E.; Brandt, M.; Thrall, S. H.; Schwartz, B. A Simple Assay for Detection of Small-Molecule Redox Activity. *J. Biomol. Screen.* **2007**, *12* (6), 881–890.

(70) Varca, A. C.; Casalena, D.; Auld, D.; Buhrlage, S. J. Identification of Deubiquitinase Inhibitors via High-Throughput Screening Using a Fluorogenic Ubiquitin-Rhodamine Assay. *STAR Protoc.* **2021**, *2* (4), 100896.

(71) Kluge, A. F.; Lagu, B. R.; Maiti, P.; Jaleel, M.; Webb, M.; Malhotra, J.; Mallat, A.; Srinivas, P. A.; Thompson, J. E. Novel Highly Selective Inhibitors of Ubiquitin Specific Protease 30 (USP30) Accelerate Mitophagy. *Bioorg. Med. Chem. Lett.* **2018**, *28* (15), 2655–2659.

(72) Wang, Y.; Jiang, Y.; Ding, S.; Li, J.; Song, N.; Ren, Y.; Hong, D.; Wu, C.; Li, B.; Wang, F.; et al. Small Molecule Inhibitors Reveal Allosteric Regulation of USP14 via Steric Blockade. *Cell Res.* **2018**, *28* (12), 1186–1194.

(73) Gersch, M.; Wagstaff, J. L.; Toms, A. V.; Graves, B.; Freund, S. M. V.; Komander, D. Distinct USP25 and USP28 Oligomerization States Regulate Deubiquitinating Activity. *Mol. Cell* **2019**, *74* (3), 436-451.e7.

(74) Ye, Y.; Scheel, H.; Hofmann, K.; Komander, D. Dissection of USP Catalytic Domains Reveals Five Common Insertion Points. *Mol. Biosyst.* **2009**, *5* (12), 1797–1808.

(75) Liu, B.; Sureda-Gómez, M.; Zhen, Y.; Amador, V.; Reverter, D. A Quaternary Tetramer Assembly Inhibits the Deubiquitinating Activity of USP25. *Nat. Commun.* **2018**, *9* (1).

(76) Zhong, B.; Liu, X.; Wang, X.; Chang, S. H.; Liu, X.; Wang, A.; Joseph, M.; Dong, C. HHS Public Access. **2013**, *13* (11), 1110–1117.

(77) Lin, D.; Zhang, M.; Zhang, M. X.; Ren, Y.; Zhao, Q.; Jin, J.; Pan, Z.; Wu, M.; Shu, H. B.; Dong, C.; et al. Induction of USP25 by Viral Infection Promotes Innate Antiviral Responses by Mediating the Stabilization of TRAF3 and TRAF6. *Proc. Natl. Acad. Sci. U. S. A.* **2015**, *112* (36), 11324–11329.

(78) Kwilas, A. R.; Donahue, R. N.; Tsang, K. Y.; Hodge, J. W. 乳鼠心肌提取 HHS Public Access.

Cancer Cell **2015**, *2* (1), 1–17.

(79) Xu, D.; Liu, J.; Fu, T.; Shan, B.; Qian, L.; Pan, L.; Yuan, J. USP25 Regulates WNT Signalling by Controlling the Stability of Tankyrases. *Genes Dev.* **2017**, *31* (10), 1024–1035.

(80) Blount, J. R.; Burr, A. A.; Denuc, A.; Marfany, G.; Todi, S. V. Ubiquitin-Specific Protease 25 Functions in Endoplasmic Reticulum-Associated Degradation. *PLoS One* **2012**, *7* (5), 1–9.

(81) Cuella-Martin, R.; Oliveira, C.; Lockstone, H. E.; Snellenberg, S.; Grolmusova, N.; Chapman, J. R. 53BP1 Integrates DNA Repair and P53-Dependent Cell Fate Decisions via Distinct Mechanisms. *Mol. Cell* **2016**, *64* (1), 51–64.

(82) Zhang, D.; Zaugg, K.; Mak, T. W.; Elledge, S. J. A Role for the Deubiquitinating Enzyme USP28 in Control of the DNA-Damage Response. *Cell* **2006**, *126* (3), 529–542.

(83) Diefenbacher, M. E.; Popov, N.; Blake, S. M.; Schülein-Völk, C.; Nye, E.; Spencer-Dene, B.; Jaenicke, L. A.; Eilers, M.; Behrens, A. The Deubiquitinase USP28 Controls Intestinal Homeostasis and Promotes Colorectal Cancer. *J. Clin. Invest.* **2014**, *124* (8), 3407–3418.

(84) Josue Ruiz, E.; Pinto-Fernandez, A.; Turnbull, A. P.; Lan, L.; Charlton, T. M.; Scott, H. C.; Damianou, A.; Vere, G.; Riising, E. M.; Da Costa, C.; et al. Usp28 Deletion and Small-Molecule Inhibition Destabilizes c-Myc and Elicits Regression of Squamous Cell Lung Carcinoma. *Elife* **2021**, *10*, 1–23.

(85) Wang, X.; Liu, Z.; Zhang, L.; Yang, Z.; Chen, X.; Luo, J.; Zhou, Z.; Mei, X.; Yu, X.; Shao, Z.; et al. Targeting Deubiquitinase USP28 for Cancer Therapy. *Cell Death Dis.* **2018**, *9* (2).

(86) Wu, Y.; Wang, Y.; Yang, X. H.; Kang, T.; Zhao, Y.; Wang, C.; Evers, B. M.; Zhou, B. P. The Deubiquitinase USP28 Stabilizes LSD1 and Confers Stem-Cell-like Traits to Breast Cancer Cells. *Cell Rep.* **2013**, *5* (1), 224–236.

(87) Schülein-Völk, C.; Wolf, E.; Zhu, J.; Xu, W.; Taranets, L.; Hellmann, A.; Jänicke, L. A.; Diefenbacher, M. E.; Behrens, A.; Eilers, M.; et al. Dual Regulation of Fbw7 Function and Oncogenic Transformation by Usp28. *Cell Rep.* **2014**, *9* (3), 1099–1109.

(88) Davis, R. J.; Welcker, M.; Clurman, B. E. Tumor Suppression by the Fbw7Ubiquitin Ligase:

Mechanisms and Opportunities. *Cancer Cell* **2014**, *26* (4), 455–464.

(89) Diefenbacher, M. E.; Chakraborty, A.; Blake, S. M.; Mitter, R.; Popov, N.; Eilers, M.; Behrens, A. Usp28 Counteracts Fbw7 in Intestinal Homeostasis and Cancer. *Cancer Res.* **2015**, *75* (7), 1181–1186.

(90) Pct, W. I. WO 2017/139778 Al. **2017**, *02453* (12).

(91) Peng, J.; Jiang, K.; Sun, X.; Wu, L.; Wang, J.; Xi, X.; Tan, X.; Liang, T.; Tan, C.; Zhang, P. Identification of a Class of Potent USP25/28 Inhibitors with Broad-Spectrum Anti-Cancer Activity. *Signal Transduct. Target. Ther.* **2022**, *7* (1), 6–8.

(92) Vlasschaert, C.; Xia, X.; Coulombe, J.; Gray, D. A. Evolution of the Highly Networked Deubiquitinating Enzymes USP4, USP15, and USP11. *BMC Evol. Biol.* **2015**, *15* (1), 1–18.

(93) Hu, B.; Zhang, D.; Zhao, K.; Wang, Y.; Pei, L.; Fu, Q.; Ma, X. Spotlight on USP4: Structure, Function, and Regulation. *Front. Cell Dev. Biol.* **2021**, *9* (February), 1–15.

(94) Yun, S. Il; Kim, H. H.; Yoon, J. H.; Park, W. S.; Hahn, M. J.; Kim, H. C.; Chung, C. H.; Kim, K. K. Ubiquitin Specific Protease 4 Positively Regulates the WNT/β-Catenin Signaling in Colorectal Cancer. *Mol. Oncol.* **2015**, *9* (9), 1834–1851.

(95) Zhang, X.; Berger, F. G.; Yang, J.; Lu, X. USP4 Inhibits P53 through Deubiquitinating and Stabilizing ARF-BP1. *EMBO J.* **2011**, *30* (11), 2177–2189.

(96) Li, Z.; Hao, Q.; Luo, J.; Xiong, J.; Zhang, S.; Wang, T.; Bai, L.; Wang, W.; Chen, M.; Wang, W.; et al. USP4 Inhibits P53 and NF-KB through Deubiquitinating and Stabilizing HDAC2. *Oncogene* **2016**, *35* (22), 2902–2912.

(97) Das, T.; Park, J. K.; Park, J.; Kim, E.; Rape, M.; Kim, E. E. K.; Song, E. J. USP15 Regulates Dynamic Protein-Protein Interactions of the Spliceosome through Deubiquitination of PRP31. *Nucleic Acids Res.* **2017**, *45* (8), 4866–4880.

(98) Zou, Q.; Jin, J.; Hu, H.; Li, H. S.; Romano, S.; Xiao, Y.; Nakaya, M.; Zhou, X.; Cheng, X.; Yang, P.; et al. USP15 Stabilizes MDM2 to Mediate Cancer-Cell Survival and Inhibit Antitumor T Cell Responses. *Nat. Immunol.* **2014**, *15* (6), 562–570.

(99) Zou, Q.; Jin, J.; Xiao, Y.; Zhou, X.; Hu, H.; Cheng, X.; Kazimi, N.; Ullrich, S. E.; Sun, S. C. T Cell Intrinsic USP15 Deficiency Promotes Excessive IFN-γ Production and an Immunosuppressive Tumor Microenvironment in MCA-Induced Fibrosarcoma. *Cell Rep.* **2015**, *13* (11), 2470–2479.

(100) Huang, X.; Langelotz, C.; Hetfeld-Pěchoč, B. K. J.; Schwenk, W.; Dubiel, W. The COP9 Signalosome Mediates β-Catenin Degradation by Deneddylation and Blocks Adenomatous Polyposis Coli Destruction via USP15. *J. Mol. Biol.* **2009**, *391* (4), 691–702.

(101) Faronato, M.; Patel, V.; Darling, S.; Dearden, L.; Clague, M. J.; Urbé, S.; Coulson, J. M. The Deubiquitylase USP15 Stabilizes Newly Synthesized REST and Rescues Its Expression at Mitotic Exit. *Cell Cycle* **2013**, *12* (12), 1964–1977.

(102) Long, L.; Thelen, J. P.; Furgason, M.; Haj-Yahya, M.; Brik, A.; Cheng, D.; Peng, J.; Yao, T. The U4/U6 Recycling Factor SART3 Has Histone Chaperone Activity and Associates with USP15 to Regulate H2B Deubiquitination. *J. Biol. Chem.* **2014**, *289* (13), 8916–8930.

(103) Fielding, A. B.; Concannon, M.; Darling, S.; Rusilowicz-Jones, E. V.; Sacco, J. J.; Prior, I. A.; Clague, M. J.; Urbé, S.; Coulson, J. M. The Deubiquitylase USP15 Regulates Topoisomerase II Alpha to Maintain Genome Integrity. *Oncogene* **2018**, *37* (17), 2326–2342.

(104) Das, T.; Song, E. J.; Kim, E. E. K. The Multifaceted Roles of Usp15 in Signal Transduction. *Int. J. Mol. Sci.* **2021**, *22* (9).

(105) Xia, X.; Huang, C.; Liao, Y.; Liu, Y.; He, J.; Shao, Z.; Hu, T.; Yu, C.; Jiang, L.; Liu, J.; et al. The Deubiquitinating Enzyme USP15 Stabilizes ERα and Promotes Breast Cancer Progression. *Cell Death Dis.* **2021**, *12* (4).

(106) Padmanabhan, A.; Candelaria, N.; Wong, K. K.; Nikolai, B. C.; Lonard, D. M.; O'Malley, B. W.; Richards, J. S. USP15-Dependent Lysosomal Pathway Controls P53-R175H Turnover in Ovarian Cancer Cells. *Nat. Commun.* **2018**, *9* (1).

(107) Chen, L. L.; Smith, M. D.; Lv, L.; Nakagawa, T.; Li, Z.; Sun, S. C.; Brown, N. G.; Xiong, Y.; Xu, Y. P. USP15 Suppresses Tumor Immunity via Deubiquitylation and Inactivation of TET2. *Sci.*

Adv. **2020**, *6* (38), 1–14.

(108) Wrigley, J. D.; Gavory, G.; Simpson, I.; Preston, M.; Plant, H.; Bradley, J.; Goeppert, A. U.; Rozycka, E.; Davies, G.; Walsh, J.; et al. Identification and Characterization of Dual Inhibitors of the USP25/28 Deubiquitinating Enzyme Subfamily. *ACS Chem. Biol.* **2017**, *12* (12), 3113–3125.

(109) Bureau, I.; Street, A.; David, J.; Drive, P. WO 2019/032863 Al. **2019**, No. 12.

(110) Zhou, D.; Xu, Z.; Huang, Y.; Wang, H.; Zhu, X.; Zhang, W.; Song, W.; Gao, T.; Liu, T.; Wang, M.; et al. Structure-Based Discovery of Potent USP28 Inhibitors Derived from Vismodegib. *Eur. J. Med. Chem.* **2023**, *254* (March), 115369.

(111) Hemelaar, J.; Galardy, P. J.; Borodovsky, A.; Kessler, B. M.; Ploegh, H. L.; Ovaa, H. Chemistry-Based Functional Proteomics: Mechanism-Based Activity-Profiling Tools for Ubiquitin and Ubiquitin-like Specific Proteases. *J. Proteome Res.* **2004**, *3* (2), 268–276.

(112) Long, M. J. C.; Lawson, A. P.; Baggio, R.; Qian, Y.; Rozhansky, L.; Fasci, D.; El Oualid, F.; Weerapana, E.; Hedstrom, L. Diarylcarbonates Are a New Class of Deubiquitinating Enzyme Inhibitor. *Bioorganic Med. Chem. Lett.* **2019**, *29* (2), 204–211.